Delft University of Technology
Faculty of Electrical Engineering, Mathematics and Computer Science
Delft Institute of Applied Mathematics

On Electromagnetically Induced Fluid Flows in Water

A thesis submitted to the
Delft Institute of Applied Mathematics
in partial fulfilment of the requirements

for the degree

MASTER OF SCIENCE
in
APPLIED MATHEMATICS

by

MICHIEL DE REUS

Delft, the Netherlands
March 2013

MSc THESIS APPLIED MATHEMATICS

"On Electromagnetically Induced Fluid Flows in Water"

MICHIEL DE REUS

Delft University of Technology

Daily Supervisor

Dr. N.V. Budko

Responsible Professor

Prof.dr.ir. C. Vuik

Other thesis committee members

Dr. J. Caro

March, 2013

Delft, the Netherlands

Preface

This document is the final result of my thesis project, a project concluding my master program in Applied Mathematics at Delft University of Technology. The subject is the result of some conversations between Neil Budko, my supervisor, and me about his current research topics. I wanted a project mixing both mathematics and physics, and my choice was a good one.

I want to thank Neil for all the time he invested in me and this project. The appointments usually took longer than expected because we ended up discussing all kinds of possible ideas to explore.

Of course I also want to thank all my friends and fellow students who supported me during my studies and in particular during this project. Special thanks go to André, Frank and Linda, for all the relaxing conversations during the coffee and lunch breaks, and the help with Latex when things got complicated. I also want to thank the board of the study association W.I.S.V. 'Christiaan Huygens' for their infinite supply of coffee, a substance essential for the completion of this project.

Furthermore I want to thank professor Vuik, my responsible professor, for his support not only during this project but throughout my whole studies in Delft, and Jaap Caro, from the physics department, for taking place in the graduation committee. I hope my thesis will be of some help in his future research.

And of course last but not least I thank my parents for their general support during the whole time and my girlfriend Carolyn whose support and friendship are invaluable.

Michiel de Reus
Delft, the Netherlands
March 2013

Contents

Chapter 1

Introduction

Electromagnetic phenomena are among the most widely researched ones in physics. One active research subject is that of optical traps. Using focussed laser beams, small dielectric particles in the micro and nano meter range are trapped by the surrounding electromagnetic fields. The first observation of this trapping force using a single beam was in the mid 1980s [1].

The trapping of these small particles has a wide range of applications. One can think of separation of particles with different sizes or electric properties on a so-called lab-on-a-chip, or the fabrication of miniature devices. For example in [16] devices are proposed that no longer need mechanical components for certain tasks such as switching a signal, but use a moving particle instead, that 'steers' a signal beam. This particle is controlled by an optical trap.

Of course for applications like this it is important that the particles react as is expected, so it is necessary to fully understand the forces acting on it, with high accuracy. As of now this is still the subject of ongoing research.

The two most important things that determine the expression of the total force on the particle are the model used for the electromagnetic field generated by the beam, and the expressions used to determine the total force on a particle given this background field. Additionally there is the question whether the electromagnetic force is the only force acting on the particle or there are more forces involved.

In practice the incoming beam is modelled as a Gaussian beam, with its parameters either deduced theoretically from the properties of the lens system, or determined empirically. As we will see later on, the Gaussian beam is an approximation that will only hold for certain choices of parameters. This is important to keep in mind when using this model.

To determine the total electromagnetic force on a particle, the force is split in a relatively large conservative part and a small non-conservative part. The conservative part is the so-called gradient force, proportional to the gradient of the electric field intensity. The non-conservative part is the so-called scattering force and points in the direction of propagation of the beam. Trapping then occurs because the gradient force is dominant compared to the scattering force, and the particle is trapped near the point of maximum intensity. Although the splitting of the total force in a gradient and scattering force is conceptually convenient, it is somewhat arbitrary, and in general incorrect. A more thorough analysis would make use of the Maxwell stress tensor and the conservation of total momentum. In [4] multiple expression for the total force on a particle inside an optical trap are compared. For larger particles these expressions deviate significantly, but for small particles,

within the Rayleigh regime, all expression result in the same total force.

In [22] an experiment is described in which the total force on small particles is measured directly. Here the non-conservative part of the trapping force is investigated. A deviation between the empirical force field and the theoretical force field based on the Gaussian beam approximation is observed.

One possibility is that there are more forces acting on the particle than just the electromagnetic force. In [20] the effect of thermophoresis is investigated. Thermophoresis is the phenomenon of an apparent force on particles submerged in a mixture of different mobile particles under influence of a temperature gradient.

We now come at the main subject of this thesis. We will investigate a phenomenon, that, if present, can lead to yet another force on the particles. We already know that particles with an electric contrast with respect to the background medium, will feel an electromagnetic force. This is the force responsible for the whole trapping to begin with. We will apply the same reasoning to the background medium itself. We determine the electromagnetic field and derive an expression for the force density corresponding to the Maxwell stress tensor. One important detail is that this stress tensor is not uniquely defined. As can be read in [6], when working in homogeneous solid media all choices will lead to the same result, since internal forces will only result in local displacements, creating internal stresses. In our case we are looking at fluids, which, by definition, cannot withstand internal stress and will start moving when forces are applied. We choose the stress tensor to be independent of the medium, assuming that all the electromagnetic reactions of the medium can be thought of as current densities induced on a vacuum background. We then use the Lorentz force expressions to determine the corresponding force density, which will result in the fluid starting to move.

1.1 Outline of this thesis

Besides the introduction this thesis consists of seven chapters and one appendix. In Chapter 2 we will investigate the electromagnetic field in general. The Maxwell equations are stated, both in vacuum and inside a medium. We will derive the complex Maxwell equations that we will use for the simulations. Also we will derive the time-averaged force density, and the heat dissipation resulting from conduction.

In Chapter 3 we discuss different external sources used to model the propagating laser beam that is used in a typical trapping experiment. We first consider the Gaussian beam approximation, after which we will discuss the so-called Gaussian dipole array, designed to reflect the properties of the Gaussian beam, without violating the Maxwell equations.

Chapter 4 focusses on the Navier-Stokes equations. Using the different conservation laws we derive the equations governing the fluid flows. These equations explicitly depend on the force density and heat dissipation terms determined in Chapter 2.

To perform the simulations themselves we need to choose a medium and domain of interest. In Chapter 5 we define the domain that we will use, and the parameters corresponding to our medium of choice, pure water, are discussed.

The numerical experiments themselves are discussed in Chapter 6. First the accuracy of the Gaussian beam source and the convergence properties of the quantities of interest for different grid sizes are investigated. Then the results of the simulations themselves are reviewed.

Finally in Chapter 7 and Chapter 8 conclusions are drawn based on the results of the simulations. Also some topics of future research are proposed.

In Appendix A some notation considering four-vectors is introduced, which is used in Chapter 2 to determine the Maxwell equations inside a possibly moving fluid.

Appendix B contains information about the software implementation used for the simulations. Some general information on the OpenFOAM package is given and the specific considerations for our implementation are mentioned.

Chapter 2

The electromagnetic field

It is well known that electromagnetic fields satisfy the Maxwell equations. In this chapter we will first consider the Maxwell equations in vacuum and derive expressions for the conversation of energy and momentum of the fields. Then we will consider the so-called macroscopic Maxwell equations in matter, where polarization of the medium will change the behaviour of the field. Also, conduction will lead to the dissipation of electromagnetic energy, resulting in exponential decay of the fields. Throughout this work we will assume that the mediums reaction to the magnetic field is negligible. This is true for most materials, particularly for water at the frequencies we will consider.

2.1 Maxwell equations in vacuum

From [7] we have the Maxwell equations in vacuum given by the coupled partial differential equations

$$-\nabla \times \mathbf{B} + \mu_0 \varepsilon_0 \frac{\partial \mathbf{E}}{\partial t} = -\mu_0 \mathbf{J}, \tag{2.1}$$

$$\nabla \times \mathbf{E} + \frac{\partial \mathbf{B}}{\partial t} = 0, \tag{2.2}$$

where $\mathbf{E} = \mathbf{E}(\mathbf{x}, t)$ is the electric field, $\mathbf{B} = \mathbf{B}(\mathbf{x}, t)$ is the magnetic field and $\mathbf{J} = \mathbf{J}(\mathbf{x}, t)$ is the (total) electric current density, and $\mathbf{x} \in \mathbb{R}^3$ is a vector in the domain of interest. The constants ε_0 and μ_0 are the permittivity of free space and permeability of free space respectively. These are considered constants by nature. We will see later on that when we consider electromagnetic fields in matter, we can model them with similar equations, with different values of these parameters. The reason there is no term at the right-hand side of the second equation is the lack of magnetic monopoles in nature. Sometimes a non-zero term is stated, which can be due to an induced magnetic source, or the application of certain mathematical techniques.

The electric current density consists of the movement of charged particles. When we consider the equations in matter, we will split the current density in different terms, corresponding to polarization and conduction. Furthermore we will have an external part, which acts as source of the initial fields. This is the part we control as part of a physical experiment.

From these two equations we can derive two compatibility equations. We assume electric charge is (locally) conserved, which can be formulated as the continuity equation

$$\frac{\partial \rho_{\mathrm{e}}}{\partial t} = -\operatorname{div} \mathbf{J}, \tag{2.3}$$

where $\rho_{\mathrm{e}} = \rho_{\mathrm{e}}(\mathbf{x}, t)$ is the (total) electric charge density. We use the subscript e to distinguish it from the mass density of the medium, which we will use in the Navier-Stokes equations. Taking the divergence of (2.1) and (2.2), and noting that the divergence of a curl is always zero, we end up with the equations

$$\begin{aligned} \varepsilon_0 \operatorname{div} \frac{\partial \mathbf{E}}{\partial t} &= -\operatorname{div} \mathbf{J}, & (2.4)\\ \operatorname{div} \frac{\partial \mathbf{B}}{\partial t} &= 0. & (2.5) \end{aligned}$$

Using (2.4) we can write

$$\varepsilon_0 \operatorname{div} \mathbf{E} = \varepsilon_0 \int_{-\infty}^{t} \frac{\mathrm{d}}{\mathrm{d}t} \operatorname{div} \mathbf{E} \, \mathrm{d}t = \int_{-\infty}^{t} \varepsilon_0 \operatorname{div} \left(\frac{\partial \mathbf{E}}{\partial t} \right) \mathrm{d}t = -\int_{-\infty}^{t} \operatorname{div} \mathbf{J} \, \mathrm{d}t = \int_{-\infty}^{t} \frac{\partial \rho_{\mathrm{e}}}{\partial t} \, \mathrm{d}t = \rho_{\mathrm{e}},$$

where we assume we can interchange the order of integration and differentiation and that there exists a t_0 such that $\mathbf{E} = 0$ and $\rho_{\mathrm{e}} = 0$ for $t \leq t_0$, or so to say, the external source is switched on at some point in time. Using the same assumptions on the second equation leads to the compatibility equations

$$\begin{aligned} \operatorname{div} \mathbf{E} &= \frac{\rho_{\mathrm{e}}}{\varepsilon_0}, & (2.6)\\ \operatorname{div} \mathbf{B} &= 0. & (2.7) \end{aligned}$$

Note that the first equation is well-known as Gauss's law or Gauss's flux theorem. To make the Maxwell equations more symmetric, we change to the magnetic field

$$\mathbf{H} = \frac{1}{\mu_0} \mathbf{B}.$$

Since we assume our medium of interest does not react magnetically, we can use the $\mathbf{H}$ with a constant coefficient. In the literature there is some debate which term belongs to which quantity. When there is a magnetic reaction of the medium to distinguish the different quantities. In this work we will work mostly with $\mathbf{H}$, and will refer to this quantity as the magnetic field. When a different quantity is implied, this will be explicitly mentioned.

Substitution in (2.1), (2.2) and (2.7) results in field equations

$$\begin{aligned} -\nabla \times \mathbf{H} + \varepsilon_0 \frac{\partial \mathbf{E}}{\partial t} &= -\mathbf{J}, & (2.8)\\ \nabla \times \mathbf{E} + \mu_0 \frac{\partial \mathbf{H}}{\partial t} &= 0, & (2.9) \end{aligned}$$

and the compatibility equations

$$\begin{aligned} \operatorname{div} \mathbf{E} &= \frac{\rho_{\mathrm{e}}}{\varepsilon_0}, && (2.10) \\ \operatorname{div} \mathbf{H} &= 0. && (2.11) \end{aligned}$$

2.1.1 Subscript notation

Sometimes it is cumbersome to work with the equations in vector notation. Especially when a lot of derivatives appear in the formulas, the notation gets quickly complex and sometimes ambiguous. For this reason, we will sometimes switch to subscript notation. This is specially suited for longer derivations, such as conservation laws. The subscript notation and vector notation are (obviously) equivalent. In subscript notations, the different components of a vector quantity are denoted with the subscripts 1, 2 and 3, or a letter, when a random component is referred. The partial derivative is replaces by the symbol ∂ with as subscript the special component to which the derivative is taken, or t for derivation with respect to time.

The wave equations in subscript notation are given by

$$\begin{aligned} -\epsilon_{ijk}\partial_j H_k + \varepsilon_0 \partial_t E_i &= -J_i, && (2.12) \\ \epsilon_{ijk}\partial_j E_k + \mu_0 \partial_t H_i &= 0, && (2.13) \end{aligned}$$

where ϵ_{ijk} is the Levi-Civita symbol. The compatibility relations are given by

$$\begin{aligned} \partial_i E_i &= \frac{\rho_{\mathrm{e}}}{\varepsilon_0}, && (2.14) \\ \partial_i H_i &= 0. && (2.15) \end{aligned}$$

We use the Einstein summation convention, which means we sum over repeated indices in one term.

2.1.2 Conservation of energy

By manipulating the Maxwell equations we can derive a conservation of energy statement for the electromagnetic fields. It turns out we can define a certain volumetric energy density and an energy flux density.

If we multiply (2.12) with E_i and (2.13) with H_i and add the results, we get as left-hand side

$$\begin{aligned} & E_i\left(-\epsilon_{ijk}\partial_j H_k + \varepsilon_0 \partial_t E_i\right) + H_i\left(\epsilon_{ijk}\partial_j E_k + \mu_0 \partial_t H_i\right) \\ &= \varepsilon_0 E_i \partial_t E_i + \mu_0 H_i \partial_t H_i - \epsilon_{ijk} E_i \partial_j H_k + \epsilon_{ijk} H_i \partial_j E_k \\ &= \partial_t \left[\frac{1}{2}\left(\varepsilon_0 E_i E_i + \mu_0 H_i H_i\right)\right] - \epsilon_{ijk} E_i \partial_j H_k + \epsilon_{ijk} H_i \partial_j E_k \\ &= \partial_t \left[\frac{1}{2}\left(\varepsilon_0 E_i E_i + \mu_0 H_i H_i\right)\right] + \epsilon_{ijk} E_j \partial_i H_k + \epsilon_{ijk} H_k \partial_i E_j \\ &= \partial_t \left[\frac{1}{2}\left(\varepsilon_0 E_i E_i + \mu_0 H_i H_i\right)\right] + \partial_i(\epsilon_{ijk} E_j H_k), \end{aligned}$$

where we have used $\epsilon_{ijk} = -\epsilon_{jik}$, and relabelled the dummy indices. As right-hand side we get

$$-E_i J_i.$$

We define the electromagnetic energy density as

$$u_{\text{em}} = \frac{1}{2}\left(\varepsilon_0 E_i E_i + \mu_0 H_i H_i\right), \tag{2.16}$$

and the Poynting vector as

$$S_i = \epsilon_{ijk} E_j H_k. \tag{2.17}$$

Then we can write the conservation of energy equation as

$$\partial_t u_{\text{em}} = -\partial_i S_i - E_i J_i, \tag{2.18}$$

or in vector notation

$$\frac{\partial u_{\text{em}}}{\partial t} = -\operatorname{div}\mathbf{S} - \mathbf{E}\cdot\mathbf{J}. \tag{2.19}$$

This is the conservation of electromagnetic energy in vacuum. We see that when electric currents are present and have a component in the same direction as the electric field, the electromagnetic energy will decrease, since the current is induced by the field present. This mechanism happens when matter is present. The other way around, if the electric field and the electric current have a component in the opposite direction, the energy increases and we have a source of electromagnetic energy. This is the idea behind the external source that will be introduced later on.

2.1.3 Conservation of (linear) momentum

It is well known that a charged particle in an electromagnetic field experiences a force, the Lorentz force. This force is given by

$$\mathbf{F} = q\mathbf{E} + \mathbf{v}\times\mathbf{B}, \tag{2.20}$$

where q is the electric charge of the particle and $\mathbf{v}$ is its velocity.

When we consider a continuous charge density and current density, we can express the Lorentz force as a force density, given by

$$\mathbf{f} = \rho_{\text{e}}\mathbf{E} + \mathbf{J}\times\mathbf{B}. \tag{2.21}$$

Switching to subscript notation and using the $\mathbf{H}$ field, the force density is given by

$$f_i = \rho_{\text{e}} E_i + \mu_0 \epsilon_{ijk} J_j H_k. \tag{2.22}$$

We can to rewrite this force density as function of the fields only by substituting (2.14) to eliminate ρ_{e}, and (2.12) to eliminate J_j. This results in

$$\begin{aligned} f_i &= \varepsilon_0(\partial_j E_j)E_i + \mu_0\epsilon_{ijk}\left(\epsilon_{jlm}\partial_l H_m - \varepsilon_0\partial_t E_j\right)H_k, \\ &= \varepsilon_0 E_i\partial_j E_j + \mu_0\epsilon_{ijk}\epsilon_{jlm}H_k\partial_l H_m - \varepsilon_0\mu_0\epsilon_{ijk}B_k\partial_t E_j, \\ &= \varepsilon_0 E_i\partial_j E_j + \mu_0\epsilon_{jki}\epsilon_{jlm}H_k\partial_l H_m - \varepsilon_0\mu_0\partial_t(\epsilon_{ijk}E_j H_k) + \varepsilon_0\mu_0\epsilon_{ijk}E_j\partial_t H_k. \end{aligned} \tag{2.23}$$

If we use the identity

$$\epsilon_{jki}\epsilon_{jlm} = \delta_{kl}\delta_{im} - \delta_{km}\delta_{il},$$

we can write

$$\begin{aligned}
\epsilon_{jki}\epsilon_{jlm}H_k\partial_l H_m &= \partial_l(\epsilon_{jki}\epsilon_{jlm}H_kH_m) - H_m\partial_l(\epsilon_{jki}\epsilon_{jlm}H_k),\\
&= \partial_l((\delta_{kl}\delta_{im} - \delta_{km}\delta_{il})H_kH_m) - H_m\partial_l((\delta_{kl}\delta_{im} - \delta_{km}\delta_{il})H_k),\\
&= \partial_l(\delta_{kl}\delta_{im}H_kH_m) - \partial_l(\delta_{km}\delta_{il}H_kH_m) - H_m\partial_l(\delta_{kl}\delta_{im}H_k) - H_m\partial_l(\delta_{km}\delta_{il}H_k),\\
&= \partial_k(H_kH_i) - \partial_i(H_kH_k) - H_i\partial_kH_k + H_k\partial_iH_k,\\
&= H_k\partial_kH_i + H_i\partial_kH_k - \partial_i(H_kH_k) - H_i\partial_kH_k + \frac{1}{2}\partial_i(H_kH_k),\\
&= H_k\partial_kH_i - \frac{1}{2}\partial_i(H_kH_k).
\end{aligned}$$

Substituting in (2.23) and using (2.17) results in

$$f_i = \varepsilon_0E_i\partial_jE_j + \mu_0H_k\partial_kH_i - \frac{1}{2}\mu_0\partial_i(H_kH_k) - \mu_0\varepsilon_0\partial_tS_i + \mu_0\varepsilon_0\epsilon_{ijk}E_j\partial_tH_k.$$

The last term on the right-hand side can be rewritten using (2.13). This results in

$$\begin{aligned}
\varepsilon_0\mu_0\epsilon_{ijk}E_j\partial_tH_k &= \varepsilon_0\epsilon_{ijk}E_j(-\epsilon_{klm}\partial_lE_m),\\
&= \varepsilon_0\epsilon_{kji}\epsilon_{klm}E_j\partial_lE_m,\\
&= \varepsilon_0E_j\partial_jE_i - \frac{1}{2}\varepsilon_0\partial_i(E_jE_j),
\end{aligned}$$

where we have used the identity we have just derived in terms of H_i. Substituting this expression, adding a term

$$\mu_0H_i\partial_jH_j = 0,$$

and rearranging and relabelling the terms results in the expression

$$f_i = \varepsilon_0\left(E_i\partial_jE_j + E_j\partial_jE_i\right) + \mu_0\left(H_i\partial_jH_j + H_j\partial_jH_i\right) - \frac{1}{2}\partial_i\left(\varepsilon_0E_jE_j + \mu_0H_jH_j\right) - \mu_0\varepsilon_0\partial_tS_i. \quad (2.24)$$

We want to write this force density as divergence of some stress tensor. This can be accomplished by defining the symmetric Maxwell stress tensor T, with components

$$T_{ij} = \varepsilon_0\left(E_iE_j - \frac{1}{2}\delta_{ij}E_kE_k\right) + \mu_0\left(H_iH_j - \frac{1}{2}\delta_{ij}H_kH_k\right), \quad (2.25)$$

with respect to the standard basis. We see that for the divergence of the stress tensor we have

$$\begin{aligned}
\partial_j T_{ij} &= \partial_j \left(\varepsilon_0 \left(E_i E_j - \frac{1}{2}\delta_{ij} E_k E_k \right) + \mu_0 \left(H_i H_j - \frac{1}{2}\delta_{ij} H_k H_k \right) \right), \\
&= \varepsilon_0 \left(E_i \partial_j E_j + E_j \partial_j E_i - \frac{1}{2}\delta_{ij} \partial_j E_k E_k \right) + \mu_0 \left(H_i \partial_j H_j + H_j \partial_i H_i - \frac{1}{2}\delta_{ij} \partial_j H_k H_k \right), \\
&= \varepsilon_0 \left(E_i \partial_j E_j + E_j \partial_j E_i - \frac{1}{2}\partial_i E_j E_j \right) + \mu_0 \left(H_i \partial_j H_j + H_j \partial_i H_i - \frac{1}{2}\partial_i H_j H_j \right).
\end{aligned}$$

Comparison with (2.24) results in

$$f_i = \partial_j T_{ij} - \mu_0 \varepsilon_0 \partial_t S_i, \tag{2.26}$$

the conservation of electromagnetic momentum. Note f_i can be interpreted as the time derivative of the momentum density. Then $\partial_j T_{ij}$ is the momentum density flux in the different directions, and $\mu_0 \varepsilon_0 S_i$ the momentum density.

In vector notation we would write the Maxwell stress tensor as

$$\overleftrightarrow{\mathbf{T}} = \varepsilon_0 \mathbf{E} \otimes \mathbf{E} + \mu_0 \mathbf{H} \otimes \mathbf{H} - \frac{1}{2} \left(\varepsilon_0 \|\mathbf{E}\|^2 + \mu_0 \|\mathbf{H}\|^2 \right) \overleftrightarrow{\mathbf{I}},$$

with $\overleftrightarrow{\mathbf{I}}$ the identity tensor. Then the conservation of momentum can be expressed as

$$\mathbf{f} = \text{ div } \overleftrightarrow{\mathbf{T}} - \mu_0 \varepsilon_0 \frac{\partial \mathbf{S}}{\partial t}. \tag{2.27}$$

We will see that inside matter we can derive a similar conservation equation.

2.2 Maxwell equations in matter

When we consider electromagnetic fields in matter, it is convenient to work with a different set of equations. Matter reacts in a certain way to electromagnetic fields. The reaction is a combination of polarization, magnetization and conduction. As mentioned earlier we assume that the magnetization is negligible, but in the derivation of the equations we will include this possibility. Furthermore we are not interested in the microscopic properties of these reactions, but will consider them from a macroscopic point of view, considering the medium as a continuum with smoothly varying properties.

2.2.1 Polarization and magnetization

For the analysis of the effect of polarization and magnetization we follow [7] and define two new quantities, the volumetric polarization density $\mathbf{P}$ and the volumetric magnetization density $\mathbf{M}$.

A polarization density gives rise to a bounded volume charge and a bounded surface charge. The bounded volume charge density is given by

$$\rho_{\mathrm{b}} = -\operatorname{div}\mathbf{P}, \tag{2.28}$$

and the bounded surface charge density is given by

$$\sigma_{\mathrm{b}} = \mathbf{P}\cdot\hat{\mathbf{n}}, \tag{2.29}$$

where $\hat{\mathbf{n}}$ is the outward pointing normal unit vector. The surface is the boundary of the medium in which polarization takes place. Furthermore, changing polarization gives rise to a polarization current, because of the bound charge moving around. The corresponding polarization current density is given by

$$\mathbf{J}_{\mathrm{p}} = \frac{\partial\mathbf{P}}{\partial t}. \tag{2.30}$$

A magnetization density gives rise to a bounded volume current and a bounded surface current. The bounded volume current density is given by

$$\mathbf{J}_{\mathrm{b}} = \nabla\times\mathbf{M}, \tag{2.31}$$

and the bounded surface current density is given by

$$\mathbf{K}_{\mathrm{b}} = \mathbf{M}\times\hat{\mathbf{n}}, \tag{2.32}$$

where again $\hat{\mathbf{n}}$ is the outward pointing normal unit vector. The surface is the boundary of the medium in which magnetization takes place.

Together with the polarization density and magnetization density, we can define two new fields, the electric displacement field

$$\mathbf{D} = \varepsilon_0\mathbf{E} + \mathbf{P}, \tag{2.33}$$

and the auxiliary magnetic field

$$\mathbf{H} = \frac{1}{\mu_0}\mathbf{B} - \mathbf{M}. \tag{2.34}$$

In order to determine the electromagnetic field we have to know how the matter will react on applied fields, that is we need to know the constitutive relations.

Using the Maxwell equations for vacuum, we will derive a new set of equivalent equations, in terms of the fields $\mathbf{D}$ and $\mathbf{H}$. The (total) current density can now be split in three parts, the current densities induced by the polarization and magnetization respectively and the free current density. That is we have

$$\begin{aligned} \mathbf{J} &= \mathbf{J}^{\mathrm{p}} + \mathbf{J}^{\mathrm{m}} + \mathbf{J}^{\mathrm{f}} \\ &= \frac{\partial \mathbf{P}}{\partial t} + \nabla \times \mathbf{M} + \mathbf{J}^{\mathrm{f}}. \end{aligned} \tag{2.35}$$

Likewise the charge density can be written as the sum of the charge density caused by the polarization and a free charge density. We have

$$\begin{aligned} \rho_{\mathrm{e}} &= \rho_{\mathrm{p}} + \rho_{\mathrm{f}} \\ &= -\operatorname{div} \mathbf{P} + \rho_{\mathrm{f}}. \end{aligned} \tag{2.36}$$

Substituting (2.33), (2.34) and (2.35) into (2.1) and rearranging terms results in the so-called Maxwell equations in matter,

$$-\nabla \times \mathbf{H} + \frac{\partial \mathbf{D}}{\partial t} = -\mathbf{J}^{\mathrm{f}}, \tag{2.37}$$

$$\nabla \times \mathbf{E} + \frac{\partial \mathbf{B}}{\partial t} = 0. \tag{2.38}$$

Substituting (2.36) and (2.34) in (2.10) results in the compatibility equations

$$\operatorname{div} \mathbf{D} = \rho_{\mathrm{f}}, \tag{2.39}$$

$$\operatorname{div} \mathbf{B} = 0. \tag{2.40}$$

To be able to solve this system of equations we need so-called constitutive relations for the displacement field, the auxiliary field and the free current density. These will be discussed in the next section.

2.2.2 Constitutive relations for fluids

The simplest way to model how matter reacts to applied electromagnetic fields, assumes linear polarization and magnetization. We assume the fields consist of a single frequency, so that there is no dispersion. In general the parameters for polarization and magnetization depend on the frequency of the field. For linear materials we have

$$\mathbf{P} = \varepsilon_0 \chi_{\mathrm{e}} \mathbf{E} \tag{2.41}$$

$$\mathbf{M} = \chi_{\mathrm{m}} \mathbf{H}. \tag{2.42}$$

The constants χ_{e} and χ_{m} which are called the electric susceptibility and magnetic susceptibility respectively. Substituting these relations in (2.33) and (2.34) in (2.10) results in the constitutive relations

$$\mathbf{D} = \varepsilon\mathbf{E} \tag{2.43}$$
$$\mathbf{B} = \mu\mathbf{H}, \tag{2.44}$$

where $\varepsilon = \varepsilon_0 (1 + \chi_{\mathrm{e}})$ is the electric permittivity and $\mu = \mu_0 (1 + \chi_{\mathrm{m}})$ the magnetic permeability. For conducting media we assume Ohm's law applies, which says that

$$\mathbf{J}^{\mathrm{f}} = \sigma\mathbf{E}, \tag{2.45}$$

where the constant σ is called the electric conductivity. In general this constant also depends on the frequency. We will see that the conduction and polarization can be modelled by one complex parameter when we consider the fields in the frequency domain.

It is interesting to note that these constitutive relations are only valid in reference frames where the medium is in rest. For non-fluid media this will usually be no problem, but when considering fluids, different material parts in general have different velocities. We will need to find the expressions for the constitutive relations in the stationary lab frame. That is we need to transform the constitutive relations from the instantaneous rest frame, to the lab frame. Following [12] we will use the four-vector framework of special relativity to determine these transformations. The notation and different tensors are defined in Appendix A.

To determine the correct constitutive relations, we will determine tensor equations, which in the instantaneous rest frame of a certain fluid particle reduce to the ordinary constitutive relation for linear media. Since by definition all the tensors obey the transformation rules, these equations will be correct in all (inertial) reference frames, in particular in the lab frame.

From (A.2) we notice that when the regular velocity is zero, the velocity four-vector is equal to

$$V^{\mu} = \begin{pmatrix} c & 0 & 0 & 0 \end{pmatrix},$$

suggesting that the correct form for the polarization is

$$D^{\mu\nu} V_{\nu} = c^2 \varepsilon F^{\mu\nu} V_{\nu}.$$

In vector notation this is equal to

$$\begin{pmatrix} 0 & c\mathbf{D} \\ -c\mathbf{D} & \cdot \times \mathbf{H} \end{pmatrix} \begin{pmatrix} -\gamma c \\ \gamma \mathbf{v} \end{pmatrix} = c^2 \varepsilon \begin{pmatrix} 0 & \frac{1}{c}\mathbf{E} \\ -\frac{1}{c}\mathbf{E} & \cdot \times \mathbf{B} \end{pmatrix} \begin{pmatrix} -\gamma c \\ \gamma \mathbf{v} \end{pmatrix}.$$

Writing out the two equations results in

$$\gamma c \mathbf{D} \cdot \mathbf{v} = c^2 \varepsilon \frac{1}{c} \gamma \mathbf{E} \cdot \mathbf{v}, \tag{2.46}$$
$$\gamma c^2 \mathbf{D} + \gamma \mathbf{v} \times \mathbf{H} = c^2 \varepsilon \gamma \mathbf{E} + c^2 \varepsilon \gamma \mathbf{v} \times \mathbf{B}. \tag{2.47}$$

Clearly this reduces to linear polarization if we substitute $\mathbf{v} = 0$. Likewise for the magnetization we have a similar expression in terms of the dual field tensors,

$$\mu H^{\nu\mu} V_\nu = G^{\nu\mu} V_\nu,$$

In vector notation this is equal to

$$\mu \begin{pmatrix} 0 & \mathbf{H} \\ -\mathbf{H} & -c(\cdot \times \mathbf{D}) \end{pmatrix} \begin{pmatrix} -\gamma c \\ \gamma \mathbf{v} \end{pmatrix} = \begin{pmatrix} 0 & \mathbf{B} \\ -\mathbf{B} & -\frac{1}{c}(\cdot \times \mathbf{E}) \end{pmatrix} \begin{pmatrix} -\gamma c \\ \gamma \mathbf{v} \end{pmatrix}.$$

Writing out the equations results in

$$\begin{aligned} \gamma\mu \mathbf{H} \cdot \mathbf{v} &= \gamma \mathbf{B} \cdot \mathbf{v}, && (2.48) \\ \gamma\mu c \mathbf{H} - \gamma\mu c \mathbf{v} \times \mathbf{D} &= \gamma c \mathbf{B} - \gamma \frac{1}{c} \mathbf{v} \times \mathbf{E}. && (2.49) \end{aligned}$$

Again we see that the equations reduce to the expected equations when $\mathbf{v} = 0$ is substituted. Rewriting (2.47) and (2.49) results in the constitutive relations

$$\begin{aligned} \mathbf{D} &= \varepsilon \mathbf{E} + \varepsilon \mathbf{v} \times \mathbf{B} - \frac{1}{c^2} \mathbf{v} \times \mathbf{H}, && (2.50) \\ \mathbf{B} &= \mu \mathbf{H} - \mu \mathbf{v} \times \mathbf{D} + \frac{1}{c^2} \mathbf{v} \times \mathbf{E}. && (2.51) \end{aligned}$$

Rewriting (2.47) and (2.49) results in the corresponding compatibility relations

$$\begin{aligned} \mathbf{D} \cdot \mathbf{v} &= \varepsilon \mathbf{E} \cdot \mathbf{v}, && (2.52) \\ \mathbf{B} \cdot \mathbf{v} &= \mu \mathbf{H} \cdot \mathbf{v}. && (2.53) \end{aligned}$$

We see that (2.50) and (2.51) are coupled. They both depend on three fields. If we assume the fluid velocity is not too large, we can simplify the expressions by neglecting higher order terms. At this point we will only consider the first correction term and neglect all terms much smaller than $\mu_0\varepsilon_0 = \frac{1}{c^2}$. Substituting (2.50) and (2.51) into each other results in

$$\begin{aligned} \mathbf{D} &= \varepsilon \mathbf{E} + \varepsilon \mathbf{v} \times \left(\mu \mathbf{H} - \mu \mathbf{v} \times \mathbf{D} + \frac{1}{c^2} \mathbf{v} \times \mathbf{E} \right) - \frac{1}{c^2} \mathbf{v} \times \mathbf{H} \\ &= \varepsilon \mathbf{E} + (\mu\varepsilon - \mu_0\varepsilon_0)\, \mathbf{v} \times \mathbf{H} - \mu\varepsilon \mathbf{v} \times (\mathbf{v} \times \mathbf{D}) + \varepsilon\mu_0\varepsilon_0 \mathbf{v} \times (\mathbf{v} \times \mathbf{E}), \\ &\approx \varepsilon \mathbf{E} + (\mu\varepsilon - \mu_0\varepsilon_0)\, \mathbf{v} \times \mathbf{H} - \mu\varepsilon \mathbf{v} \times (\mathbf{v} \times \mathbf{D}), \\ &= \varepsilon \mathbf{E} + (\mu\varepsilon - \mu_0\varepsilon_0)\, \mathbf{v} \times \mathbf{H} - \mu\varepsilon \mathbf{v} \times \left(\mathbf{v} \times \left(\varepsilon \mathbf{E} + \varepsilon \mathbf{v} \times \mathbf{B} - \frac{1}{c^2} \mathbf{v} \times \mathbf{H} \right) \right), \\ &\approx \varepsilon \mathbf{E} + (\mu\varepsilon - \mu_0\varepsilon_0)\, \mathbf{v} \times \mathbf{H}. \end{aligned}$$

Likewise we get the same result for $\mathbf{B}$,

$$\mathbf{B} \approx \mu \mathbf{H} - (\mu\varepsilon - \mu_0\varepsilon_0) \mathbf{v} \times \mathbf{E}.$$

Finally we need the free current density. In non-conducting media this will of course be zero. When we have positive electric conductivity, we again construct a tensor equation that reduces to the correct equation for $\mathbf{v} = 0$. It is clear that the correct expression is given by

$$\sigma F^{\mu\nu} V_\nu = (J_{\mathrm{f}})^\mu.$$

In vector notation this is equal to

$$\sigma \begin{pmatrix} 0 & \frac{1}{c}\mathbf{E} \\ -\frac{1}{c}\mathbf{E} & \cdot \times \mathbf{B} \end{pmatrix} \begin{pmatrix} -\gamma c \\ \gamma \mathbf{v} \end{pmatrix} = \begin{pmatrix} c\rho_{\mathrm{f}} \\ \mathbf{J}^{\mathrm{f}} \end{pmatrix}$$

Working out these equations results in

$$\begin{aligned} \gamma \frac{1}{c} \sigma \mathbf{E} \cdot \mathbf{v} &= c\rho_{\mathrm{f}}, \\ \gamma\sigma\mathbf{E} + \gamma\sigma\mathbf{v} \times \mathbf{B} &= \mathbf{J}^{\mathrm{f}}. \end{aligned}$$

Rewriting results in the in the equations

$$\begin{aligned} \rho_{\mathrm{f}} &= \gamma \frac{1}{c^2} \sigma \mathbf{E} \cdot \mathbf{v}, \\ \mathbf{J}^{\mathrm{f}} &= \gamma\sigma\mathbf{E} + \gamma\sigma\mathbf{v} \times \mathbf{B}. \end{aligned}$$

We see that for $\mathbf{v} = 0$ this reduces to $\mathbf{J}^{\mathrm{f}} = \sigma\mathbf{E}$ and $\rho_{\mathrm{f}} = 0$. For low velocities we have $\gamma \approx 1$, and $\frac{\|\mathbf{v}\|}{c^2} \approx 0$, so we can write

$$\begin{aligned} \rho_{\mathrm{f}} &\approx 0, \\ \mathbf{J}^{\mathrm{f}} &\approx \sigma \left(\mathbf{E} + \mathbf{v} \times \mathbf{B} \right). \end{aligned}$$

Finally we want to know the induced current in terms of the $\mathbf{H}$ field instead of the $\mathbf{B}$ field. If we substitute for $\mathbf{B}$ and only keep the largest term we get as result

$$\mathbf{J}^{\mathrm{f}} = \sigma \left(\mathbf{E} + \mu\mathbf{v} \times \mathbf{H} \right).$$

So to conclude we have the constitutive relations

$$\begin{aligned} \mathbf{D} &= \varepsilon\mathbf{E} + (\mu\varepsilon - \mu_0\varepsilon_0)\, \mathbf{v} \times \mathbf{H}, && (2.54) \\ \mathbf{B} &= \mu\mathbf{H} - (\mu\varepsilon - \mu_0\varepsilon_0)\mathbf{v} \times \mathbf{E}, && (2.55) \\ \mathbf{J}^{\mathrm{f}} &= \sigma \left(\mathbf{E} + \mu\mathbf{v} \times \mathbf{H} \right), && (2.56) \\ \rho_{\mathrm{f}} &= 0. && (2.57) \end{aligned}$$

where we have only kept the lowest order term involving the fluids velocity. In general we see that the velocity field has an effect on the electromagnetic field. This interaction is responsible for energy and momentum exchange between the electromagnetic field and the fluids particles, in particular the electromagnetic energy is changed in kinetic energy because the Lorentz force will do work on the fluid particles.

2.2.3 Modified Maxwell equations in fluids

We will now substitute all the constitutive relations in the field equations to derive the final equations governing the electromagnetic field inside a (possibly) moving fluid. If we substitute the relations (2.54) and (2.56) into equation (2.37) we get

$$-\nabla \times \mathbf{H} + \frac{\partial}{\partial t}\left[\varepsilon \mathbf{E} + (\mu\varepsilon - \mu_0\varepsilon_0)\,\mathbf{v} \times \mathbf{H}\right] = -\sigma\left(\mathbf{E} + \mu \mathbf{v} \times \mathbf{H}\right).$$

We assume that the velocity field is constant in time, so that the time derivative of the velocity disappears. Rewriting then results in

$$-\nabla \times \mathbf{H} + \varepsilon_0 \frac{\partial \mathbf{E}}{\partial t} = -(\varepsilon - \varepsilon_0)\frac{\partial \mathbf{E}}{\partial t} - (\mu\varepsilon - \mu_0\varepsilon_0)\left(\mathbf{v} \times \frac{\partial \mathbf{H}}{\partial t}\right) - \sigma\left(\mathbf{E} + \mu \mathbf{v} \times \mathbf{H}\right).$$

Likewise, if we substitute (2.55) in (2.38) we get

$$\nabla \times \mathbf{E} + \frac{\partial}{\partial t}\left(\mu \mathbf{H} - (\mu\varepsilon - \mu_0\varepsilon_0)\mathbf{v} \times \mathbf{E}\right) = 0,$$

which results in

$$\nabla \times \mathbf{E} + \mu_0 \frac{\partial \mathbf{H}}{\partial t} = -\left(\mu - \mu_0\right)\frac{\partial \mathbf{H}}{\partial t} + (\mu\varepsilon - \mu_0\varepsilon_0)\left(\mathbf{v} \times \frac{\partial \mathbf{E}}{\partial t}\right).$$

We now define the induced electric and magnetic current densities. They are minus the right-hand sides of the modified Maxwell equations we have just derived. So we have

$$-\mathbf{J}^{\mathrm{ind}} = -(\varepsilon - \varepsilon_0)\frac{\partial \mathbf{E}}{\partial t} - (\mu\varepsilon - \mu_0\varepsilon_0)\left(\mathbf{v} \times \frac{\partial \mathbf{H}}{\partial t}\right) - \sigma\left(\mathbf{E} + \mu \mathbf{v} \times \mathbf{H}\right), \tag{2.58}$$

$$-\mathbf{K}^{\mathrm{ind}} = -\left(\mu - \mu_0\right)\frac{\partial \mathbf{H}}{\partial t} + (\mu\varepsilon - \mu_0\varepsilon_0)\left(\mathbf{v} \times \frac{\partial \mathbf{E}}{\partial t}\right). \tag{2.59}$$

We see that if the fluid is moving this creates an induced current. These terms, depending on $\mathbf{v}$, create a coupling between the velocity field governed by the Navier-Stokes equations and the Maxwell equations, and this system of coupled equations is highly non-linear and hard to solve.

In addition to the induced currents there will be external currents. These are controlled currents, independent of the fields. It are these currents that deliver the field's energy and momentum in the first place. The final Maxwell equations governing the fields are given by

$$-\nabla \times \mathbf{H} + \varepsilon_0 \frac{\partial \mathbf{E}}{\partial t} = -\mathbf{J}^{\mathrm{ind}} - \mathbf{J}^{\mathrm{ext}}, \tag{2.60}$$

$$\nabla \times \mathbf{E} + \mu_0 \frac{\partial \mathbf{H}}{\partial t} = -\mathbf{K}^{\mathrm{ind}} - \mathbf{K}^{\mathrm{ext}}. \tag{2.61}$$

We will also derive the corresponding compatibility relations. Taking the divergence of (2.60), results in (2.4) so we get the corresponding compatibility equation

$$\operatorname{div} \mathbf{E} = \frac{\rho_{\mathrm{e}}}{\varepsilon_0}.$$

Although magnetic monopoles do not exist, we have seen that in matter magnetic currents can be induced, and we need (induced) magnetic charge to keep the framework complete. Stipulating local conservation of magnetic charge, we define

$$\rho_{\mathrm{m}} = -\operatorname{div}\mathbf{K}, \tag{2.62}$$

which is a continuity equation like (2.3). Now taking the divergence of (2.61) results in

$$\mu_0 \operatorname{div}\frac{\partial \mathbf{H}}{\partial t} = -\operatorname{div}\mathbf{K}. \tag{2.63}$$

Following the exact same derivation for the first equation and assuming, by causality, that $\mathbf{K} = 0$ for $t \leq t_0$ for certain t_0, we arrive at the compatibility relation

$$\operatorname{div}\mathbf{H} = \frac{\rho_{\mathrm{m}}}{\mu_0}. \tag{2.64}$$

We will see in Chapter 6 that the velocities will be so small that the induced currents depending on the velocity can be neglected for our purposes.

2.2.4 Boundary conditions

In order to determine the electromagnetic field in a certain region of space, we need appropriate boundary conditions.

We have boundaries where the material properties are not continuous or there are surface currents. We assume the boundaries are fixed in space and time.

The derivation of the boundary conditions can be found for example in [7]. They follow directly from the Maxwell equations. Here we will only state the results.

At a boundary we can write the electric and magnetic field as the sum of a orthogonal and tangential component,

$$\begin{aligned}\mathbf{E} &= \mathbf{E}_{\mathrm{ort}} + \mathbf{E}_{\mathrm{tan}},\\ \mathbf{H} &= \mathbf{H}_{\mathrm{ort}} + \mathbf{H}_{\mathrm{tan}}.\end{aligned}$$

Furthermore at a boundary we have two separate regions A and B, each on one side of the boundary. We denote by $\hat{\mathbf{n}}$ the unit normal vector pointing from region B to A. On the boundary itself we have possibly electric and magnetic charge densities σ_{e} and σ_{m}, and current densities $\mathbf{J}_{\mathrm{surf}}$ and $\mathbf{K}_{\mathrm{surf}}$. The four boundary conditions for the field components are then given by

$$\mathbf{E}_{A,\mathrm{tan}} - \mathbf{E}_{B,\mathrm{tan}} = \mathbf{K}_{\mathrm{surf}} \times \hat{\mathbf{n}}, \tag{2.65}$$

$$\mathbf{E}_{A,\mathrm{ort}} - \mathbf{E}_{B,\mathrm{ort}} = \frac{\sigma_{\mathrm{e}}}{\varepsilon_0}, \tag{2.66}$$

$$\mathbf{H}_{A,\mathrm{tan}} - \mathbf{H}_{B,\mathrm{tan}} = \mathbf{J}_{\mathrm{surf}} \times \hat{\mathbf{n}}, \tag{2.67}$$

$$\mathbf{H}_{A,\mathrm{ort}} - \mathbf{H}_{B,\mathrm{ort}} = \frac{\sigma_{\mathrm{m}}}{\mu_0}. \tag{2.68}$$

These four boundary conditions together with the Maxwell equations and the charge and current densities completely determine the fields.

Of course in cases with certain symmetries we can consider different boundary conditions, so that we can reduce the geometry.

2.3 Energy and momentum inside a fluid

We have derived the field equations inside a (possibly moving) fluid. We will now derive equations for the energy and momentum conservation. We proceed as in the vacuum case.

2.3.1 Energy equation

For simplicity we will use subscript notation here. If we multiply (2.60) with E_i and (2.61) with H_i and add the results, we get as left-hand side

$$\begin{aligned}
&E_i\left(-\epsilon_{ijk}\partial_j H_k + \varepsilon_0\partial_t E_i\right) + H_i\left(\epsilon_{ijk}\partial_j E_k + \mu_0\partial_t H_i\right)\\
&= \varepsilon_0 E_i\partial_t E_i + \mu_0 H_i\partial_t H_i - \epsilon_{ijk}E_i\partial_j H_k + \epsilon_{ijk}H_i\partial_j E_k\\
&= \partial_t\left[\frac{1}{2}\left(\varepsilon_0 E_i E_i + \mu_0 H_i H_i\right)\right] - \epsilon_{ijk}E_i\partial_j H_k + \epsilon_{ijk}H_i\partial_j E_k\\
&= \partial_t\left[\frac{1}{2}\left(\varepsilon_0 E_i E_i + \mu_0 H_i H_i\right)\right] + \epsilon_{ijk}E_j\partial_i H_k + \epsilon_{ijk}H_k\partial_i E_j\\
&= \partial_t\left[\frac{1}{2}\left(\varepsilon_0 E_i E_i + \mu_0 H_i H_i\right)\right] + \partial_i(\epsilon_{ijk}E_j H_k),
\end{aligned}$$

where we have used $\epsilon_{ijk} = -\epsilon_{jik}$, and relabelled the dummy indices. As right-hand side we get

$$-E_i J_i - H_i K_i.$$

If we now define the energy density as

$$u_{\mathrm{em}} = \frac{1}{2}\left(\varepsilon_0 E_i E_i + \mu_0 H_i H_i\right), \tag{2.69}$$

and the Poynting vector

$$S_i = \epsilon_{ijk}E_j H_k, \tag{2.70}$$

we can write the equation as

$$\partial_t u_{\mathrm{em}} = -\partial_i S_i - E_i J_i - H_i K_i, \tag{2.71}$$

or in vector notation

$$\frac{\partial u_{\mathrm{em}}}{\partial t} = -\operatorname{div}\mathbf{S} - \mathbf{E}\cdot\mathbf{J} - \mathbf{H}\cdot\mathbf{K}. \tag{2.72}$$

This is the conservation of electromagnetic energy in matter. Although the expression does not explicitly depend on the velocity $\mathbf{v}$, the currents do, so the energy density also depends on the fluid velocity.

2.3.2 Momentum equation

We can also derive the momentum equation, from which the force density follows. Multiplying (2.60) by μ_0 and taking the cross product with $\mathbf{H}$ results in

$$-\mu_0\epsilon_{ijk}\epsilon_{klm}H_j\partial_l H_m + \mu_0\varepsilon_0\epsilon_{ijk}H_j\partial_t E_k = -\mu_0\epsilon_{ijk}H_j J_k.$$

Rewriting using the identity

$$\epsilon_{ijk}\epsilon_{klm}H_j\partial_l H_m = -H_k\partial_k H_i + \frac{1}{2}\partial_i(H_k H_k),$$

results in

$$\mu_0 H_k\partial_k H_i - \frac{1}{2}\mu_0\partial_i(H_k H_k) + \mu_0\varepsilon_0\epsilon_{ijk}H_j\partial_t E_k = \mu_0\epsilon_{ijk}J_j H_k.$$

Using (2.64) we have

$$\begin{aligned}\mu_0 H_k\partial_k H_i &= \mu_0\partial_k(H_k H_i) - \mu_0 H_i\partial_k H_k,\\ &= \mu_0\partial_k(H_k H_i) - \rho_{\mathrm{m}}H_i.\end{aligned}$$

Rearranging terms and relabelling results in the equation

$$\partial_j\left[\mu_0 H_j H_i - \frac{1}{2}\mu_0\delta_{ij}H_k H_k\right] - \mu_0\varepsilon_0\epsilon_{ijk}(\partial_t E_j)H_k = \rho_{\mathrm{m}}H_i + \mu_0\epsilon_{ijk}J_j H_k. \tag{2.73}$$

Likewise multiplying (2.61) by ε_0 and taking the cross product with $\mathbf{E}$ results in

$$\varepsilon_0\epsilon_{ijk}\epsilon_{klm}E_j\partial_l E_m + \mu_0\varepsilon_0\epsilon_{ijk}E_j\partial_t H_k = -\varepsilon_0\epsilon_{ijk}E_j K_k,$$

which we can rewrite to

$$-\varepsilon_0 E_k\partial_k E_i + \frac{1}{2}\varepsilon_0\partial_i(E_k E_k) + \mu_0\varepsilon_0\epsilon_{ijk}E_j\partial_t H_k = \varepsilon_0\epsilon_{ijk}K_j E_k.$$

Using (2.63) we have

$$\begin{aligned}\varepsilon_0 E_k\partial_k E_i &= \varepsilon_0\partial_k(E_k E_i) - \varepsilon_0 E_i\partial_k E_k,\\ &= \varepsilon_0\partial_k(E_k E_i) - \rho_{\mathrm{e}}E_i.\end{aligned}$$

Rearranging terms and relabelling results in the equation

$$-\partial_j\left[\varepsilon_0 E_j E_i - \frac{1}{2}\varepsilon_0\delta_{ij}E_k E_k\right] + \mu_0\varepsilon_0\epsilon_{ijk}E_j\partial_t H_k = -\rho_{\mathrm{e}}E_i + \varepsilon_0\epsilon_{ijk}K_j E_k. \tag{2.74}$$

Defining the stress tensor T_{ij} by

$$T_{ij} = \mu_0(H_j H_i) + \varepsilon_0(E_j E_i) - \frac{1}{2}\mu_0\delta_{ij}(H_k H_k) - \frac{1}{2}\varepsilon_0\delta_{ij}(E_k E_k), \tag{2.75}$$

subtracting (2.74 from (2.73) and using (2.70) we can write

$$f_i = \partial_j T_{ij} - \partial_t S_i, \tag{2.76}$$

where f_i is the force density given by

$$f_i = \rho_\mathrm{e} E_i + \rho_\mathrm{m} H_i + \mu_0 \epsilon_{ijk} J_j H_k - \varepsilon_0 \epsilon_{ijk} K_j E_k. \tag{2.77}$$

Equation (2.76) is the expression of momentum conservation in the medium, and couples the stress tensor to the forces exerted on the fluid particle.

In vector notation this force density is equal to

$$\mathbf{f} = \rho_\mathrm{e}\mathbf{E} + \rho_\mathrm{m}\mathbf{H} + \mu_0 \mathbf{J} \times \mathbf{H} - \varepsilon_0 \mathbf{K} \times \mathbf{E}. \tag{2.78}$$

This force density is exerted by the electromagnetic field on the fluid particles, and will be used as source term in the Navier-Stokes equations.

2.4 Maxwell in the frequency domain

Up until now we have only considered the fields and equations in the time domain. Using Fourier transforms in the time variable we can switch to the frequency domain. This transformation works well with the Maxwell equations because they are linear in the field components. In the frequency domain we can investigate the interesting phenomenon of the electric permittivity being a function of the frequency. As we will see this leads to distortion of a wave and dissipation.

2.4.1 Complex fields

In general the fields will be a superposition of several frequency components, and using Fourier transformations, we can write the (real) fields in the time domain as an integral over a complex field, which is a function of the space coordinates and the frequency variable ω. For an arbitrary field $f(\mathbf{x}, t)$ we can write

$$f(\mathbf{x}, t) = \frac{1}{2} \int_{-\infty}^{+\infty} \hat{f}(\mathbf{x}, \omega) e^{-i\omega t} \, \mathrm{d}\omega.$$

Note that the constant coefficient is just a convention, so that the expression we will use have a simpler form. Since the time-domain fields are real-valued, we have the relation

$$f(\mathbf{x}, t) = \bar{f}(\mathbf{x}, t) = \frac{1}{2} \int_{-\infty}^{+\infty} \bar{\hat{f}}(\mathbf{x}, \omega) e^{i\omega t} \, \mathrm{d}\omega = \frac{1}{2} \int_{-\infty}^{+\infty} \bar{\hat{f}}(\mathbf{x}, -\omega) e^{-i\omega t} \, \mathrm{d}\omega,$$

so we see for the complex field that we have $\hat{f}(\mathbf{x}, \omega) = \bar{\hat{f}}(\mathbf{x}, -\omega)$. Using this relation we can write

$$\begin{aligned} f(\mathbf{x},t) &= \frac{1}{2}\int_{-\infty}^{+\infty} \hat{f}(\mathbf{x},\omega)e^{-i\omega t}\,\mathrm{d}\omega \\ &= \frac{1}{2}\left[\int_{-\infty}^{0} \hat{f}(\mathbf{x},\omega)e^{-i\omega t}\,\mathrm{d}\omega + \int_{0}^{+\infty} \hat{f}(\mathbf{x},\omega)e^{-i\omega t}\,\mathrm{d}\omega\right] \\ &= \frac{1}{2}\left[\overline{\int_{0}^{+\infty} \bar{\hat{f}}(\mathbf{x},-\omega)e^{-i\omega t}\,\mathrm{d}\omega} + \int_{0}^{+\infty} \hat{f}(\mathbf{x},\omega)e^{-i\omega t}\,\mathrm{d}\omega\right] \\ &= \mathrm{Re}\left\{\int_{0}^{+\infty} \hat{f}(\mathbf{x},\omega)e^{-i\omega t}\,\mathrm{d}\omega\right\}, \end{aligned} \tag{2.79}$$

So to determine the time-domain fields we need to take the real part of the complex fields. For our electromagnetic fields we have the expressions

$$E_i(\mathbf{x},t) = \frac{1}{2}\int_{-\infty}^{+\infty} \hat{E}_i(\mathbf{x},\omega)e^{-i\omega t}\,\mathrm{d}\omega, \tag{2.80}$$

$$H_i(\mathbf{x},t) = \frac{1}{2}\int_{-\infty}^{+\infty} \hat{H}_i(\mathbf{x},\omega)e^{-i\omega t}\,\mathrm{d}\omega, \tag{2.81}$$

$$D_i(\mathbf{x},t) = \frac{1}{2}\int_{-\infty}^{+\infty} \hat{D}_i(\mathbf{x},\omega)e^{-i\omega t}\,\mathrm{d}\omega, \tag{2.82}$$

$$B_i(\mathbf{x},t) = \frac{1}{2}\int_{-\infty}^{+\infty} \hat{B}_i(\mathbf{x},\omega)e^{-i\omega t}\,\mathrm{d}\omega. \tag{2.83}$$

Likewise we can write the electric and magnetic current densities as integrals over the frequency parameter.

2.4.2 Dispersion of the permittivity

Up until now we have assumed that matter reacts the same to any applied electromagnetic field, regardless how fast the fields change in time. One of the consequences of this property is that polarization and conduction occur instantaneously, that is, given a certain change in the electromagnetic fields, the matter instantaneously rearranges itself to retain the linear relationships $\mathbf{D} = \varepsilon\mathbf{E}$ and $\mathbf{J}_\mathrm{f} = \sigma\mathbf{E}$. Of course such an instantaneous reaction cannot occur on physical grounds, so a more complex mechanism has to govern the polarization. Following [12] we assume the polarization is not only a function of the present electric field strength but of all values in the past. In general this means we can write

$$D_i(\mathbf{x},t) = \varepsilon_0 E_i(\mathbf{x},t) + \varepsilon_0 \int_0^{\infty} f(\tau)E_i(\mathbf{x},t-\tau)\,\mathrm{d}\tau. \tag{2.84}$$

This means that the polarization is not local any more in the temporal variable. In the space variables we assume it still to be local. The precise way in which the medium reacts depends on our choice of $f(\tau)$. Note that for the special choice

$$f(\tau) = \chi_\mathrm{e}\delta(\tau),$$

we get the original model with instantaneous response back.

To further analyse the dispersion relation, we consider the complex fields. If we substitute (2.82) and (2.80) into (2.84) and interchange the order of integration we get as result

$$\begin{aligned}
&\int_{-\infty}^{+\infty} \hat{D}_i(\mathbf{x},\omega)e^{-i\omega t}\,\mathrm{d}\omega = \\
&= \varepsilon_0 \int_{-\infty}^{+\infty} \hat{E}_i(\mathbf{x},\omega)e^{-i\omega t}\,\mathrm{d}\omega + \varepsilon_0 \int_0^{\infty} f(\tau)\left[\int_{-\infty}^{+\infty} \hat{E}_i(\mathbf{x},\omega)e^{-i\omega(t-\tau)}\,\mathrm{d}\omega\right]\mathrm{d}\tau, \\
&= \varepsilon_0 \int_{-\infty}^{+\infty} \hat{E}_i(\mathbf{x},\omega)e^{-i\omega t}\left[1+\int_0^{\infty} f(\tau)e^{i\omega\tau}\,\mathrm{d}\tau\right]\mathrm{d}\omega, \\
&= \int_{-\infty}^{+\infty} \varepsilon_0\hat{E}_i(\mathbf{x},\omega)\left[1+\int_0^{\infty} f(\tau)e^{i\omega\tau}\,\mathrm{d}\tau\right]e^{-i\omega t}\,\mathrm{d}\omega,
\end{aligned}$$

so we see that for the complex field vectors we have the relation

$$\hat{D}_i(\mathbf{x},\omega) = \hat{\varepsilon}(\omega)\hat{E}_i(\mathbf{x},\omega), \tag{2.85}$$

where we have defined the complex electric permittivity by

$$\hat{\varepsilon}(\omega) = \varepsilon_0\left[1+\int_0^{\infty} f(\tau)e^{i\omega\tau}\,\mathrm{d}\tau\right]. \tag{2.86}$$

We see that when we assume the permittivity is local in the space coordinates we get a linear complex permittivity relation. Through the function $f(\tau)$ this relation depends on the specific media. We will not dig in the microscopic properties of matter to determine $f(\tau)$, instead we will take the values of $\hat{\varepsilon}(\omega)$ for the media of our interest from the literature.

It is interesting to see how we can relate the real permittivity and conductivity to the complex permittivity. Consider (2.60) together with (2.58) and assume $\mathbf{v} = 0$. Then we have

$$-\epsilon_{ljk}\partial_j H_k + \varepsilon_0\partial_t E_l = -(\varepsilon-\varepsilon_0)\partial_t E_l - \sigma E_l - J_l^{\mathrm{ext}}.$$

Rewriting and substituting (2.80 results in

$$-\epsilon_{ljk}\partial_l \hat{H}_k - i\omega\left(\varepsilon + i\frac{\sigma}{\omega}\right)\hat{E}_l = -\hat{J}_l^{\mathrm{ext}}.$$

Comparing with (2.85) we can identify

$$\hat{\varepsilon}(\omega) = \varepsilon'(\omega) + i\varepsilon''(\omega) = \varepsilon(\omega) + i\frac{\sigma(\omega)}{\omega},$$

where we made the frequency dependency explicit. We see that the imaginary part of the complex permittivity can be associated with conductivity. This suggests intuitively that it is associated with energy dissipation from the electromagnetic fields to the medium.

2.4.3 Complex Maxwell equations

To determine the equations governing the complex fields we substitute the fields written as integrals over the frequency parameter in both sides of the Maxwell equations (2.60) and (2.61). After interchanging the integration and differentiation and performing the time derivation, we get for each fixes ω the equations

$$\begin{aligned} -\varepsilon_{ijk}\partial_j \hat{H}_k - i\omega\varepsilon_0 \hat{E}_i &= -\hat{J}_i^{\text{ind}} - \hat{J}_i^{\text{ext}}, & (2.87)\\ \varepsilon_{ijk}\partial_j \hat{E}_k - i\omega\mu_0 \hat{H}_i &= -\hat{K}_i^{\text{ind}} - \hat{K}_i^{\text{ext}}. & (2.88) \end{aligned}$$

In order to determine the complex induced currents, we take the same steps for (2.58) and (2.59), and we use that $\sigma = \omega\varepsilon''$ and write $\varepsilon = \varepsilon'$ for the real permittivity. This results in

$$\begin{aligned} -\hat{\mathbf{J}}^{\text{ind}} &= i\omega(\varepsilon' - \varepsilon_0)\hat{\mathbf{E}} + i\omega(\mu\varepsilon' - \mu_0\varepsilon_0)\mathbf{v}\times\hat{\mathbf{H}} - \omega\varepsilon''\left(\hat{\mathbf{E}} + \mu\mathbf{v}\times\hat{\mathbf{H}}\right). & (2.89)\\ -\hat{\mathbf{K}}^{\text{ind}} &= i\omega(\mu - \mu_0)\hat{\mathbf{H}} - i\omega(\mu\varepsilon' - \mu_0\varepsilon_0)(\mathbf{v}\times\hat{\mathbf{E}}). & (2.90) \end{aligned}$$

If we assume $\mu = \mu_0$, and write $\hat{\varepsilon} = \varepsilon' + i\varepsilon''$ we get after rearranging the terms the equations

$$\begin{aligned} -\nabla\times\hat{\mathbf{H}} - i\omega\hat{\varepsilon}\hat{\mathbf{E}} &= i\omega\mu_0\left(\hat{\varepsilon} - \varepsilon_0\right)\mathbf{v}\times\hat{\mathbf{H}} - \hat{\mathbf{J}}^{\text{ext}}, & (2.91)\\ \nabla\times\hat{\mathbf{E}} - i\omega\mu_0\hat{\mathbf{H}} &= -i\omega\mu_0(\varepsilon - \varepsilon_0)\mathbf{v}\times\hat{\mathbf{E}} - \hat{\mathbf{K}}^{\text{ext}}. & (2.92) \end{aligned}$$

Notice that at the right-hand side of (2.92) we only need the real part of the permittivity. We expect the fluid velocity to be small, so that the first terms on the right-hand side of the equations can be neglected. This results in the equations

$$\begin{aligned} -\nabla\times\hat{\mathbf{H}} - i\omega\hat{\varepsilon}\hat{\mathbf{E}} &= -\hat{\mathbf{J}}^{\text{ext}}, & (2.93)\\ \nabla\times\hat{\mathbf{E}} - i\omega\mu_0\hat{\mathbf{H}} &= -\hat{\mathbf{K}}^{\text{ext}}, & (2.94) \end{aligned}$$

which is the form we will use most of the time. Taking the divergence on both sides results in the compatibility relations

$$\begin{aligned} i\omega\nabla\cdot(\hat{\varepsilon}\hat{\mathbf{E}}) &= \nabla\cdot\hat{\mathbf{J}}^{\text{ext}}, & (2.95)\\ i\omega\mu_0\nabla\cdot\hat{\mathbf{H}} &= \nabla\cdot\hat{\mathbf{K}}^{\text{ext}}, & (2.96) \end{aligned}$$

We see that for each frequency component the complex fields satisfy these complex Maxwell equations. It is important to realize that the induced currents in general are functions of the frequency ω. Since a lot of real-life sources are highly localized in the frequency domain, that is their intensity is centred around one frequency, we will approximate these sources as if they consist of only one frequency, and we write $\hat{f}(\mathbf{x},\omega';\omega) = \delta(\omega-\omega')f(\mathbf{x})$. Substitution in (2.79) results in the expression

$$f(\mathbf{x},t) = \text{Re}\left\{\hat{f}(\mathbf{x})e^{-i\omega t}\right\}. \quad (2.97)$$

In Chapter 3 we will use these single frequency fields most of the time.

If we split the equations in real and imaginary parts, we end up with four equations. For equation (2.93) this results in

$$-\nabla \times \mathbf{H}' + \omega\left(\varepsilon''\mathbf{E}' + \varepsilon'\mathbf{E}''\right) = -\mathrm{Re}\left\{\hat{\mathbf{J}}^{\mathrm{ext}}\right\}, \tag{2.98}$$

$$-\nabla \times \mathbf{H}'' - \omega\left(\varepsilon'\mathbf{E}' - \varepsilon''\mathbf{E}''\right) = -\mathrm{Im}\left\{\hat{\mathbf{J}}^{\mathrm{ext}}\right\}. \tag{2.99}$$

For (2.94) we get as equations

$$\nabla \times \mathbf{E}' + \omega\mu_0\mathbf{H}'' = -\mathrm{Re}\left\{\hat{\mathbf{K}}^{\mathrm{ext}}\right\}, \tag{2.100}$$

$$\nabla \times \mathbf{E}'' - \omega\mu_0\mathbf{H}' = -\mathrm{Im}\left\{\hat{\mathbf{K}}^{\mathrm{ext}}\right\}. \tag{2.101}$$

We will use these equations in a later stage to see how well the calculated fields satisfy the Maxwell equations on different grids.

2.4.4 Complex index of refraction

Up until now we have mostly worked with the complex permittivity parameter. In optics the complex index of refraction $\hat{n}$ and the complex wave number $\hat{k}$ are often used. We define the complex index of refraction $\hat{n} = n + \imath\kappa$ by

$$\varepsilon_0\hat{n}^2 = \hat{\varepsilon}, \tag{2.102}$$

where we take the root with positive imaginary part, so that $\kappa \geq 0$. Furthermore we define the complex wave number $\hat{k} = k + \imath\alpha$ by

$$\hat{k} = \frac{\omega}{c}\hat{n}. \tag{2.103}$$

We will use these quantities often, specially because the properties of the medium we will use are can be found in terms of these parameters in the literature.

2.5 Time-averaged quantities

Our main goal is to couple the Maxwell equations with the Navier-Stokes equations. It is important to realize that there are two temporal scales in this situation. On one hand there is the time scale at which the electromagnetic fields oscillate, on the other hand there is the time scale on which the fluid reacts, and the particles move and accelerate as response to the forces. When we focus on electromagnetic fields with wavelengths in the micrometer region, the frequencies are of the order $10^{13}\,\mathrm{s}^{-1}$ and higher. We are not interested in the field properties, such as energy transfer or Lorentz forces, at this time scale, but in the time-averaged properties.

We will focus on single frequency sources, so that the time-domain fields and frequency-domain fields are related by (2.97). We see that the time-domain fields are periodic in t, with period $T = \frac{2\pi}{\omega}$. In order to determine the time-averaged values, we integrate from $-\frac{T}{2}$ to $\frac{T}{2}$. The time-averaged

value of a periodic quantity we denote by $\langle\cdot\rangle$. We will first focus on two arbitrary fields f and g. For the field intensity itself we have

$$\begin{aligned}
\langle f(\mathbf{x},t)\rangle &= \frac{1}{T}\int_{-\frac{T}{2}}^{\frac{T}{2}} \mathrm{Re}\left\{\hat{f}(\mathbf{x})e^{-\imath\omega t}\right\}\,\mathrm{d}t,\\
&= \frac{1}{T}\mathrm{Re}\left\{\left[-\frac{1}{\imath\omega}\hat{f}(\mathbf{x})e^{-\imath\omega t}\right]_{\frac{T}{2}}^{\frac{T}{2}}\right\},\\
&= \frac{1}{T}\mathrm{Re}\left\{-\frac{1}{\imath\omega}\hat{f}(\mathbf{x})\left(e^{-\frac{\imath\omega T}{2}}-e^{\frac{\imath\omega T}{2}}\right)\right\}\\
&= 0,
\end{aligned}$$

which is intuitively clear since the field intensity is consists of an oscillating sine and cosine. More interesting is the result for quantities that are the product of two complex fields, such as the components of the Poynting vector or the Maxwell stress tensor. We have

$$\begin{aligned}
\langle f(\mathbf{x},t)\cdot g(\mathbf{x},t)\rangle &= \frac{1}{T}\int_{-\frac{T}{2}}^{\frac{T}{2}} \mathrm{Re}\left\{\hat{f}(\mathbf{x})e^{-\imath\omega t}\right\}\cdot\mathrm{Re}\left\{\hat{g}(\mathbf{x})e^{-\imath\omega t}\right\}\,\mathrm{d}t,\\
&= \frac{1}{4T}\int_{-\frac{T}{2}}^{\frac{T}{2}} \left[\hat{f}(\mathbf{x})e^{-\imath\omega t}+\bar{\hat{f}}(\mathbf{x})e^{\imath\omega t}\right]\cdot\left[\hat{g}(\mathbf{x})e^{-\imath\omega t}+\bar{\hat{g}}(\mathbf{x})e^{\imath\omega t}\right]\,\mathrm{d}t,\\
&= \frac{1}{4T}\int_{-\frac{T}{2}}^{\frac{T}{2}} \left[\hat{f}(\mathbf{x})\hat{g}(\mathbf{x})e^{-2\imath\omega t}+\hat{f}(\mathbf{x})\bar{\hat{g}}(\mathbf{x})+\bar{\hat{f}}(\mathbf{x})\hat{g}(\mathbf{x})+\bar{\hat{f}}(\mathbf{x})\bar{\hat{g}}(\mathbf{x})e^{2\imath\omega t}\right]\,\mathrm{d}t,\\
&= \frac{1}{4}\left[\hat{f}(\mathbf{x})\bar{\hat{g}}(\mathbf{x})+\bar{\hat{f}}(\mathbf{x})\hat{g}(\mathbf{x})\right],\\
&= \frac{1}{2}\mathrm{Re}\left\{\hat{f}(\mathbf{x})\bar{\hat{g}}(\mathbf{x})\right\},
\end{aligned}$$

where in the fourth line we used that the integration is over two periods of the complex exponential. We see that although the two field quantities integrate to zero their product is not zero in general. This time-averaged non-zero value will give rise to the heat dissipation and force term we will need. One final quantity we need to average is the time derivative of the product of two field quantities. We have

$$\begin{aligned}
\left\langle\frac{\partial}{\partial t}\left[f(\mathbf{x},t)\cdot g(\mathbf{x},t)\right]\right\rangle &= \frac{1}{T}\int_{-\frac{T}{2}}^{\frac{T}{2}}\frac{\partial}{\partial t}\left[\mathrm{Re}\left\{\hat{f}(\mathbf{x})e^{-\imath\omega t}\right\}\cdot\mathrm{Re}\left\{\hat{g}(\mathbf{x})e^{-\imath\omega t}\right\}\right]\,\mathrm{d}t, &(2.104)\\
&= \frac{1}{T}\left[\mathrm{Re}\left\{\hat{f}(\mathbf{x})e^{-\imath\omega t}\right\}\cdot\mathrm{Re}\left\{\hat{g}(\mathbf{x})e^{-\imath\omega t}\right\}\right]_{-\frac{T}{2}}^{\frac{T}{2}}, &(2.105)\\
&= 0. &(2.106)
\end{aligned}$$

In the last line we again use that the complex exponential is periodic.

We can now determine the time-averaged versions of the conservation equations we have derived earlier. For the Poynting vector we get

$$\langle \mathbf{S} \rangle = \langle \mathbf{E} \times \mathbf{H} \rangle = \frac{1}{2} \mathrm{Re} \left\{ \hat{\mathbf{E}} \times \bar{\mathbf{H}} \right\}.$$

This equality will be our motivation to define the complex Poynting vector as

$$\hat{\mathbf{S}} = \frac{1}{2} \hat{\mathbf{E}} \times \bar{\mathbf{H}}. \tag{2.107}$$

If we time-average (2.72) we see that the left-hand side vanishes because of the time derivative, and after rearranging terms we end up with the conservation equation

$$\mathrm{div}\, \mathrm{Re} \left\{ \hat{\mathbf{S}} \right\} = -\frac{1}{2} \mathrm{Re} \left\{ \hat{\mathbf{E}} \cdot \bar{\mathbf{J}} \right\} - \frac{1}{2} \mathrm{Re} \left\{ \hat{\mathbf{H}} \cdot \bar{\mathbf{K}} \right\}.$$

Substituting (2.89) results for the first term on the left-hand side in

$$\begin{aligned}
-\frac{1}{2} \mathrm{Re} \left\{ \hat{\mathbf{E}} \cdot \bar{\mathbf{J}} \right\} &= \frac{1}{2} \mathrm{Re} \left\{ \hat{\mathbf{E}} \cdot \left(-\imath\omega(\varepsilon' - \varepsilon_0) \bar{\mathbf{E}} - \imath\omega\mu_0(\varepsilon' - \varepsilon_0) \mathbf{v} \times \bar{\mathbf{H}} - \omega\varepsilon'' \left(\bar{\mathbf{E}} + \mu_0 \mathbf{v} \times \bar{\mathbf{H}} \right) \right) \right\}, \\
&= \frac{1}{2} \mathrm{Re} \left\{ \hat{\mathbf{E}} \cdot \left(-\imath\omega\mu_0(\varepsilon' - \varepsilon_0) \mathbf{v} \times \bar{\mathbf{H}} - \omega\varepsilon'' \left(\bar{\mathbf{E}} + \mu_0 \mathbf{v} \times \bar{\mathbf{H}} \right) \right) \right\}, \\
&= \frac{1}{2} \omega\mu_0(\varepsilon' - \varepsilon_0) \mathrm{Im} \left\{ (\mathbf{v} \times \bar{\mathbf{H}}) \cdot \hat{\mathbf{E}} \right\} - \frac{1}{2} \omega\mu_0\varepsilon'' \mathrm{Re} \left\{ (\mathbf{v} \times \bar{\mathbf{H}}) \cdot \hat{\mathbf{E}} \right\} - \frac{1}{2} \omega\varepsilon'' \hat{\mathbf{E}} \cdot \bar{\mathbf{E}}, \\
&= -\omega\mu_0(\varepsilon' - \varepsilon_0) \mathrm{Im} \left\{ \hat{\mathbf{S}} \right\} \cdot \mathbf{v} + \omega\mu_0\varepsilon'' \mathrm{Re} \left\{ \hat{\mathbf{S}} \right\} \cdot \mathbf{v} - \frac{1}{2} \omega\varepsilon'' \hat{\mathbf{E}} \cdot \bar{\mathbf{E}}.
\end{aligned}$$

Likewise if we substitute (2.90) in the second term we get

$$\begin{aligned}
-\frac{1}{2} \mathrm{Re} \left\{ \hat{\mathbf{H}} \cdot \bar{\mathbf{K}} \right\} &= -\frac{1}{2} \mathrm{Re} \left\{ \hat{\mathbf{H}} \cdot \left(\imath\omega\mu_0(\varepsilon' - \varepsilon_0)(\mathbf{v} \times \bar{\mathbf{E}}) \right\} \right), \\
&= \frac{1}{2} \omega\mu_0(\varepsilon' - \varepsilon_0) \mathrm{Im} \left\{ (\mathbf{v} \times \bar{\mathbf{E}}) \cdot \hat{\mathbf{H}} \right\}, \\
&= -\omega\mu_0(\varepsilon' - \varepsilon_0) \mathrm{Im} \left\{ \hat{\mathbf{S}} \right\} \cdot \mathbf{v}.
\end{aligned}$$

This results in the equation

$$\mathrm{div}\, \mathrm{Re} \left\{ \hat{\mathbf{S}} \right\} = -2\omega\mu_0(\varepsilon' - \varepsilon_0) \mathrm{Im} \left\{ \hat{\mathbf{S}} \right\} \cdot \mathbf{v} + \omega\mu_0\varepsilon'' \mathrm{Re} \left\{ \hat{\mathbf{S}} \right\} \cdot \mathbf{v} - \frac{1}{2} \omega\varepsilon'' \hat{\mathbf{E}} \cdot \bar{\mathbf{E}}.$$

We see when we neglect the back-action of the velocity of the fluid we get

$$\mathrm{div}\, \mathrm{Re} \left\{ \hat{\mathbf{S}} \right\} = -\frac{1}{2} \omega\varepsilon'' \hat{\mathbf{E}} \cdot \bar{\mathbf{E}},$$

which we can identify with the heat dissipation generated by the conductance of the fluid. This dissipation term will be denoted by

$$q_{\mathrm{em}} = \frac{1}{2} \omega\varepsilon'' \hat{\mathbf{E}} \cdot \bar{\mathbf{E}}, \tag{2.108}$$

which is the energy conservation equation for the time-averaged fields.

For the force we also want to determine the time-averaged value. If we again neglect the current terms depending on $\mathbf{v}$ and assume we have a homogeneous medium, we have $\rho_{\mathrm{e}} = 0$ and $\rho_{\mathrm{m}} = 0$. Furthermore $\hat{\mathbf{K}} = 0$, so we end up with

$$\langle \mathbf{f} \rangle = \frac{1}{2}\mu_0 \mathrm{Re}\left\{ \hat{\mathbf{J}}^{\mathrm{ind}} \times \bar{\mathbf{H}} \right\}.$$

We assume the back-action of the fluid on the fields is negligible. Substituting (2.89) with $\mathbf{v} = 0$ then results in

$$\begin{aligned} \langle \mathbf{f} \rangle &= -\frac{1}{2}\omega\mu_0 \mathrm{Re}\left\{ \imath(\hat{\varepsilon} - \varepsilon_0)\hat{\mathbf{E}} \times \bar{\mathbf{H}} \right\}, \\ &= \omega\mu_0 \mathrm{Im}\left\{ (\hat{\varepsilon} - \varepsilon_0)\hat{\mathbf{S}} \right\}, \\ &= \omega\mu_0 \left[\varepsilon'' \mathrm{Re}\left\{ \hat{\mathbf{S}} \right\} + (\varepsilon' - \varepsilon_0)\mathrm{Im}\left\{ \hat{\mathbf{S}} \right\} \right]. \end{aligned}$$

So when we are considering the Navier-Stokes equations, we have as external force density the term

$$\mathbf{f}_{\mathrm{em}} = \omega\mu_0 \left[\varepsilon'' \mathrm{Re}\left\{ \hat{\mathbf{S}} \right\} + (\varepsilon' - \varepsilon_0)\mathrm{Im}\left\{ \hat{\mathbf{S}} \right\} \right]. \tag{2.109}$$

The first term is proportional to ε'', which is the parameter associated with heat dissipation, so we refer to this term as f_{dis}. The second term is proportional to ε', which is associated with polarization, and we refer to this term is f_{pol}. So we can write the electromagnetic force density as

$$\mathbf{f}_{\mathrm{em}} = \mathbf{f}_{\mathrm{pol}} + \mathbf{f}_{\mathrm{dis}}. \tag{2.110}$$

Which term is dominant will depend on the properties of the medium. In particular, for transparent frequencies $\mathbf{f}_{\mathrm{dis}}$ will be very small.

We can also express the moment conservation from (2.76) in terms of the time-averaged fields. This results in

$$\mathbf{f}_{\mathrm{em}} = \nabla \cdot \langle \overleftrightarrow{T} \rangle, \tag{2.111}$$

where the time-averaged stress tensor is given by time-averaging (2.75), resulting in

$$\langle T_{ij} \rangle = \frac{1}{2}\mathrm{Re}\left\{ \varepsilon_0 E_i E_j^* + \mu_0 H_i H_j^* \right\} - \frac{1}{4}\delta_{ij}\left(\varepsilon_0 E_i E_j^* + \mu_0 H_i H_i^* \right).$$

We now have all the (theoretical) information we need regarding the electromagnetic properties of our problem. In order to run a simulation we need to determine the (complex) fields using equations (2.93) and (2.94). With these field we can determine the complex Poynting vector using (2.107). Then we can determine the electromagnetic heat dissipation and electromagnetic force term using (2.108) and (2.109) respectively. In order to proceed we still need to choose the external sources, which will be the subject of the next chapter.

Chapter 3

External electromagnetic sources

In the previous chapter we derived the equations governing the electromagnetic fields, but we still need to choose an external source to create the fields in the first place. There are different kind of sources, and they can be modelled in multiple ways. We will first consider the so-called Gaussian beam approximation, which is used frequently because it is a good model for the fields create by a laser, and it has good properties to use in combination with lenses. The main down-side is that it is only an approximate solution for the Maxwell equations, so we cannot expect the resulting fields and other quantities depending on the fields to be exact. Since we are interested in the force field, we need to make sure the approximations are good enough for our purpose.

As an alternative method we will create a source that does satisfy the Maxwell equations. We will model an aperture with an external current density using an array of perfect dipoles. We will see that this source does satisfy the Maxwell equations exact.

3.1 Gaussian beam approximations

On approximation that is regularly used for modelling the electromagnetic field of a laser is the so-called Gaussian beam. We will not assume an explicit external source, but solve for the potential in a more general setting. We will derive the Gaussian beam solution of the paraxial approximation of the Maxwell equations in a linear, homogeneous, non magnetic, lossy medium. From Section 2.4.3 we have the frequency domain Maxwell equations given by

$$\begin{aligned} -\epsilon_{ijk}\partial_j H_k - \imath\omega\hat{\varepsilon}E_i &= 0, & (3.1)\\ \epsilon_{ijk}\partial_j E_k - \imath\omega\mu_0 H_i &= 0, & (3.2) \end{aligned}$$

with $\hat{\varepsilon} = \varepsilon' + \imath\varepsilon''$ the complex permittivity. For non-magnetic media we have $\hat{\varepsilon} = \hat{n}^2\varepsilon_0$, so that $\varepsilon' = (n^2 - \kappa^2)\varepsilon_0$ and $\varepsilon'' = 2n\kappa\varepsilon_0$. Taking divergence on both sides results in the compatibility relations

$$\begin{aligned} \partial_i E_i &= 0, & (3.3)\\ \partial_i H_i &= 0. & (3.4) \end{aligned}$$

Following [3] we will express the equations in terms of a vector potential and solve for the potential instead of the fields. Then we can derive the field variables from the solution of the potential. The main advantage of the method is that we can assume the potential only has one non-zero component, orthogonal to the direction of propagation, while for the fields themselves this is not possible. We define the vector potential A_i such that

$$H_i = \epsilon_{ijk}\partial_j A_k, \tag{3.5}$$

which is possible because H is divergent-less. Substitution in (3.2) and rewriting results in

$$\epsilon_{ijk}\partial_j \left(E_k - \imath\omega\mu_0 A_k\right) = 0.$$

We know that when the curl of a vector field vanishes there exists a scalar field such that the vector field is equal to the gradient of the scalar field, so there exists V such that

$$E_i = \imath\omega\mu_0 A_i - \partial_i V. \tag{3.6}$$

Substitution in (3.1) results in

$$-\epsilon_{ijk}\partial_j(\epsilon_{klm}\partial_l A_k) - \imath\omega\hat{\varepsilon}\left(\imath\omega\mu_0 A_i - \partial_i V\right) = 0.$$

This can be rewritten to

$$-\partial_i(\partial_j A_j) + \partial_j^2 A_i + \imath\omega\hat{\varepsilon}\partial_i V + \omega^2\mu_0\hat{\varepsilon}A_i = 0.$$

Choosing the Lorenz gauge, such that

$$\partial_j A_j = \imath\omega\hat{\varepsilon}V, \tag{3.7}$$

the equation reduces to

$$\partial_j^2 A_i + \omega^2\mu_0\hat{\varepsilon}A_i = 0.$$

Using (2.103), we can write this equation as

$$\partial_j^2 A_i + \hat{k}^2 A_i = 0,$$

the Helmholtz equation with complex coefficient. We have $\hat{k} = k + \imath\alpha$, the complex wave number. We assume our vector potential has non-zero component $A = A_2$ and $A_1 = A_3 = 0$, so that we end up with the equation

$$\partial_1^2 A + \partial_2^2 A + \partial_3^2 A + \hat{k}^2 A = 0. \tag{3.8}$$

We assume the laser beam propagates in the x_3 direction, and we write A as

$$A = \psi(x_1, x_2, x_3)e^{\imath\hat{k}x_3}. \tag{3.9}$$

Note that

$$\begin{aligned}\partial_3^2 A &= \partial_3^2\left(\psi e^{\imath\hat{k}x_3}\right),\\ &= \partial_3\left[e^{\imath\hat{k}x_3}\left(\partial_3\psi+\imath\hat{k}\psi\right)\right],\\ &= e^{\imath\hat{k}x_3}\left(\partial_3^2\psi+\imath\hat{k}\partial_3\psi+\imath\hat{k}\partial_3\psi-\hat{k}^2\psi\right),\end{aligned}$$

Substitution in (3.8) results in

$$e^{\imath\hat{k}x_3}\left[\partial_1^2\psi+\partial_2^2\psi+\partial_3^2\psi+2\imath\hat{k}\partial_3\psi\right]=0.$$

Dividing by $e^{\imath\hat{k}x_3}$ results in the equation

$$\partial_1^2\psi+\partial_2^2\psi+\partial_3^2\psi+2\imath\hat{k}\partial_3\psi=0. \tag{3.10}$$

We now define a characteristic length scale w_0 which later on will be identified as the waist size of the beam. We also define $\hat{l}=\hat{k}w_0^2$, and transform to the coordinates

$$\begin{aligned}x_1 &\rightarrow w_0x_1,\\ x_2 &\rightarrow w_0x_2,\\ x_3 &\rightarrow \hat{l}x_3.\end{aligned}$$

The partial derivatives transform as

$$\begin{aligned}\partial_1 &\rightarrow \frac{1}{w_0}\partial_1,\\ \partial_2 &\rightarrow \frac{1}{w_0}\partial_2,\\ \partial_3 &\rightarrow \frac{1}{\hat{l}}\partial_3.\end{aligned}$$

Substitution in (3.10) and multiplying by w_0^2 results in

$$\partial_1^2\psi+\partial_2^2\psi+2\imath\partial_3\psi+\hat{s}^2\partial_3^2\psi=0, \tag{3.11}$$

with $\hat{s}=\frac{w_0}{\hat{l}}=\frac{1}{\hat{k}w_0}$. We want to approximate the solution ψ by expanding it around $\hat{s}$ and solving for the first term. This will give us an accurate approximation for $|\hat{s}|\ll 1$. We write

$$\psi=\sum_{n=0}^{\infty}\psi_n\hat{s}^n. \tag{3.12}$$

Substituting in (3.11) and using linearity results in

$$\sum_{n=0}^{\infty}\left[\partial_1^2\psi_n+\partial_2^2\psi_n+2\imath\partial_3\psi_n\right]\hat{s}^n+\partial_3^2\psi_n\hat{s}^{n+2}=0. \tag{3.13}$$

Equating terms of equal power in $\hat{s}$ results for $n = 0$ in the equation

$$\partial_1^2\psi_0 + \partial_2^2\psi_0 + 2\imath\partial_3\psi_0 = 0. \tag{3.14}$$

Note that higher order equations depend on lower order solutions. For $n = 2$ for example we have

$$\partial_1^2\psi_2 + \partial_2^2\psi_2 + 2\imath\partial_3\psi_2 = -\partial_3^2\psi_0.$$

In order to solve (3.14) we substitute the solution

$$\psi_0 = \exp\left(\imath P(x_3) + \imath\frac{1}{2}\frac{\rho^2}{q(x_3)}\right), \tag{3.15}$$

with $\rho^2 = x_1^2 + x_2^2$, and $q(x_3)$ a function of x_3 that we will make explicit later. For the derivatives we have

$$\begin{aligned}
\partial_1\psi_0 &= \psi_0 \cdot \imath\frac{x_1}{q}, \\
\partial_1^2\psi_0 &= \psi_0\left[\imath\frac{1}{q} - \frac{x_1^2}{q^2}\right], \\
\partial_2^2\psi_0 &= \psi_0\left[\imath\frac{1}{q} - \frac{x_2^2}{q^2}\right], \\
\partial_3\psi_0 &= \psi_0\left[\imath\partial_3 P - \imath\frac{1}{2}\frac{\rho^2}{q^2}\partial_3 q\right].
\end{aligned}$$

Substitution in (3.14) results in

$$\begin{aligned}
0 &= \psi_0\left[\imath\frac{1}{q} - \frac{x_1^2}{q^2}\right] + \psi_0\left[\imath\frac{1}{q} - \frac{x_2^2}{q^3}\right] + 2\imath\psi_0\left[\imath\partial_3 P - \imath\frac{1}{2}\frac{\rho^2}{q^2}\partial_3 q\right], \\
&= \left[2\imath\frac{1}{q} - \frac{x_1^2 + x_2^2}{q^2} - 2\partial_3 P + \frac{\rho^2}{q^2}(\partial_3 q)\right]\psi_0.
\end{aligned}$$

Setting $\partial_3 q = 1$ makes the terms in ρ^2 vanish, and we end up with the condition

$$\partial_3 P = \frac{\imath}{q}. \tag{3.16}$$

We will consider both terms in the exponential of (3.15) separately. First we focus on the second term, then on the first term.

3.1.1 Second term

Focussing on the second term in the exponential of (3.15), we choose

$$q(x_3) = (x_3 - z_0) - q_0, \tag{3.17}$$

with z_0 and q_0 constants, so that $\partial_3 q = 1$. We have z_0 the (transformed) point of focus. Furthermore we write

$$q_0 = \imath \frac{z_R}{w_0^2 \hat{k}},$$

with z_R the Rayleigh range given by

$$z_\mathrm{R} = \frac{w_0^2}{2} k. \tag{3.18}$$

This choice of parameters coincides with the choices in the literature. If we transform back to the original variables, we can write

$$\frac{1}{q(x_3)} = \frac{1}{(x_3 - z_0) - q_0} \to \frac{1}{\frac{1}{w_0^2 \hat{k}}(x_3 - z_0) - \imath \frac{z_R}{w_0^2 \hat{k}}} = \frac{w_0^2 \hat{k}}{(x_3 - z_0) - \imath z_R}.$$

Substitution in the second term of the exponential in (3.15) and using $x_1 \to \frac{1}{w_0} x_1$ and $x_2 \to \frac{1}{w_0} x_2$, so that $\rho^2 \to \frac{1}{w_0^2} \rho^2$, results in

$$\begin{aligned} \exp\left(\imath \frac{1}{2} \frac{\rho^2}{q(x_3)}\right) &= \exp\left(\imath \hat{k} \frac{1}{2} \frac{\rho^2}{(z - z_0) - \imath z_R}\right), \\ &= \exp\left(\imath (k + \imath \alpha) \frac{1}{2} \rho^2 \frac{(z - z_0) + \imath z_R}{(z - z_0)^2 + z_R^2}\right). \end{aligned}$$

We define the radius of curvature as

$$R(z) = (z - z_0) \left[1 + \left(\frac{z_\mathrm{R}}{z - z_0}\right)^2\right], \tag{3.19}$$

and the spot size

$$w(z) = w_0 \sqrt{1 + \left(\frac{z - z_0}{z_\mathrm{R}}\right)^2}, \tag{3.20}$$

both in the original coordinates. Note that

$$\frac{1}{R(z)} = \frac{z - z_0}{(z - z_0)^2 + z_R^2},$$

and

$$\frac{w_0^2}{w(z)^2} = \frac{z_R^2}{(z - z_0)^2 + z_R^2},$$

so we have

$$\frac{(z - z_0) + \imath z_R}{(z - z_0)^2 + z_R^2} = \frac{1}{R(z)} + \imath \frac{w_0^2}{w(z)^2} \frac{1}{z_R}.$$

Substitution results in

$$\begin{aligned}
\exp\left(\imath\frac{1}{2}\frac{\rho^2}{q(x_3)}\right) &= \exp\left(\imath(k+\imath\alpha)\frac{1}{2}\rho^2\left[\frac{1}{R(z)}+\imath\frac{w_0^2}{w(z)^2}\frac{1}{z_R}\right]\right),\\
&= \exp\left(\imath(k+\imath\alpha)\frac{\rho^2}{2R(z)}\right)\exp\left(-(k+\imath\alpha)\frac{1}{2}\rho^2\frac{w_0^2}{w(z)^2}\frac{1}{z_R}\right),\\
&= \exp\left(\imath(k+\imath\alpha)\frac{\rho^2}{2R(z)}\right)\exp\left(-k\frac{1}{2}\rho^2\frac{w_0^2}{w(z)^2}\frac{2}{w_0^2k}\right)\exp\left(-\imath\alpha\frac{1}{2}\rho^2\frac{w_0^2}{w(z)^2}\frac{2}{w_0^2k}\right),\\
&= \exp\left(\imath(k+\imath\alpha)\frac{\rho^2}{2R(z)}\right)\exp\left(-\frac{\rho^2}{w(z)^2}\right)\exp\left(-\imath\frac{\alpha}{k}\frac{\rho^2}{w(z)^2}\right),
\end{aligned}$$

So finally we can write the second term as

$$\exp\left(\imath\frac{1}{2}\frac{\rho^2}{q(x_3)}\right) = \exp\left(\imath(k+\imath\alpha)\frac{\rho^2}{2R(z)}\right)\exp\left(-\frac{\rho^2}{w(z)^2}\right)\exp\left(-\imath\frac{\alpha}{k}\frac{\rho^2}{w(z)^2}\right). \tag{3.21}$$

Furthermore we have

$$\partial_3 R^{-1}(z) = \frac{z_R^2-(z-z_0)^2}{((z-z_0)^2+z_R^2)^2}, \tag{3.22}$$

and

$$\partial_3 w(z) = \frac{w_0^2}{z_R}\frac{z-z_0}{z_R}\frac{1}{w(z)}. \tag{3.23}$$

An interesting result with respect to the Gaussian beam solution in a lossless medium is the extra phase shift $-\frac{\alpha}{k}\frac{\rho^2}{w(z)^2}$. So we can not just replace the wave number k with a complex wave number $\hat{k}$ in the usual expression for the Gaussian beam solution.

3.1.2 First term

We will now focus on the first term in the exponential of (3.15). Using (3.16) and (3.17) we have

$$\imath\partial_3 P = -\frac{1}{z-z_0-q_0}.$$

The anti-derivative is given by

$$\imath P = -\mathrm{Log}\left(1-\frac{z-z_0}{q_0}\right),$$

where the constant of integration will later on be added as the complex overall constant A_0 giving the amplitude and phase. Note that transferring back to the dimensioned coordinates we have

$$\left(1-\frac{z-z_0}{q_0}\right)\rightarrow\left(1-\frac{z-z_0}{\hat{k}w_0^2}\frac{w_0^2\hat{k}}{\imath z_R}\right) = \left(1+\imath\frac{z-z_0}{z_R}\right).$$

We see that the real part of the argument of the complex logarithm is strictly positive, so we are on the principal branch for every value of z and the integration is valid. We can now rewrite the expression as

$$\begin{aligned} -\mathrm{Log}\left(1+\imath\frac{z-z_0}{z_R}\right) &= -\log\left(\sqrt{1+\left(\frac{z-z_0}{z_R}\right)^2}\right)-\imath\mathrm{Arg}\left(1+\imath\frac{z-z_0}{z_R}\right), \\ &= -\log\left(\frac{w(z)}{w_0}\right)-\imath\arctan\left(\frac{z-z_0}{z_R}\right). \end{aligned}$$

We have as final result for this term

$$\exp(\imath P)=\exp\left(-\log\left(\frac{w(z)}{w_0}\right)-\imath\arctan\left(\frac{z-z_0}{z_R}\right)\right)=\frac{w_0}{w(z)}\exp\left(-\imath\arctan\left(\frac{z-z_0}{z_R}\right)\right). \quad (3.24)$$

3.1.3 Total result

Finally if we substitute (3.24) and (3.21) in (3.15) we get as solution of (3.14) the expression

$$\psi_0=\frac{w_0}{w(z)}\exp\left(\imath\hat{k}\frac{\rho^2}{2R(z)}-\frac{\rho^2}{w(z)^2}-\imath\frac{\alpha}{k}\frac{\rho^2}{w(z)^2}-\imath\zeta(z)\right). \quad (3.25)$$

Substitution of (3.25) in (3.9) results in the vector potential

$$A(x_1,x_2,x_3)\approx A_0\frac{w_0}{w(z)}\exp\left[\imath\hat{k}x_3+\imath\hat{k}\frac{\rho^2}{2R(z)}-\frac{\rho^2}{w(z)^2}-\imath\frac{\alpha}{k}\frac{\rho^2}{w(z)^2}-\imath\zeta(z)\right], \quad (3.26)$$

with the Gouy phase given by

$$\zeta(z)=\arctan\left(\frac{z-z_0}{z_R}\right), \quad (3.27)$$

and A_0 the complex amplitude determined by the total power and phase. We see that the extinction coefficient not only governs the extinction of the potential but also induces a phase shift. Note that the derivative for the Gouy phase is given by

$$\partial_3\zeta(z)=\frac{z_R}{z_R^2+(z-z_0)^2}. \quad (3.28)$$

3.1.4 Electric field

From the vector potential we can determine the electric field. Combining (3.6) and (3.7) we get

$$E_i=\imath\omega\mu_0A_i+\imath\frac{1}{\omega\hat{\varepsilon}}\partial_i\partial_jA_j,$$

which using $A_1=A_3=0$ results in

$$\begin{aligned} E_1 &= \imath\frac{1}{\omega\hat{\varepsilon}}\partial_1\partial_2 A_2, \\ E_2 &= \imath\frac{1}{\omega\hat{\varepsilon}}\partial_2^2 A_2 + \imath\omega\mu_0 A_2, \\ E_3 &= \imath\frac{1}{\omega\hat{\varepsilon}}\partial_3\partial_2 A_2. \end{aligned}$$

Substituting

$$A_2 = A_0 \exp(\imath\hat{k}x_3)\psi(x_1, x_2, x_3)$$

and using $\hat{\varepsilon} = \varepsilon_0\hat{n}^2$ results for the first component in

$$\begin{aligned} E_1 &= \imath\frac{1}{\varepsilon_0\hat{n}^2\omega}A_0 \exp(\imath\hat{k}x_3)\partial_1\partial_2\psi, \\ &\rightarrow \imath\frac{\omega}{\varepsilon_0 c^2\hat{k}^2 w_0^2}A_0 \exp(\imath\hat{k}^2 w_0^2 x_3)\partial_1\partial_2\psi, \\ &= \imath\omega\mu_0 A_0\hat{s}^2 \exp\left(\imath\frac{x_3}{\hat{s}^2}\right)\partial_1\partial_2\psi. \end{aligned}$$

Defining

$$E_0 = \imath\omega\mu_0 A_0 \tag{3.29}$$

results in

$$E_1 = E_0\hat{s}^2 \exp\left(\imath\frac{x_3}{\hat{s}^2}\right)\partial_1\partial_2\psi.$$

Likewise for the second component we get

$$E_2 = E_0\left[\hat{s}^2 \exp\left(\imath\frac{x_3}{\hat{s}^2}\right)\partial_2^2\psi + \exp(\imath\hat{k}x_3)\psi\right].$$

For the third component we get

$$\begin{aligned} E_3 &= \imath\frac{1}{\varepsilon_0\hat{n}^2\omega}A_0\partial_3\left(\exp(\imath\hat{k}x_3)\partial_2\psi\right), \\ &\rightarrow \imath\frac{\omega}{\varepsilon_0 c^2\hat{k}^2}A_0\frac{1}{\hat{k}w_0^2}\partial_3\left(\exp(\imath\hat{k}^2 w_0^2)\frac{1}{w_0}\partial_2\psi\right), \\ &= \imath\omega\mu_0 A_0\hat{s}^3\partial_3\left(\exp\left(\imath\frac{x_3}{\hat{s}^2}\right)\partial_2\psi\right), \\ &= E_0\left[\hat{s}^3 \exp\left(\imath\frac{x_3}{\hat{s}^2}\right)\partial_3\partial_2\psi + \imath\hat{s} \exp\left(\imath\frac{x_3}{\hat{s}^2}\right)\partial_2\psi\right]. \end{aligned}$$

If we now substitute (3.12) in these expressions and neglect all terms of order $\hat{s}^2$ and higher, we obtain

$$\begin{aligned} E_1 &= 0, \\ E_2 &= E_0 \exp\left(\imath \frac{x_3}{\hat{s}^2}\right) \psi_0, \\ E_3 &= \imath \hat{s} E_0 \exp\left(\imath \frac{x_3}{\hat{s}^2}\right) \partial_2 \psi_0. \end{aligned}$$

In the original coordinates this finally results in expressions of the electric field components given by

$$E_1 = 0, \tag{3.30}$$

$$E_2 = E_0 \exp(\imath \hat{k} x_3) \psi_0, \tag{3.31}$$

$$E_3 = E_0 \exp\left(\imath \hat{k} x_3\right) \psi_0 \left[-\frac{1}{R(z)} - \frac{2\imath}{\hat{k} w(z)^2} + \frac{2\alpha}{k \hat{k} w(z)^2} \right] x_2, \tag{3.32}$$

where we have used

$$\partial_2 \psi_0 = \psi_0 \left[\frac{\imath \hat{k}}{R(z)} - \frac{2}{w(z)^2} - \frac{2\imath\alpha}{k w(z)^2} \right] x_2.$$

3.1.5 Magnetic field

For the magnetic field components we use (3.5). Since $A_1 = A_3 = 0$ we see directly that $H_2 = 0$. For H_1 we have

$$\begin{aligned} H_1 &= -\partial_3 A_2, \\ &= -\partial_3 \left[A_0 \exp\left(\imath \hat{k} x_3\right) \psi \right], \\ &\rightarrow -\frac{1}{\hat{k} w_0^2} A_0 \partial_3 \left[\exp\left(\imath \frac{1}{\hat{s}} x_3\right) \psi \right], \\ &= -\hat{k} \hat{s}^2 A_0 \left[\imath \frac{1}{\hat{s}^2} \exp\left(\imath \frac{1}{\hat{s}} x_3\right) \psi + \exp\left(\imath \frac{1}{\hat{s}} x_3\right) \partial_3 \psi \right], \\ &= -\imath \hat{k} A_0 \exp\left(\imath \frac{1}{\hat{s}^2} x_3\right) \psi - \hat{k} \hat{s}^2 A_0 \exp\left(\imath \frac{1}{\hat{s}} x_3\right) \partial_3 \psi. \end{aligned}$$

For H_3 we get as results

$$\begin{aligned} H_3 &= \partial_1 A_2, \\ &= \partial_1 \left[A_0 \exp\left(\imath \hat{k} x_3\right) \psi \right], \\ &\rightarrow \frac{1}{w_0} A_0 \exp\left(\imath \frac{1}{\hat{s}^2} x_3\right) \partial_1 \psi, \\ &= \hat{k} \hat{s} A_0 \exp\left(\imath \frac{1}{\hat{s}^2} x_3\right) \partial_1 \psi, \end{aligned}$$

Substitution in (3.12), using (3.29) and neglecting all terms of order $\hat{s}^2$ and higher, we obtain

$$\begin{aligned} H_1 &= -\frac{\hat{k}}{\omega\mu_0} E_0 \exp\left(\imath\hat{k}x_3\right)\psi_0, && (3.33)\\ H_2 &= 0, && (3.34)\\ H_3 &= -\imath\frac{1}{\omega\mu_0} E_0 \exp\left(\imath\hat{k}x_3\right)\partial_1\psi_0. && (3.35) \end{aligned}$$

Substituting the expression

$$\partial_1\psi_0 = \psi_0\left[\frac{\imath\hat{k}}{R(z)} - \frac{2}{w(z)^2} - \frac{2\imath\alpha}{kw(z)^2}\right]x_1,$$

results in the magnetic field components

$$\begin{aligned} H_1 &= -\frac{\hat{k}}{\omega\mu_0} E_0 \exp\left(\imath\hat{k}x_3\right)\psi_0, && (3.36)\\ H_2 &= 0, && (3.37)\\ H_3 &= -\frac{1}{\omega\mu_0} E_0 \exp\left(\imath\hat{k}x_3\right)\psi_0\hat{k}\left[-\frac{1}{R(z)} - \frac{2\imath}{\hat{k}w(z)^2} + \frac{2\alpha}{k\hat{k}w(z)^2}\right]x_1. && (3.38) \end{aligned}$$

3.1.6 Implementation

When implementing these quantities we need to separate the real and imaginary parts. We have

$$\begin{aligned} \psi_0 &= \exp\left[\log(\frac{w_0}{w(z)}) + \imath\hat{k}\frac{\rho^2}{2R(z)} - \frac{\rho^2}{w(z)^2} - \imath\frac{\alpha}{k}\frac{\rho^2}{w(z)^2} - \imath\zeta(z)\right],\\ &= \frac{w_0}{w(z)}\exp\left[-\alpha\frac{\rho^2}{2R(z)} - \frac{\rho^2}{w(z)^2}\right]\exp\left[\imath\left(k\frac{\rho^2}{2R(z)} - \frac{\alpha}{k}\frac{\rho^2}{w(z)^2} - \zeta(z)\right)\right] \end{aligned}$$

We define the quantities

$$B(x_1, x_2, x_3) = E_0\exp(\imath\hat{k}x_3)\psi_0,$$

and

$$\begin{aligned} C(x_1, x_2, x_3) &= -\frac{1}{R(z)} - \frac{2\imath}{\hat{k}w(z)^2} + \frac{2\alpha}{k\hat{k}w(z)^2},\\ &= -\frac{1}{R(z)} - \frac{2(\imath k + \alpha)}{(k^2+\alpha^2)w(z)^2} + \frac{2\alpha(k - \imath\alpha)}{k(k^2+\alpha^2)w(z)^2},\\ &= -\frac{1}{R(z)} - \imath\frac{2}{(k^2+\alpha^2)w(x_3)^2}\left(\frac{\alpha^2}{k} + k\right). \end{aligned}$$

and

$$\begin{aligned} D(x_1,x_2,x_3) &= \hat{k}\left[-\frac{1}{R(z)}-\frac{2\imath}{\hat{k}w(z)^2}+\frac{2\alpha}{k\hat{k}w(z)^2}\right], \\ &= -\frac{\hat{k}}{R(z)}-\frac{2\imath}{w(z)^2}+\frac{2\alpha}{kw(z)^2}, \\ &= -\frac{k}{R(z)}+\frac{2\alpha}{kw(z)^2}-\imath\left[\frac{\alpha}{R(z)}+\frac{2}{w(z)^2}\right], \end{aligned}$$

and assume E_0 is real so that

$$\begin{aligned} \mathrm{Re}\{B\} &= E_0\frac{w_0}{w(z)}\exp\left[-\alpha x_3-\alpha\frac{\rho^2}{2R(z)}-\frac{\rho^2}{w(z)^2}\right]\cos\left(kx_3+k\frac{\rho^2}{2R(z)}-\frac{\alpha}{k}\frac{\rho^2}{w(z)^2}-\zeta(z)\right), \\ \mathrm{Im}\{B\} &= E_0\frac{w_0}{w(z)}\exp\left[-\alpha x_3-\alpha\frac{\rho^2}{2R(z)}-\frac{\rho^2}{w(z)^2}\right]\sin\left(kx_3+k\frac{\rho^2}{2R(z)}-\frac{\alpha}{k}\frac{\rho^2}{w(z)^2}-\zeta(z)\right), \end{aligned}$$

and

$$\begin{aligned} \mathrm{Re}\{C\} &= -\frac{1}{R(z)}, \\ \mathrm{Im}\{C\} &= -\frac{2}{(k^2+\alpha^2)w(x_3)^2}\left(\frac{\alpha^2}{k}+k\right). \end{aligned}$$

Split in real and imaginary parts the fields are then given by

$$\begin{aligned} E_2' &= \mathrm{Re}\{B\}, \\ E_2'' &= \mathrm{Im}\{B\}, \\ E_3' &= (\mathrm{Re}\{B\}\mathrm{Re}\{C\}-\mathrm{Im}\{B\}\mathrm{Im}\{C\})\,x_2, \\ E_3'' &= (\mathrm{Re}\{B\}\mathrm{Im}\{C\}+\mathrm{Im}\{B\}\mathrm{Re}\{C\})\,x_2, \\ H_1' &= -\frac{1}{\omega\mu_0}(k\mathrm{Re}\{B\}-\alpha\mathrm{Im}\{B\}), \\ H_1'' &= -\frac{1}{\omega\mu_0}(\alpha\mathrm{Re}\{B\}+k\mathrm{Im}\{B\}), \\ H_3' &= -\frac{1}{\omega\mu_0}(\mathrm{Re}\{B\}\mathrm{Re}\{D\}-\mathrm{Im}\{B\}\mathrm{Im}\{D\})\,x_1, \\ H_3'' &= -\frac{1}{\omega\mu_0}(\mathrm{Re}\{B\}\mathrm{Im}\{D\}+\mathrm{Im}\{B\}\mathrm{Re}\{D\})\,x_1, \end{aligned}$$

and $E_1 = H_2 = 0$. This is the form of the equations as we will use them in the implementation.

3.1.7 Accuracy

We saw that, by design, the Gaussian beam solution only satisfies the Maxwell equations approximately. To get physically significant results we must ensure that this approximation is accurate enough, and we need some measure to see how well the solution satisfies the equations, and also how accurate the derived quantities are. Since we have determine the Gaussian beam solution by expanding the Maxwell equations around $\hat{s}$, we know that for $|\hat{s}|$ small the solution should satisfy the original equation well. Using (2.102) we can write

$$\hat{s} = \frac{c}{\omega w_0}\frac{1}{\hat{n}} = \frac{\lambda_0}{2\pi w_0 \hat{n}}. \tag{3.39}$$

We can determine what the corresponding requirement for the waist size w_0. We have

$$|\hat{s}| = \frac{\lambda_0}{2\pi w_0}\frac{1}{\sqrt{n^2+\kappa^2}}.$$

For a good approximation we must have $|\hat{s}| \ll 1$, which results in the relation

$$w_0 \gg \frac{\lambda_0}{2\pi}\frac{1}{\sqrt{n^2+\kappa^2}},$$

between the waist size and the wave length.

From (3.18) we see that a larger waist size results in a larger Rayleigh range. We then see from (3.20) that the spot size as function of the direction of propagation gets closer to w_0, its value at the point of focus. This implies that there is less focus in the direction of propagation, so this poses a problem for us. The more accurate we want to model the electromagnetic fields, the less focussing we can have in the direction of propagation. Furthermore, on of the purposes of this project is to see the influence of flows on Rayleigh particles that are captured using optical tweezers, so we need wavelengths that are relatively high compared to the size of these particles, and again for higher wavelengths, the Gaussian beam approximation gets less accurate. This is the reason why in the next section we will develop an external source that satisfies the Maxwell equation exactly, and still had focussing properties.

Since we have the analytic solution, we can in principle determine what the analytic residual will be. Furthermore once we have chosen a grid on which we determine the fields, we can also calculate numerically the residual. We will determine the numerical residual by using central difference schemes for the derivatives in the Maxwell equations.

For the analytical residual, we use (3.2). We first choose a grid with grid points $\mathbf{x}_i$, on which we calculate the analytical expression for all the derivatives of the electric field. Then we determine both the real and imaginary part of the residual, given by

$$\begin{aligned}\mathbf{R}'(\mathbf{x}_i) &= \nabla \times \mathbf{E}'(\mathbf{x}_i) + \omega\mu_0 \mathbf{H}''(\mathbf{x}_i),\\ \mathbf{R}''(\mathbf{x}_i) &= \nabla \times \mathbf{E}''(\mathbf{x}_i) - \omega\mu_0 \mathbf{H}'(\mathbf{x}_i).\end{aligned}$$

Then the scalar residual is given by

$$R(\mathbf{x}_i) = \mathbf{R}'(\mathbf{x}_i)\cdot\mathbf{R}'(\mathbf{x}_i) + \mathbf{R}''(\mathbf{x})_i \cdot \mathbf{R}''(\mathbf{x}_i).$$

This quantity we integrate numerically over the whole domain, where we use a midpoint rule. This results in the total residual

$$R = \sum_{\mathbf{x}_i \in V} R(\mathbf{x}_i) V_i,$$

where V_i is the volume of the corresponding cell. To normalize we determine the norm of the second term of (3.2),

$$N = \omega^2 \mu_0^2 \sum_{\mathbf{x_i} \in V} \left(\mathbf{H}'(\mathbf{x}_i) \cdot \mathbf{H}'(\mathbf{x}_i) + \mathbf{H}''(\mathbf{x}_i) \cdot \mathbf{H}''(\mathbf{x}_i) \right) V_i.$$

The relative residual is then given by

$$R_{\text{rel}} = \sqrt{\frac{R}{N}}.$$

In order to determine $\mathbf{R}'$ and $\mathbf{R}''$, we need the derivatives of $\mathbf{E}'$ and $\mathbf{E}''$ with respect to all the spatial coordinates. Using the expressions derived in the previous section, we can easily determine the derivatives, which results in

$$\begin{aligned}
\partial_1 B' &= -B'' \left[\frac{k x_1}{R(x_3)} - 2\frac{\kappa}{n} \frac{x_1}{w(x_3)^2} \right] - B' \left[\alpha \frac{x_1}{R(x_3)} + \frac{2x_1}{w(x_3)^2} \right], \\
\partial_1 B'' &= B' \left[\frac{k(x_1 - x_0)}{R(x_3)} - 2\frac{\kappa}{n} \frac{(x_1 - x_0)}{w(x_3)^2} \right] - B'' \left[\alpha \frac{(x_1 - x_0)}{R(x_3)} + \frac{2(x_1 - x_0)}{w(x_3)^2} \right], \\
\partial_2 B' &= -B'' \left[\frac{k x_2}{R(x_3)} - 2\frac{\kappa}{n} \frac{x_2}{w(x_3)^2} \right] - B' \left[\alpha \frac{x_2}{R(x_3)} + \frac{2x_2}{w(x_3)^2} \right], \\
\partial_2 B'' &= B' \left[\frac{k(x_2 - y_0)}{R(x_3)} - 2\frac{\kappa}{n} \frac{(x_2 - y_0)}{w(x_3)^2} \right] - B'' \left[\alpha \frac{(x_2 - y_0)}{R(x_3)} + \frac{2(x_2 - y_0)}{w(x_3)^2} \right], \\
\partial_3 B' &= -\frac{1}{w(x_3)} B' \partial_3 w(x_3) + \left[-\alpha - \frac{\alpha \rho^2}{2} \partial_3 R^{-1}(x_3) + \frac{2\rho^2}{w(x_3)^3} \partial_3 w(x_3) \right] B' \\
&\quad - \left[k + k\frac{\rho^2}{2} \partial_3 R^{-1}(x_3) - \frac{2\kappa}{n} \frac{\rho^2}{w(x_3)^3} \partial_3 w(x_3) - \partial_3 \zeta(x_3) \right] B'', \\
\partial_3 B'' &= -\frac{1}{w(x_3)} B'' \partial_3 w(x_3) + \left[-\alpha - \frac{\alpha \rho^2}{2} \partial_3 R^{-1}(x_3) + \frac{2\rho^2}{w(x_3)^3} \partial_3 w(x_3) \right] B'' \\
&\quad + \left[k + k\frac{\rho^2}{2} \partial_3 R^{-1}(x_3) - \frac{2\kappa}{n} \frac{\rho^2}{w(x_3)^3} \partial_3 w(x_3) - \partial_3 \zeta(x_3) \right] B'.
\end{aligned}$$

Substitution in the field expressions derived in the previous section results directly to analytical expressions of the derivatives of the fields, which are used in the next section to calculate the residuals.

Since the electromagnetic field components are accurate up to order $|\hat{s}|$, we expect the analytical approximation of $\mathbf{E}$ and $\mathbf{H}$ to be of order $\mathcal{O}(|\hat{s}|^2)$. In Chapter 6 we will check this by calculating the fields for different parameters.

We will also determine the numerical residual, in exactly the same way. We will check both Maxwell equations (3.1) and (3.2). The rotations are now determined using central differencing, and for the integral we again use a midpoint rule. We expect for wavelengths small compared to

the grid size that the numerical error due to the central differencing will be dominant, while for larger wavelengths, the error will be dominated by the fact that we are using the Gaussian beam approximation. Again we will investigate this in Chapter 6.

3.2 Gaussian dipole array

At the end of Section 3.1 we saw that using the Gaussian beam approximation, we get solutions that do not satisfy the Maxwell equations, and for tighter and tighter focussing this approximation gets worse and worse. In this section we will construct fields that do satisfy the Maxwell equations exactly, and still have highly focussing behaviour. We will construct our external source density as an array of perfect dipoles in a source plane. We orientate these dipoles so that they are proportional to the field of an incoming Gaussian Beam in that source plane. Then, suggested by the Huygens principle, we get a resulting electromagnetic field, mimicking a Gaussian beam. We will use a Green's function method to construct the expressions for the fields. We will first derive the Green's function and its derivatives, and develop expressions for the electric and magnetic fields. Then we will describe how we model our Gaussian type beam.

3.2.1 Green's function

We assume the external current is zero everywhere inside the domain of interest. Then, from (2.96) we have $\nabla \cdot \mathbf{H} = 0$. It is well-known that a divergence-less vector field can be written as the rotation of another vector field, so we can define $\mathbf{A}$ such that

$$\mathbf{H} = \nabla \times \mathbf{A}.$$

Substitution in (2.94) results in

$$\nabla \times (\mathbf{E} - \imath\omega\mu_0\mathbf{A}) = 0,$$

where we have assumed there is no magnetic current density.

It is also well-known that every curl-less vector field can be written as the gradient of a scalar potential, so there exists a scalar function V such that

$$\mathbf{E} - \imath\omega\mu_0\mathbf{A} = -\nabla V. \tag{3.40}$$

Substitution in (2.93) results in

$$-\nabla \times (\nabla \times \mathbf{A}) - \imath\omega\hat{\varepsilon}(\imath\omega\mu_0\mathbf{A} - \nabla V) = -\mathbf{J}^{\text{ext}},$$

or

$$-\nabla(\nabla \cdot \mathbf{A}) + \nabla^2\mathbf{A} + \omega^2\mu_0\hat{\varepsilon}\mathbf{A} + \imath\omega\hat{\varepsilon}\nabla V = -\mathbf{J}^{\text{ext}}.$$

Again we choose the Lorenz gauge, given by (3.7),

$$\nabla \cdot \mathbf{A} = \imath\omega\hat{\varepsilon}V,$$

so that the equation simplifies to

$$\nabla^2\mathbf{A} + \omega^2\mu_0\hat{\varepsilon}\mathbf{A} = -\mathbf{J}^{\text{ext}}.$$

Here we have assumed the permittivity is homogeneous throughout the whole medium. The equation for the potential can now be written as

$$\nabla^2 \mathbf{A} + \hat{k}^2 \mathbf{A} = -\mathbf{J}^{\text{ext}}. \tag{3.41}$$

The electric field is then obtained by substituting (3.7) in (3.40). Rewriting results in

$$\mathbf{E} = \imath\omega\mu_0 \mathbf{A} - \frac{1}{\imath\omega\hat{\varepsilon}} \nabla(\nabla \cdot \mathbf{A}).$$

The fields can now be written as

$$\begin{aligned} \mathbf{E} &= \imath\omega\mu_0 \left[\mathbf{A} + \frac{1}{\hat{k}^2} \nabla(\nabla \cdot \mathbf{A}) \right], & (3.42) \\ \mathbf{H} &= \nabla \times \mathbf{A}. & (3.43) \end{aligned}$$

Taking the Fourier transform of (3.41) results in

$$-(m_1^2 + m_2^2 + m_3^2)\tilde{\mathbf{A}} + \hat{k}^2 \tilde{\mathbf{A}} = -\tilde{\mathbf{J}}^{\text{ext}},$$

where m_i are the spatial Fourier coordinates. Solving for $\tilde{\mathbf{A}}$ results in

$$\tilde{\mathbf{A}} = \frac{1}{\|\mathbf{m}\|^2 - \hat{k}^2} \tilde{\mathbf{J}}^{\text{ext}}.$$

We now formally define the Fourier transform of the Green's function as

$$\tilde{g}(\mathbf{m}) = \frac{1}{\|\mathbf{m}\|^2 - \hat{k}^2}.$$

Given that the inverse exists, the potential is given by taking the inverse Fourier transform,

$$\mathbf{A}(\mathbf{x}) = \int_{\mathbf{y} \in \mathbb{R}^3} g(\mathbf{x} - \mathbf{y}) \mathbf{J}^{\text{ext}}(\mathbf{y}) \, \mathrm{d}V, \tag{3.44}$$

where we have used the convolution theorem. To determine $g(\mathbf{x})$, we perform the inverse integrations explicit in spherical coordinates. We have

$$g(\mathbf{x}) = \frac{1}{(2\pi)^3} \int_{\mathbf{m} \in \mathbb{R}^3} \hat{g}(\mathbf{m}) e^{\imath \mathbf{m} \cdot \mathbf{x}} \, \mathrm{d}V. \tag{3.45}$$

For fixed $\mathbf{x} \neq 0$ we define as basis for m-space a right-handed orthonormal basis $\{\hat{\mathbf{m}}_1, \hat{\mathbf{m}}_2, \hat{\mathbf{m}}_3\}$, such that $\hat{\mathbf{m}}_1 = \frac{\mathbf{x}}{\|\mathbf{x}\|}$. We parameterize the vectors (m_1, m_2, m_3) as

$$\begin{aligned} m_1 &= r\cos\theta, \\ m_2 &= r\sin\theta\cos\phi, \\ m_3 &= r\sin\theta\sin\phi, \end{aligned}$$

with $0 \leq r$, $0 \leq \theta < \pi$ and $0 \leq \phi < 2\pi$. Note that this is just a form of spherical coordinates, with the Jacobian of this transformation given by $J = r^2 \sin\theta$. Furthermore note that

$$\mathbf{x} \cdot \mathbf{m} = \|\mathbf{x}\| \hat{\mathbf{m}}_1 \cdot \mathbf{m} = \|\mathbf{x}\| \hat{\mathbf{m}}_1 \cdot (m_1 \hat{\mathbf{m}}_1) = \|\mathbf{x}\| r\cos\theta,$$

and $\|\mathbf{m}\|^2 = r^2$, so we can write (3.45) as

$$g(\mathbf{x}) = \frac{1}{(2\pi)^3}\int_0^\infty \int_0^\pi \int_0^{2\pi} \frac{1}{r^2 - \hat{k}^2} e^{\imath\|\mathbf{x}\| r\cos\theta}(r^2\sin\theta)\,\mathrm{d}\phi\,\mathrm{d}\theta\,\mathrm{d}r.$$

Performing the integration over ϕ and changing parameter to $y = \cos\theta$ results in

$$g(\mathbf{x}) = \frac{1}{(2\pi)^2}\int_0^\infty \int_{-1}^1 \frac{r^2}{r^2 - \hat{k}^2} e^{\imath\|\mathbf{x}\| ry}\,\mathrm{d}y\,\mathrm{d}r.$$

Performing the integration over y results in

$$\begin{aligned}
\frac{1}{(2\pi)^2}\int_0^\infty \int_{-1}^1 \frac{r^2}{r^2 - \hat{k}^2} e^{\imath\|\mathbf{x}\| ry}\,\mathrm{d}y\,\mathrm{d}r &= \frac{1}{(2\pi)^2}\int_0^\infty \left[\frac{1}{\imath\|\mathbf{x}\| r}\frac{r^2}{r^2 - \hat{k}^2} e^{\imath\|\mathbf{x}\| ry}\right]_{-1}^{1}\mathrm{d}r, \\
&= -\frac{\imath}{(2\pi)^2\|\mathbf{x}\|}\int_0^\infty \frac{r}{r^2 - \hat{k}^2}\left[e^{\imath\|\mathbf{x}\| r} - e^{-\imath\|\mathbf{x}\| r}\right]\mathrm{d}r, \\
&= -\frac{\imath}{(2\pi)^2\|\mathbf{x}\|}\int_{-\infty}^\infty \frac{r}{r^2 - \hat{k}^2} e^{\imath\|\mathbf{x}\| r}\,\mathrm{d}r.
\end{aligned}$$

This final integral can be determined by considering it a complex contour integral around a semi-disk in the upper half of the complex plane, centred around the origin. By using Jordan's lemma and assuming $\hat{k}$ has positive imaginary part, the integral over the semi-circle vanishes in the limit of the radius going to infinity. The only pole in the upper half-plane is at $z_0 = \hat{k}$ where we take the root with positive imaginary part. Using z as complex parameter, we can write the integrand as

$$\frac{z}{(z - z_0)(z + z_0)} e^{\imath\|\mathbf{x}\| z}.$$

Using the residue theorem from complex calculus we then know that

$$\begin{aligned}
\int_{-\infty}^\infty \frac{r}{r^2 - \hat{k}^2} e^{\imath\|\mathbf{x}\| r}\,\mathrm{d}r &= 2\pi\imath \mathrm{Res}\left(\frac{z}{(z - z_0)(z + z_0)} e^{\imath\|\mathbf{x}\| z}, z_0\right), \\
&= 2\pi\imath \lim_{z\to z_0} \frac{z}{z + z_0} e^{\imath\|\mathbf{x}\| z}, \\
&= \imath\pi e^{\imath\|\mathbf{x}\| z_0}.
\end{aligned}$$

This finally results in the expression for the Green's function,

$$g(\mathbf{x}) = \frac{1}{4\pi\|\mathbf{x}\|} e^{\imath\hat{k}\|\mathbf{x}\|}. \tag{3.46}$$

Expressions for the derivatives

In this section we will derive the expressions for the derivatives of the Green's function that we need. Since in (3.44) we have the expression $g(\mathbf{x} - \mathbf{y})$, we will focus on this expression. Note that

the derivatives are taken with respect to $\mathbf{x}$. We define $\mathbf{r} = \mathbf{x} - \mathbf{y}$, and $r = \|\mathbf{x} - \mathbf{y}\|$. The Green's function then becomes

$$g(\mathbf{r}) = \frac{1}{4\pi r} e^{\imath \hat{k} r}.$$

Notice that in Cartesian coordinates

$$\partial_i r = \frac{r_i}{r},$$

or in vector notation,

$$\nabla r = \frac{\mathbf{r}}{r} = \hat{\mathbf{r}}.$$

We now have

$$\partial_i g(\mathbf{r}) = g(\mathbf{r}) \left[\imath \hat{k} - \frac{1}{r} \right] \frac{r_i}{r},$$

or in vector notation

$$\nabla g(\mathbf{r}) = g(\mathbf{r}) \left[\imath \hat{k} - \frac{1}{r} \right] \hat{\mathbf{r}}. \tag{3.47}$$

The second derivatives are given by the symmetric tensor with Cartesian coordinates

$$\begin{aligned} \partial_j \partial_i g(\mathbf{r}) &= g(\mathbf{r}) \frac{r_i r_j}{r^2} \left(\imath \hat{k} - \frac{1}{r} \right)^2 + g(\mathbf{r}) \frac{r^2 \delta_{ij} - r_i r_j}{r^3} \left(\imath \hat{k} - \frac{1}{r} \right) + g(\mathbf{r}) \frac{r_i r_j}{r^4}, \\ &= g(\mathbf{r}) \left[-\hat{k}^2 \frac{r_i r_j}{r^2} + \frac{1}{r^2} \left(3 \frac{r_i r_j}{r^2} - \delta_{ij} \right) + \frac{\imath \hat{k}}{r} \left(\delta_{ij} - 3 \frac{r_i r_j}{r^2} \right) \right], \end{aligned}$$

where we have used the expression

$$\partial_j \hat{r_i} = \frac{r^2 \delta_{ij} - r_i r_j}{r^3}. \tag{3.48}$$

In vector notation we can write this tensor as

$$\nabla \nabla g(\mathbf{r}) = -g(\mathbf{r}) \left[\hat{k}^2 \hat{\mathbf{r}} \otimes \hat{\mathbf{r}} + \frac{\imath \hat{k}}{r} \left(3 \hat{\mathbf{r}} \otimes \hat{\mathbf{r}} - \mathbb{I} \right) - \frac{1}{r^2} \left(3 \hat{\mathbf{r}} \otimes \hat{\mathbf{r}} - \mathbb{I} \right) \right], \tag{3.49}$$

with $\mathbb{I}$ the identity operator.

3.2.2 Perfect dipole

Before focussing on complex external current densities, we will first consider as external source an oscillating perfect electric dipole, given by

$$\mathbf{J}^{\text{ext}}(\mathbf{x}, t) = \delta(\mathbf{x} - \mathbf{x}_{\text{s}}) I_0 \cos(\omega t - \varphi) \hat{\mathbf{d}},$$

with I_0 the strength, φ the phase factor and $\hat{\mathbf{d}}$ the orientation. The orientation $\hat{\mathbf{d}}_i$ determines the polarization of the resulting fields. We see that if we define the complex, time harmonic, external source as

$$\mathbf{J}^{\text{ext}}(\mathbf{x}) = \delta(\mathbf{x}-\mathbf{x}_{\text{s}})I_0 e^{\imath\varphi}\hat{\mathbf{d}}, \tag{3.50}$$

we have

$$\mathbf{J}^{\text{ext}}(\mathbf{x},t) = \text{Re}\left\{\mathbf{J}^{\text{ext}}(\mathbf{x})e^{-\imath\omega t}\right\}.$$

Substituting (3.50) in (3.44) results in the expression for the potential

$$\mathbf{A}(\mathbf{x}) = g(\mathbf{x}-\mathbf{x}_{\text{s}})I_0 e^{\imath\varphi}\hat{\mathbf{d}}. \tag{3.51}$$

For simplicity we will absorb the phase factor φ in the Green's function g, which results in

$$g(\mathbf{r}) = \frac{1}{4\pi r}e^{\imath(\hat{k}r+\varphi)},$$

so that we can write

$$\mathbf{A}(\mathbf{x}) = g(\mathbf{x}-\mathbf{x}_{\text{s}})I_0\hat{\mathbf{d}}. \tag{3.52}$$

Note that this does not alter any of the derivatives. We now define $\mathbf{r} = \mathbf{x}-\mathbf{x}_{\text{s}}$ and $r = \|\mathbf{x}-\mathbf{x}_{\text{s}}\|$. From (3.52) we can derive the electric and magnetic fields. Substituting (3.52) in (3.42) and using (3.49) results in

$$\begin{aligned}
\mathbf{E} &= \imath\omega\mu_0\left[g(\mathbf{r})I_0\hat{\mathbf{d}} + \frac{1}{\hat{k}^2}\nabla(\nabla\cdot(g(\mathbf{r})I_0\hat{\mathbf{d}}))\right], \\
&= \imath\omega\mu_0 I_0\left[g(\mathbf{r})\hat{\mathbf{d}} + \frac{1}{\hat{k}^2}(\hat{\mathbf{d}}\cdot\nabla)(\nabla g(\mathbf{r}))\right], \\
&= \imath\omega\mu_0 I_0 g(\mathbf{r})\left[\hat{\mathbf{d}} - (\hat{\mathbf{d}}\cdot\hat{\mathbf{r}})\hat{\mathbf{r}} - \frac{\imath}{\hat{k}r}\left(3(\hat{\mathbf{d}}\cdot\hat{\mathbf{r}})\hat{\mathbf{r}} - \hat{\mathbf{d}}\right) + \frac{1}{\hat{k}^2r^2}\left(3(\hat{\mathbf{d}}\cdot\hat{\mathbf{r}})\hat{\mathbf{r}} - \hat{\mathbf{d}}\right)\right].
\end{aligned}$$

We want to split this field in a real and imaginary part. First notice that

$$\frac{1}{\hat{k}} = \frac{k-\imath\alpha}{k^2+\alpha^2},$$

and

$$\frac{1}{\hat{k}^2} = \frac{k^2-\alpha^2-2\imath k\alpha}{(k^2+\alpha^2)^2}.$$

The electric field can now be written as

$$\begin{aligned}
\mathbf{E} &= \omega\mu_0 I_0 g(\mathbf{r})\left[\imath\left(\hat{\mathbf{d}} - (\hat{\mathbf{d}}\cdot\hat{\mathbf{r}})\hat{\mathbf{r}}\right) + \left(\frac{1}{\hat{k}r} + \frac{\imath}{\hat{k}^2r^2}\right)\left(3(\hat{\mathbf{d}}\cdot\hat{\mathbf{r}})\hat{\mathbf{r}} - \hat{\mathbf{d}}\right)\right]. \\
&= \omega\mu_0 I_0 g(\mathbf{r})\left[\imath\left(\hat{\mathbf{d}} - (\hat{\mathbf{d}}\cdot\hat{\mathbf{r}})\hat{\mathbf{r}}\right) + \left(\frac{k-\imath\alpha}{(k^2+\alpha^2)r} + \frac{\imath(k^2-\alpha^2)+2k\alpha}{(k^2+\alpha^2)^2r^2}\right)\left(3(\hat{\mathbf{d}}\cdot\hat{\mathbf{r}})\hat{\mathbf{r}} - \hat{\mathbf{d}}\right)\right]
\end{aligned} \tag{3.53}$$

Splitting in a real and imaginary part results in

$$\mathbf{E}' = -\omega\mu_0 I_0 \left(g''\mathbf{v}_1 - (c_1 g' + c_2 g'')\,\mathbf{v}_2\right), \tag{3.54}$$
$$\mathbf{E}'' = \omega\mu_0 I_0 \left(g'\mathbf{v}_1 + (c_1 g'' - c_2 g')\,\mathbf{v}_2\right), \tag{3.55}$$

where we have defined the vectors

$$\begin{aligned}\mathbf{v}_1 &= \hat{\mathbf{d}} - (\hat{\mathbf{d}}\cdot\hat{\mathbf{r}})\hat{\mathbf{r}},\\ \mathbf{v}_2 &= 3(\hat{\mathbf{d}}\cdot\hat{\mathbf{r}})\hat{\mathbf{r}} - \hat{\mathbf{d}},\end{aligned}$$

and the scalars

$$\begin{aligned}c_1 &= \frac{k}{(k^2+\alpha^2)r} + \frac{2k\alpha}{(k^2+\alpha^2)^2 r^2},\\ c_2 &= \frac{\alpha}{(k^2+\alpha^2)r} - \frac{k^2-\alpha^2}{(k^2+\alpha^2)^2 r^2}.\end{aligned}$$

For the magnetic field we substitute (3.52) in (3.43) and use (3.47), which results in

$$\begin{aligned}\mathbf{H} &= I_0 \nabla g(\mathbf{r}) \times \hat{\mathbf{d}},\\ &= I_0 \left(g(\mathbf{r})\left[\imath\hat{k} - \frac{1}{r}\right]\hat{\mathbf{r}}\right) \times \hat{\mathbf{d}},\\ &= I_0 g(\mathbf{r}) \left(\imath\hat{k} - \frac{1}{r}\right)\hat{\mathbf{r}} \times \hat{\mathbf{d}}.\end{aligned} \tag{3.56}$$

Splitting in real and imaginary part we get as expression for the magnetic field

$$\mathbf{H}' = -I_0 \left(\left(\alpha + \frac{1}{r}\right) g' + k g''\right)\hat{\mathbf{r}} \times \hat{\mathbf{d}}, \tag{3.57}$$
$$\mathbf{H}'' = -I_0 \left(\left(\alpha + \frac{1}{r}\right) g'' - k g'\right)\hat{\mathbf{r}} \times \hat{\mathbf{d}}. \tag{3.58}$$

So we now have expressions for the electric and magnetic field of a perfect dipole, which satisfy the Maxwell equations exactly.

3.2.3 Gaussian source plane as array of dipoles

In the previous section we constructed a simple exact solution for the Maxwell equations. We can now use this solution to construct more interesting fields, by using the superposition principle. We can place multiple perfect dipoles at different spatial locations, and we know by linearity of the Maxwell equations that the total electromagnetic field will be the sum of the partial fields. It is important to notice that is it only the fields that can be added, not the derived quantities

such as the heat dissipation or the Poynting vector. To determine these we first determine the total electromagnetic field and then calculate the derived quantity. We will work with the vector potential, using (3.44). Once we have determined the vector potential for our solution, we can easily calculate the electric and magnetic fields by (3.42) and (3.43).

For an arbitrary external electric current density $\mathbf{J}^{\text{ext}}(\mathbf{x})$, we have

$$\mathbf{A}(\mathbf{x}) = \int_D g(\mathbf{x}-\mathbf{y})\mathbf{J}^{\text{ext}}(\mathbf{y})\,\mathrm{d}y, \tag{3.59}$$

where D is the region where the current density is non-zero. We assume we are interested in the field values at locations $\mathbf{x}$, so that $r = \|\mathbf{x}-\mathbf{y}_i\|$ is not too small, that is, we look at points not too close to the source region. In this case we do not need to take care of the singularity in the Green's function. Since the Green's function contains a factor $\exp \imath kr$, it also oscillates over D, so when discretizing (3.59), we have to make sure our grid is fine enough. Furthermore the spatial variation of the current density have to be taken into account when determining the grid size. We will approximate the integral by using the second order midpoint scheme. If we divide the volume D in cells with label i, and denote the volume V_i and centres $\mathbf{y}_i$, we can approximate the integral as

$$\mathbf{A}(\mathbf{x}) \approx \sum_i g(\mathbf{x}-\mathbf{y}_i)\mathbf{J}^{\text{ext}}(\mathbf{y}_i)V_i, \tag{3.60}$$

where $\mathbf{x}$ is the fixed point where we want to determine the field values.

We now have to determine the current density to use. We will apply the same idea behind the Huygens-Fresnel principle, which says that the fields of a propagating wave are equal to the superposition of the fields resulting of point sources in a plane through which the wave front travels. We will use this principle, by choosing a source plane, through which the beam enters. Then we use the Gaussian beam approximation to determine the electric field components in this plane, and we use as external electric currents point sources that are proportional to the (complex) field values at those point. Mathematically, we choose a plane S, orthogonal to the direction of propagation, which in Section 3.1 was the z direction, so for each vector $\mathbf{y} \in S$, we have $z = z_{\text{s}}$, where s is the subscript for the source. We will denote the center of the beam in the source plane as $\mathbf{x}_{\text{s}} = (x_{\text{s}}, y_{\text{s}}, z_{\text{s}})$.

Using (3.30) and the proportionality requirement we can thus write the external electric current density as

$$\begin{aligned} J_1 &= 0, \\ J_2 &\propto \exp(\imath\hat{k}z)\psi_0, \\ J_3 &\propto \exp\left(\imath\hat{k}z\right)\psi_0\left(-\frac{1}{R(z)} - \frac{2\imath}{\hat{k}w(z)^2} + \frac{2\alpha}{k\hat{k}w(z)^2}\right)y. \end{aligned}$$

We will determine the strength of the currents not directly, but through a normalization procedure as described in Section 5.1.1. Since $z = z_{\text{s}}$ is fixed, we only have to consider factors depending on x and y. It is essential that we look at the complex field values, because in general the different components do not have to be in phase with each other. Using (3.25) we have

$$\psi_0 \propto \exp\left(-\frac{\rho^2}{w(z_{\text{s}}-z_{\text{f}})^2} + \imath\hat{k}\frac{\rho^2}{2R(z_{\text{s}}-z_{\text{f}})} - \imath\frac{\alpha}{k}\frac{\rho^2}{w(z_{\text{s}}-z_{\text{f}})^2}\right),$$

where we have substituted $z = z_s - z_f$, the (oriented) distance between the source plane and the focal plane and $\rho^2 = (x - x_s)^2 + (y - y_s)^2$, with (x_s, y_s) the axial line through the center of the beam. If we now define complex parameters $\hat{\beta}$ and $\hat{\gamma} = \hat{\gamma}(\rho)$ such that

$$\begin{aligned}
\hat{\beta} &= -\frac{1}{R(z_s - z_f)} - \frac{2\imath}{\hat{k}w(z_s - z_f)^2} + \frac{2\alpha}{k\hat{k}w(z_s - z_f)^2}, \\
&= -\frac{1}{R(z_s - z_f)} - \imath\frac{2}{kw(z_s - z_f)^2}, \qquad (3.61) \\
\hat{\gamma} &= \exp\left(-\frac{\rho^2}{w(z_s - z_f)^2} + \imath\hat{k}\frac{\rho^2}{2R(z_s - z_f)} - \imath\frac{\alpha}{k}\frac{\rho^2}{w(z_s - z_f)^2}\right), \qquad (3.62)
\end{aligned}$$

we can write $J_2^{\text{ext}} \propto \hat{\gamma}$ and $J_3^{\text{ext}} \propto \hat{\gamma}\hat{\beta}y$. Note that although $\hat{\gamma}$ occurs in both components, we can not divide by it, because of the dependence on ρ. Denoting the normalization constant as I_0, we can write the external current as

$$\begin{aligned}
J_1^{\text{ext}} &= 0, \\
J_2^{\text{ext}} &= \hat{\gamma}I_0\delta(z - z_s), \\
J_3^{\text{ext}} &= \hat{\gamma}\hat{\beta}(y - y_s)I_0\delta(z - z_s),
\end{aligned}$$

where the δ function reflects that the source only acts in a plane. Substitution in (3.59) and applying the discretization that has lead to (3.60) results in the discretized expresions for the vector potential,

$$\begin{aligned}
A_1 &= 0, \\
A_2 &= I_0 \sum_i \hat{\gamma}_i g(\mathbf{x} - \mathbf{y}_i), \\
A_3 &= I_0\hat{\beta} \sum_i (y_i - y_s)\hat{\gamma}_i g(\mathbf{x} - \mathbf{y}_i),
\end{aligned}$$

where the δ function is taken into account by fixing $z = z_s$ in the integration vector $\mathbf{y}$, changing from a volume integral to an area integral and we added a subscript to $\hat{\gamma}$ to denote its dependency on ρ. Furthermore we have assumed the cells are of equal area, and absorbed this into the I_0 parameter, which will be normalized by the procedure explained in Section 5.1.1. So for our final discretized vector potential we can write

$$\mathbf{A}(\mathbf{x}) = I_0 \sum_{i=1}^{n} \hat{\gamma}_i g(\mathbf{x} - \mathbf{y}_i) \left[\hat{\mathbf{y}} + \hat{\beta}(y_i - y_s)\hat{\mathbf{z}}\right], \qquad (3.63)$$

where $\hat{\mathbf{y}}$ and $\hat{\mathbf{z}}$ are the standard unit basis vectors. If we compare the expression for this vector potential with (3.51) we see that it is a superposition of perfect dipoles, with two dipoles with orthogonal orientation for each source vector $\mathbf{y}_i$. This means that in order to determine the vector potential, and the resulting electric and magnetic fields, we can directly use the expressions derived in Section 3.2.2, substituting $I_0 e^{\imath\varphi}\hat{\mathbf{d}} = I_0\hat{\gamma}_i\hat{\mathbf{y}}$ and $I_0 e^{\imath\varphi}\hat{\mathbf{d}} = I_0\hat{\gamma}_i\hat{\beta}y\hat{\mathbf{z}}$, for the y and z component respectively.

We still need to address the discretization domain. We will assume the domain is a square patch in the source plane, centred around $\mathbf{x}_s = (x_\mathrm{s}, y_\mathrm{s}, z_\mathrm{s})$ and having length L in both directions. The dimensions of this square are determined by how fast the amplitude of the external current density decays. Since I_0 is constant on the whole domain we ignore its values, since it is the relative contribution we are interested in. The amplitude for the y component is then given by $|\hat{\gamma}|$. For the z component we have $|\hat{\beta}||\hat{\gamma}|y$. From (3.62) it is easily seen that

$$|\hat{\gamma}| = \exp\left(-\frac{\rho^2}{w(z_\mathrm{s}-z_\mathrm{f})^2} - \alpha\frac{\rho^2}{2R(z_\mathrm{s}-z_\mathrm{f})}\right),$$

so the coefficient decays exponentially in ρ^2, which means the amplitude for the y component is a decreasing function for all ρ. For the z component special care is needed because of the factor y. Of course we know because of the exponential decay eventually the amplitude starts decreasing. For fixed y we again have exponential decay in $|x - x_\mathrm{s}|^2$ for all x. In the y direction the amplitude will initially grow towards a maximum after which it starts decaying. It is important that our domain contains this maximum. In order to determine the location we calculate the partial derivative with respect to y. We have

$$\begin{aligned}\frac{\partial}{\partial y}\left(|\hat{\beta}||\hat{\gamma}|y\right) &= |\hat{\beta}|\left(\frac{\partial|\hat{\gamma}|}{\partial y}y + |\hat{\gamma}|\right)\\ &= |\hat{\beta}||\hat{\gamma}|\left(1 - \frac{2y^2}{w(z_\mathrm{s}-z_\mathrm{f})^2}\right).\end{aligned}$$

At the maximum this partial derivative will equal zero, so we have

$$y = y_\mathrm{max} = \frac{1}{\sqrt{2}}w(z_\mathrm{s} - z_\mathrm{f}).$$

For $y > y_\mathrm{max}$ the amplitude will again be a decreasing function of ρ, so we will always choose the length of the source domain such that

$$L > 2y_\mathrm{max} = \sqrt{2}w(z_\mathrm{s} - z_\mathrm{f}). \tag{3.64}$$

The amplitudes depend on both w_0 and $z_\mathrm{s} - z_\mathrm{f}$. To determine a specific value of L, we choose a tolerance $0 < \epsilon_\mathrm{s} < 1$. Now we will choose L such that the relative amplitudes in both directions are smaller than this tolerance, that is, we have $|\hat{\gamma}| < \epsilon_\mathrm{s}$ and $|\hat{\beta}||\hat{\gamma}|\frac{L}{2} < \epsilon_\mathrm{s}$, in addition to (3.64). We will always choose $\epsilon_\mathrm{s} = 0.001$ except when stated otherwise. Such a small value will ensure that extending the source domain will not lead to significantly changing the resulting fields. Using this approach, we choose the model the complete Gaussian source beam. It could be that in a experimental situation, the incoming beam is larger than the aperture on which it is pointed, in which case it would be more suitable to cut off the source domain at the appropriate value, so that the modelled fields will approach the physical ones more closely, introducing side lobes from the edge of the aperture. We will not use this approach here and we will model the complete beam.

Finally we have to make sure the discretization of the grid is fine enough. We already noticed that the Green's function oscillates. This is due to the complex exponential $\exp(\imath kr)$. When evaluating the integral over the source plane, $\mathbf{x}$ is considered constant, so the period of oscillation depends on how r varies over the source plane with respect to this fixed $\mathbf{x}$. In the limiting case

$z \to z_\mathrm{s}$ the component of $\mathbf{r}$ outside the source plane will tend to zero, and we see that r will approach ρ, resulting in a factor $\exp(\imath k\rho)$, which oscillates in the source plane with period $\frac{2\pi}{k}$. This gives a lower bound for the period.

From 3.62) we see that the external current density will also oscillate over the source plane, due to the complex exponential

$$\exp\left[\imath\left(k\frac{\rho^2}{2R(z_\mathrm{s}-z_\mathrm{f})}-\frac{\alpha}{k}\frac{\rho^2}{w(z_\mathrm{s}-z_\mathrm{f})^2)}\right)\right].$$

We see that the period increases for increasing ρ, so by fixing L, the size of the source domain, we implicitly fix some lower bound for this period.

We will not further analyse this oscillating behaviour analytically. Instead, in Chapter 6 we will show the consequences of different grid sizes for the source domain, and we will quantitative estimate the errors involved, to make sure we will choose a grid fine enough for the simulations.

Chapter 4

Navier-Stokes equations

In this chapter we will outline the different equations governing the flow of a fluid. All the equations follow from the different conservation laws. In particular we use the conservation of mass, linear momentum, angular momentum and energy.

We have $\mathbf{v}$ the velocity of the fluid, which in general is a function of position and time, so $\mathbf{v} = \mathbf{v}(\mathbf{x}, t)$. We will now determine the equations for $\mathbf{v}$ in terms of the material properties and other variables.

4.1 Conservation of mass

For the fluid in motion we assume that mass is (locally) conserved. From [2] we have the continuity equation given by

$$\frac{\partial \rho}{\partial t} + \operatorname{div}(\rho \mathbf{v}) = 0, \tag{4.1}$$

where $\rho(\mathbf{x}, t)$ is the mass density and $\mathbf{v}(\mathbf{x}, t)$ the velocity of the fluid. In subscript notation this becomes

$$\partial_t \rho + \partial_j(\rho v_j) = 0. \tag{4.2}$$

Expanding the differentiation results in

$$\partial_t \rho + \rho \partial_j v_j + v_j \partial_j \rho = 0. \tag{4.3}$$

This equation can be simplified using certain assumptions on the flow, such as incompressibility. If we introduce the operator

$$\frac{\mathrm{D}}{\mathrm{D}t} = \frac{\partial}{\partial t} + \mathbf{v} \cdot \nabla, \tag{4.4}$$

called the material derivative, we can write the continuity equation as

$$\frac{1}{\rho}\frac{\mathrm{D}\rho}{\mathrm{D}t} = -\operatorname{div} \mathbf{v}. \tag{4.5}$$

The material derivative is the derivative along the path of a fluid particle. It can be applied to field variables, that is variables that are functions of $\mathbf{u}$ and t. In subscript notation we will write D_t, so we can write

$$\frac{1}{\rho}\mathrm{D}_t\rho = -\partial_i v_i. \tag{4.6}$$

We see that if the material derivative of the mass density is zero, the divergence of the velocity vanishes.

4.2 Conservation of (linear) momentum

Using conservation of (linear) momentum and following the derivation from [2], we arrive at the general expression for conservation of linear momentum,

$$\rho\mathrm{D}_t v_i = \partial_j T_{ij} + f_i^{\mathrm{b}}, \tag{4.7}$$

where $f_i^{\mathrm{b}}(\mathbf{x}, t)$ is the volumetric body force density and T_{ij} the stress tensor.

Writing out the material derivative results in

$$\rho\left(\partial_t v_i + v_j\partial_j v_i\right) = \partial_j T_{ij} + f_i^{\mathrm{b}}. \tag{4.8}$$

We have to determine the relation between the stress tensor and the other quantities that describe the flow of the fluid. First of all we write the stress tensor as the sum of an isotropic part and a non-isotropic part

$$T_{ij} = -p\delta_{ij} + T'_{ij}, \tag{4.9}$$

with p the mechanical pressure and T'_{ij} the non-isotropic part of the stress tensor or the deviatoric stress tensor. If we consider the fluid to be a Newtonian fluid, the deviatoric stress tensor can be written as

$$T'_{ij} = 2\mu\left(e_{ij} - \frac{1}{3}\Delta\delta_{ij}\right), \tag{4.10}$$

where μ is the dynamic viscosity, e_{ij} is given by

$$e_{ij} = \frac{1}{2}\left(\partial_j u_i + \partial_i u_j\right),$$

and $\Delta = e_{kk} = \partial_k v_k$, with summation over k implied. In general the dynamic viscosity is a function of the temperature.

Substitution of (4.10)and (4.9) in (4.8) results in

$$\begin{aligned}
\rho\left(\partial_t v_i + v_j\partial_j v_i\right) &= \partial_j\left[-p\delta_{ij} + 2\mu\left(e_{ij} - \frac{1}{3}\Delta\delta_{ij}\right)\right] + f_i^{\mathrm{b}}, \\
&= -\partial_i p + 2\partial_j(\mu e_{ij}) - \frac{2}{3}\partial_i(\mu\Delta) + f_i^{\mathrm{b}}, \\
&= -\partial_i p + \partial_j\left(\mu\left(\partial_j v_i + \partial_i v_j\right)\right) - \frac{2}{3}\partial_i(\mu\partial_j v_j) + f_i^{\mathrm{b}}.
\end{aligned}$$

This is the most general form for Newtonian fluids. If we assume temperature differences are small, then the viscosity is homogeneous and can be taken out of the derivatives. This results in the simpler form

$$\rho\left(\partial_t v_i + v_j \partial_j v_i\right) = -\partial_i p + \mu \partial_j^2 v_i + \frac{1}{3}\mu \partial_i (\partial_j v_j) + f_i^{\mathrm{b}}, \tag{4.11}$$

where we have interchanged the order of differentiation to combine two terms.

A final important simplification is to consider the flow incompressible. This means that the material derivative of the mass density of the fluid is zero. From (4.6) it follows directly that

$$\partial_i v_i = 0.$$

If we substitute this in (4.11) we have as result the incompressible Navier-Stokes equations with constant viscosity,

$$\rho\left(\partial_t v_i + v_j \partial_j v_i\right) = -\partial_i p + \mu \partial_j^2 v_i + f_i^{\mathrm{b}}. \tag{4.12}$$

We can write this slightly different if we use

$$v_j \partial_j v_i = \partial_j (v_j v_i) - v_i \partial_j v_j = \partial_j (v_j v_i).$$

The result then is

$$\rho\left(\partial_t v_i + \partial_j (v_j v_i)\right) = -\partial_i p + \mu \partial_j^2 v_i + f_i^{\mathrm{b}}. \tag{4.13}$$

In general the Navier-Stokes equation together with the continuity equation are four equations in five unknowns, v_i, ρ and p, so our system is not complete yet. In the incompressible case, the equation $\mathrm{D}_t \rho = 0$ is this final equation. When we consider compressible flow we need to take into account an energy equation and a thermodynamic relation too. We will consider incompressible flow throughout this work, but since we do expect there to be heating in the fluid we need these extra equations, to take care of the heat dissipation.

4.3 Conservation of energy

When the fluid contains heat sources, and heat transfer plays a role we have to take conservation of energy into account. In general we define the total energy density as the sum of the internal energy and the kinetic energy,

$$E = \rho\left(e + \frac{1}{2} v_i v_i\right), \tag{4.14}$$

with e the specific internal energy (per unit mass). Since we assume our fluid is incompressible, additional heat will have no effect on the density, and we consider only the internal energy. Of course under this assumption there will be no interaction between the internal and kinetic energy at all, but in order to investigate whether heat driven currents exists we need a heat equation. Further details can be found in Section 4.4. The specific internal energy can be written as

$$e = c_{\mathrm{p}} T,$$

where in general c_p is a function of T. We assume that the temperature differences will be small, so that we can assume c_p is constant.

If we consider a control volume V we can then write for the internal energy,

$$\frac{\mathrm{d}}{\mathrm{d}t}\int_V \rho c_\mathrm{p} T \,\mathrm{d}V = -\int_S \rho c_\mathrm{p} T v_i \hat{n}_i \,\mathrm{d}A + Q. \tag{4.15}$$

The first term on the right-hand side is the convection term, in the second term Q is the sum of the heat source and heat flux through the surface of the control volume. We can write Q as

$$Q = \int_V q \,\mathrm{d}V - \int_S q_i^* \hat{n}_i \,\mathrm{d}A, \tag{4.16}$$

with q the heat source density and q_i^* the heat flux. For the heat flux we use Fourier's law,

$$q_i^* = -k\partial_i T,$$

with $k \geq 0$ the heat conduction coefficient. In general $k = k(T)$, but we assume the temperature differences are small enough to consider k constant.

If we substitute (4.16) in (4.15), interchanging the integration and differentiation in (4.15) and apply the divergence theorem, we get the integral heat equation

$$\int_V \partial_t(\rho c_\mathrm{p} T)\,\mathrm{d}V = -\int_V \partial_i(\rho c_\mathrm{p} T v_i)\,\mathrm{d}V + \int_V \partial_i(k\partial_i T)\,\mathrm{d}V + \int_V q\,\mathrm{d}V.$$

Since we have chosen V arbitrarily, the integrands have to be equal. Taking out the constant parameters and using the incompressibility results in the heat equation,

$$\rho c_\mathrm{p}\partial_t T = -\rho c_\mathrm{p} v_i \partial_i T + k\partial_i^2 T + q. \tag{4.17}$$

This is the heat equation we will work with.

4.4 Boussinesq approximation

Since we have a heat source density q generally not equal to zero, it is possible that temperature differences might lead to small currents, under the influence of gravity. This effect called natural convection is small for small temperature differences, but since we expect our external electromagnetic forces to be small too, we want to take them into account so that we can investigate which effect is dominant for different electromagnetic properties. In order to achieve this we use the Boussinesq approximation.

In general when gravity is taken into account, we have as one of the body forces ρg_i, with g_i the gravity acceleration. In the Boussinesq approximation, we assume the density is constant in all the terms, except this one. Following [13] and [5] we write the density and the temperature as the difference between a reference value and a small deviation, $\rho = \rho_0 + \rho'$ and $T = T_0 + T'$. Since ρ' is small, we can write it as

$$\rho' = \left(\frac{\partial \rho_0}{\partial T}\right)_p T' = -\rho_0 \beta T',$$

with β the thermal expansion coefficient. Using this expression we have for the density the expression

$$\rho = \rho_0 \left(1 - \beta(T - T_0)\right). \tag{4.18}$$

We now define the modified pressure as

$$p' = p + \rho g x_2, \tag{4.19}$$

where we assume gravity works in the negative x_2 direction. Substitution in the two important terms of the left-hand side of the momentum equation results in

$$-\partial_i p - \rho g \hat{x}_2 = -\partial_i (p' - \rho g x_2) - \rho g \hat{x}_2 = -\partial_i p' + \rho g \hat{x}_2 + g x_2 \partial_i \rho - \rho g \hat{x}_2 = -\partial_i p' + g x_2 \partial_i \rho.$$

Substitution in (4.13) results in the modified Navier-Stokes equation

$$\rho_0 \left(\partial_t v_i + \partial_j (v_j v_i)\right) = -\partial_i p' + g x_2 \partial_i \rho + \mu \partial_j^2 v_i + f_i^{\mathrm{b}}, \tag{4.20}$$

where from f_i^{b} gravity is now excluded.

In [5] it is stated that for water the errors introduced by using this approximation are approximately 1% for temperatures differences of 2 K or smaller. For larger differences this error grows, and the solutions can even become qualitatively different. This is important to keep in keep, and we always have to check whether we are still in the domain of validity of this approximation.

4.5 Steady-state equations

We have derived a number of conservation equations and other relations that govern the flow of the fluid. Also we made a number of assumptions on our fluid and flow. In particular we assume the density is constant and equal to ρ_0. We will now state the final equations that we will use to determine the steady-state flows in our fluid. As a consequence, the partial time derivatives are equal to zero. From (4.2), (4.20) and (4.17) we have

$$\begin{aligned}
\partial_i v_i &= 0, && (4.21)\\
\rho_0 v_j \partial_j v_i &= -\partial_i p' + g x_2 \partial_i \rho + \mu \partial_j^2 v_i + f_i^{\mathrm{em}}, && (4.22)\\
\rho_0 c_{\mathrm{p}} v_i \partial_i T &= k \partial_i^2 T + q_{\mathrm{em}}, && (4.23)
\end{aligned}$$

with the modified pressure p' given by (4.19) and the variable density by (4.18). Furthermore we have identified the heat source and the body force with the expression from (2.109) and (2.108). If we divide the second equation by ρ_0 we see we get as coefficient for the viscous term

$$\nu = \frac{\mu}{\rho_0}.$$

This quantity is called the kinematic viscosity, and is it usually stated in the literature.

4.6 Boundary conditions

In order to solve the equations stated earlier we need boundary conditions for the velocity and temperature. Information about the boundary conditions can be found in [5]. For the velocity at a solid boundary there are two common possibilities. In the inviscid case we assume the velocity is parallel to the boundary, that is, no fluid particle penetrates the boundary,

$$\mathbf{v} \cdot \hat{\mathbf{n}} = 0,$$

with $\hat{\mathbf{n}}$ the unit normal vector. In case of a viscous fluid, we assume the no-slip boundary condition, which says that the fluid 'sticks' to the boundary and its velocity is zero,

$$\mathbf{v} = 0.$$

This boundary condition we will use for the simulations.

For the temperature we can either assume the boundary is perfectly insulated, so that the normal derivative of the temperature is zero, or that a certain heat flux is present. The latter is implemented by using a reference temperature and possibly a certain heat coefficient, modelling the walls heat properties.

For boundaries where fluid is allowed to cross we need different boundary conditions. The most common situation we will consider is a domain with an inflow and an outflow boundary. At the inflow we prescribe a certain velocity and temperature. At the outflow we assume the normal gradient of these quantities is zero.

Notice that we did not specify the pressure. The value of the pressure will usually follow from the equations. In case that the velocity at an inflow is not known we can prescribe the pressure. The velocity at the boundary then follows from the equations.

4.7 Discrezation and the SIMPLE algorithm

In order to solve our system of equations we need to discretize the equations and use an algorithm to obtain the steady-state solutions of the different quantities. The two difficulties are that the momentum equation is non-linear, and coupled with the pressure. The non-linearity will be solved by using the velocity field of the previous iteration for one of the terms. The coupling of the pressure is handled by using the momentum equation to determine a predictor of the velocity field and solving the pressure equation to determine the pressure field, and create a correction for the velocity field which obeys the continuity equation. Since we are interested in steady-state solutions we will use the SIMPLE (Semi-Implicit Method for Pressure Linked Equations) algorithm, which is described in [15]. Details about the implementation used can be found in [10]. We will give an overview of the procedure.

First a prediction is made for the velocity components, by solving the momentum equation. Than this prediction is used to determine a new temperature and density field. Using these predicted fields, the pressure field is determined by solving a pressure equation, and using the new pressure field, the velocity field is corrected so that it is divergence free, and the continuity equation is satisfied. This procedure is iterated until certain conditions are met, which in practice means the residuals of all the fields involved are smaller than a certain tolerance.

We will use an equidistant rectangular co-located grid. Quantities in the centre of a control volume have the superscript c, where as quantities in the centre of the faces have the superscript f.

To obtain quantities at the face centres, second order linear interpolation is used. For differentiation we use the second order central differencing.

The whole procedure starts with a initial pressure field and velocity field, for example uniform.

4.7.1 Momentum equation

The predicted velocity is determined by solving the discretized momentum equation (4.22). The whole equation is divided by ρ_0. We integrate both sides over the control volume. For the flux terms the divergence theorem is applied. For the right-hand side term we get

$$\int_V v_j \partial_j v_i \,\mathrm{d}V = \int_V \partial_j (v_j v_i) \,\mathrm{d}V = \int_S v_j v_i \hat{n}_j \,\mathrm{d}S \approx \sum A_j v_i^{\mathrm{f}} v_j^{\mathrm{f}} \hat{n}_j^{\mathrm{f}},$$

with A_j the area of the corresponding face. For v_j we use the velocity field of the previous iteration. For the viscous term we write $\nu = \frac{\mu}{\rho_0}$ and we get

$$\nu \int_V \partial_j^2 v_i \,\mathrm{d}V = \nu \int_S \partial_j v_i \hat{n}_j \,\mathrm{d}S \approx \nu \sum A_j (\partial_j v_i)^{\mathrm{f}} \hat{n}_j^{\mathrm{f}}.$$

The quantity in parentheses is determined using central differencing with the values in neighbouring cell centres. For the external force term, the electromagnetic force, we use a second order mid-point scheme, so that

$$\frac{1}{\rho_0} \int_V f_i^{\mathrm{em}} \,\mathrm{d}V \approx \frac{V}{\rho_0} \cdot (f_i^{\mathrm{em}})^{\mathrm{c}},$$

with V the volume of the control volume. For the pressure term and the extra buoyancy term special care is needed. If we would determine the gradient using the scheme

$$\int_V \partial_i \phi \,\mathrm{d}V = \int_S \phi \hat{n}_i \,\mathrm{d}A \approx \sum_{j=1}^{6} A_j \phi_j^{\mathrm{f}} (\hat{n}_i)_j^{\mathrm{f}},$$

and use linear interpolation for ϕ_j^{f} we see that because the $(\hat{n}_i)_j^{\mathrm{f}}$ are oriented in opposite direction for faces with the same orientation, the contribution of ϕ^{c} cancels. This decoupling can lead to so-called checker board oscillations. See [15] for more details. The solution we use is to use so-called Rhie and Chow interpolation [18], where the gradient value in the cell centre is determined as a weighted average of the estimated values on the cell faces,

$$\int_V \partial_i \phi \,\mathrm{d}V \approx \frac{V}{A} \sum_{j=1}^{6} A_j (\partial_i \phi)_j^{\mathrm{f}},$$

where A is the summed area of the faces. The $(\partial_i \phi)_j^{\mathrm{f}}$ terms are determined with linear interpolation between the value in the control volume and the different neighbouring volumes.

All the terms of the momentum equations are now described, and we can assemble the whole system in the matrix system

$$C^k \mathbf{v}^k = \mathbf{r}^k,$$

where the coefficients of C^k depend on $\mathbf{v}^{k-1}$ and the coefficients of $\mathbf{r}^k$ on p^{k-1} and ρ^{k-1}.

This equation is solved iteratively. We use a diagonal incomplete-LU preconditioned bi-conjugate gradient method. We iterate until the residual is smaller than a certain tolerance. For the exact definition of the residual, and the normalisation see ([10] page 173-181). This gives a prediction of the velocity field.

4.7.2 Energy equation

The energy equation resembles the momentum equation almost completely. Both are forms of a more general transport equation. As a result the numerical treatment is almost equal. The equation is divided by $\rho_0 c_\mathrm{p}$, and rewriting results in

$$\partial_i(v_i T) = \frac{k}{\rho_0 c_\mathrm{p}} \partial_i^2 T + \frac{1}{\rho_0 c_\mathrm{p}} q_\mathrm{em}.$$

The convective term on the left-hand side is handled exactly as the convective term in momentum equation, where for the velocity field the values of the previous iteration are used, so that continuity is assured. Furthermore the conductive term is also implemented the same way as the viscous term in the momentum equation. The source term is approximated by a second order mid-point scheme, like the external force term in the momentum equation. This results in a matrix equation

$$A^k \mathbf{T}^k = \mathbf{s}^k,$$

where again the coefficient of the matrix A^k depends on the solution of the velocity field at the previous iteration, $\mathbf{v}^{k-1}$. Again we use a diagonal incomplete-LU preconditioned bi-conjugate gradient method so solve the system.

From the new temperature field we can determine the updated density using (4.18).

4.7.3 Pressure equation

After solving the velocity predictor we can now determine the new pressure field. We write the momentum equation in the semi-discretized form

$$A\mathbf{v} = -\nabla \mathbf{p}' + \mathbf{f}.$$

We now split A in the diagonal and non-diagonal part and write for the corrected velocity field $\tilde{\mathbf{v}}$ and substitute the corrected field, resulting in

$$D\mathbf{v}' + B\mathbf{v} = -\nabla \mathbf{p}' + \mathbf{f}.$$

Since D is diagonal the inverse is simple and we can solve for $\mathbf{v}'$, resulting in

$$\mathbf{v}' = -D^{-1}B\mathbf{v} - \nabla D^{-1}\mathbf{p}' + D^{-1}\mathbf{f}. \tag{4.24}$$

Taking the divergence on both sides and assuming that $\nabla \cdot \mathbf{v}' = 0$ results in the Poisson equation

$$\nabla^2 \left[D^{-1}\mathbf{p}'\right] = -\nabla \cdot \left[D^{-1}B\mathbf{v} - D^{-1}\mathbf{f}\right].$$

Solving this equation results in a corrected pressure $\mathbf{p}'$. Once this pressure is obtained we can determine the corrected velocity by substitution in (4.24). Having determined the new fields we can go on to next iteration.

4.7.4 Under relaxation

In order to use the iterative methods, the system matrix should be diagonally dominant. For time-dependent problems this dominance is taken care of by the discretization of the time-derivative. For steady-state problems we need to enhance the diagonal dominance of the system, which is done through implicit under relaxation. Following ([10] page 115) we have for each system $A\mathbf{x} = \mathbf{b}$ we define the relaxation parameter $0 < \alpha \leq 1$. We split A in the diagonal and non-diagonal parts $A = D + B$. Then to both sides of the equation we add a term resulting in

$$(D + B)\mathbf{x}^n + \frac{1-\alpha}{\alpha} D\mathbf{x}^n = \mathbf{b} + \frac{1-\alpha}{\alpha} D\mathbf{x}^{n-1},$$

where $\mathbf{x}^n$ is the solution vector and $\mathbf{x}^{n-1}$ is the solution vector of the previous iteration. Note that once steady-state is reached, both terms will coincide. The resulting system is

$$(\frac{1}{\alpha} D + B)\mathbf{x}^n = \mathbf{b} + \frac{1-\alpha}{\alpha} D\mathbf{x}^{n-1},$$

and we see that the diagonal dominance of the system matrix is higher. The down-side is that more iterations are needed in general to obtain the steady-state solution. For the moment and energy equation we use the value $\alpha = 0.7$. For the pressure equation $\alpha = 0.3$ is used.

$$\begin{aligned} \partial_i v_i &= 0, && (4.25)\\ \rho_0 v_j \partial_j v_i &= -\partial_i p' + g x_2 \partial_i \rho + \mu \partial_j^2 v_i + f_i^{\mathrm{em}}, && (4.26)\\ \rho_0 c_{\mathrm{p}} v_i \partial_i T &= k \partial_i^2 T + q_{\mathrm{em}}, && (4.27) \end{aligned}$$

Chapter 5

Choice of medium and domain

In the previous chapters we have determined all the equations governing the electromagnetic fields, and the fluid flows that we want to investigate, but we still have to determine the domain in which we want to determine these quantities and the parameters we want to choice. In this short chapter we will determine the domain we use to investigate the flows, and the parameters we use for the numerical experiments.

5.1 Domain and boundary

The domain we consider will be a three dimensional square box, with sides of 10 µm. We define our axis so that the $(x, y, z) = (0, 0, 0)$ point coincides with one of the lower corner points of the boundary of the box, and $(x, y, z) = (10\,\mu\text{m}, 10\,\mu\text{m}, 10\,\mu\text{m})$ will be the opposite corner point.

We choose the y direction as the vertical one, so that gravity is working in the negative y direction. The positive z direction will be the direction of propagation of our electromagnetic fields, and we place the source at negative z, centred around $(x, y) = (5\,\mu\text{m}, 5\,\mu\text{m})$. Whenever we use a focussed source, we will use the middle point $(x, y, z) = (5\,\mu\text{m}, 5\,\mu\text{m}, 5\,\mu\text{m})$ as point of focus.

See Figure (5.1) for a schematic overview of our system.

We assume the fluid satisfies the no-slip boundary condition at all boundaries, so that we have $\mathbf{v} = 0$ at all points on the boundary. As mentioned before we do not need to impose a boundary condition for the pressure. Furthermore we assume the domain is in thermal equilibrium with the environment, so that the boundaries are at constant temperature. We choose $T_0 = 300\,\text{K}$, as reference temperature. All the parameters are determined corresponding to either 20° Celsius or 25° Celsius, corresponding to 293 K and 298 K, close to the reference temperature. In the end it is only the gradient of the temperature that is essential, so we choose a rounded reference temperature, so that differences are easy to determine.

5.1.1 Electromagnetic normalization

When simulating the electromagnetic source, we assume the whole space has the electric properties of water, so that we can assume the permittivity of the whole space is homogeneous. This was one of the assumptions made in the derivations of the analytic expressions for the sources. Of course one of the consequences is that in a medium with losses the fields start already decaying outside

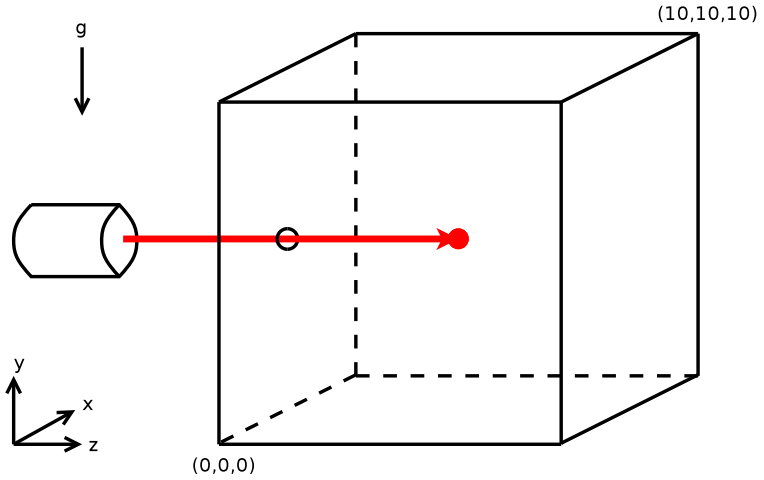

Figure 5.1: Schematic overview of domain and source.

the domain of interest. Furthermore is it hard to determine an analytic expression for the radiated energy of the sources in the first place, specially when there is no symmetry in the plane of the source perpendicular to the direction of propagation. Otherwise the total energy radiated in the direction of propagation would be half the total radiated energy. To coop with this problem, we determine numerically the total power through the boundary patch through which the beam enters, then we normalize the fields so that this power equals the number of mW we want. We already saw that the real part of the complex Poynting vector gives a measure for the power flow, so that the total amount of power through a patch is given by

$$P_0 = \int_S \mathrm{Re}\{\mathbf{S}\} \cdot \hat{\mathbf{n}} \, \mathrm{d}A,$$

where S is the patch of interest and $\hat{\mathbf{n}}$ is the normal vector orientated in the direction of propagation. See Figure (5.2) for a schematic overview of this normalization. The integral is taken over the blue shaded patch, with the normal vector orientated in the positive z direction. Since the Poynting vector is the product of the electric and magnetic field vectors, we know that the total power is proportional to I_0^2 when a dipole source is used, and E_0^2 when we consider a Gaussian beam source.

5.2 Parameters

The parameters depend on the properties of the fluid we use. For this project we will only consider liquid water. The main reason is that most experimental set-ups use this fluid. Furthermore most biological particles dwell well inside water, since that is their natural habitat. Most parameters we will use are for purified water, and they will change for water containing minerals. We are not too concerned with the exact parameters, since we do not expect flow results to be significantly

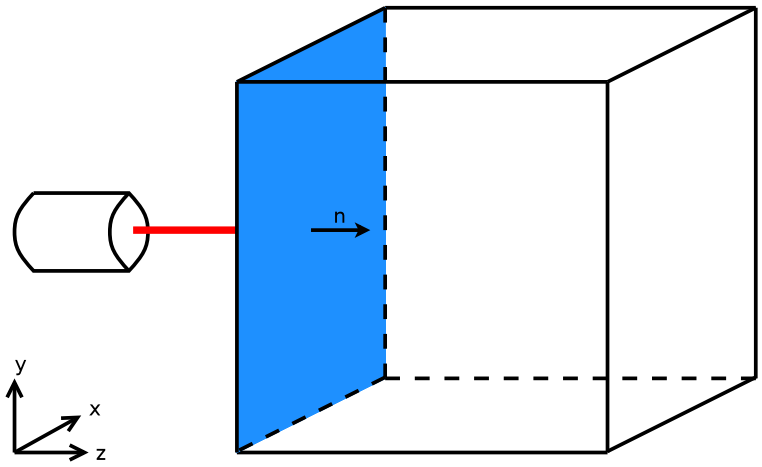

Figure 5.2: Normalization of the electromagnetic field.

property	symbol	value	unit
density	ρ_0	997	$\mathrm{kg\,m^{-3}}$
specific heat (at constant pressure)	c_p	4.18×10^3	$\mathrm{J\,kg^{-1}\,K^{-1}}$
coefficient of thermal expansion	β	2.57×10^{-4}	$\mathrm{K^{-1}}$
kinematic viscosity	ν	9.02×10^{-7}	$\mathrm{m^2\,s^{-1}}$
thermal conductivity	k	6.01	$\mathrm{W\,m^{-1}\,K^{-1}}$

Table 5.1: Parameter values in SI units.

different if the parameters vary slightly. Of course when highly accurate quantitative experiments are performed, the accuracy of parameters will become more important.

5.2.1 Dynamic parameters

For the dynamic parameters, we use [9] as reference. Although this book is mostly about water in natural occurrences, it also contains values for pure water. The thermal conductivity is taken from [17], where we linearly interpolated the value. We will use three significant digits, and the reference temperature of 25° Celsius. The values can be found in Table 5.1. All values are in SI units.

5.2.2 Electric parameters

As already mentioned we assume the liquid does not respond magnetically to an electromagnetic field. For water this is a good approximation. The only medium parameter we need for water is then the index of refraction $\hat{n}$. In general this will be a complex number, depending on the frequency of the fields. We use the data from [8], which is compiled from several experimental sources. Values are tabulated for vacuum wavelengths between 0.2 µm and 200 µm. All the values are determined

for the reference temperature of 25° Celsius. Figure (5.3) shows the real and imaginary part of the complex index of refraction $\hat{n} = n + \imath\kappa$.

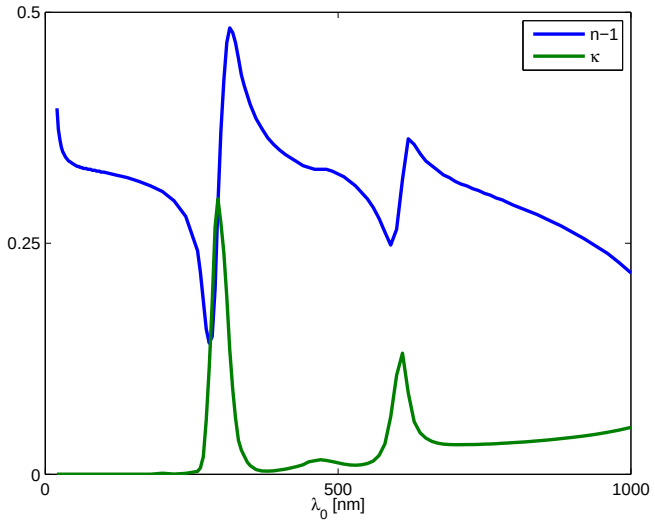

Figure 5.3: Overview of the refractive index in water for vacuum wavelengths up to 1 µm. Both the real and complex part are shown, and the real part is shifted down by 1.

We see that in the micrometer range there are two spikes that are interesting. Both are a consequence of the vibrational modes of the water molecules. We will focus on the first absorption spike, stretching from 2.4 µm to 3.8 µm. Furthermore we will investigate one small wavelength, for which the absorption is very small. From (2.109) we see that the coefficients for the two force terms are

$$\frac{\omega}{c^2}\left(\frac{\varepsilon'}{\varepsilon_0} - 1\right) = \frac{\omega}{c^2}\delta\varepsilon'_{\text{rel}} \quad \text{and} \quad \frac{\omega}{c^2}\frac{\varepsilon''}{\varepsilon_0} = \frac{\omega}{c^2}\varepsilon''_{\text{rel}}.$$

Figure (5.4) shows the values of $\delta\varepsilon'_{\text{rel}}$ and $\varepsilon''_{\text{rel}}$. Furthermore four vacuum wavelengths are highlighted, 1.2 µm, 2.4 µm, 2.8 µm and 3.2 µm respectively. These are the wavelengths we will investigate.

At the first point, only the force term proportional to $\delta\varepsilon'_{\text{rel}}$ will contribute. Furthermore the absorption will be low, so that the motion due to buoyancy will also be low. For the second and third wavelengths, the absorption will be comparable. Furthermore at the second wavelength the two force term are of equal scale, while for the third point we will have the maximum total force. It is important to note that these are vacuum wavelengths. Inside the medium, the wavelength will be different, depending on the real index of refraction. In Figure (5.5) we plotted the same region but now as function of the wavelength inside the water. Note that the function is no longer single valued, as a result of the dependency on the index of refraction itself. This means that we have different vacuum wavelengths with the same wavelength inside the water, but with different absorption

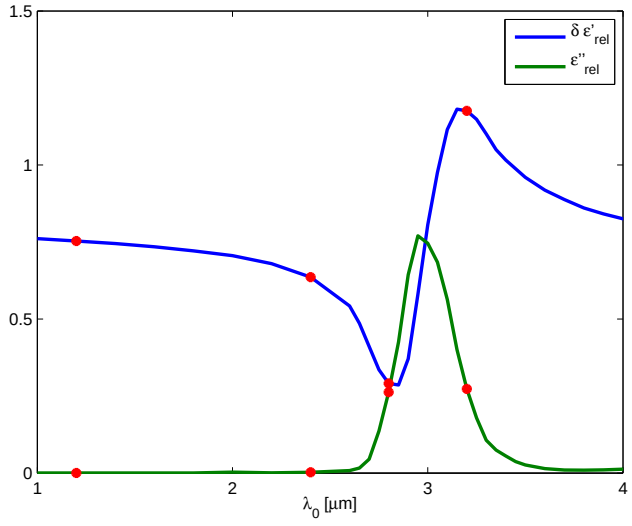

Figure 5.4: Absorption spike and points of interest, 1.2 µm, 2.4 µm, 2.8 µm and 3.2 µm respectively. The difference of the real and imaginary part of the relative permittivity compared to the vacuum are shown.

values. The corresponding wavelengths inside the water are 0.91 µm, 1.88 µm, 2.45 µm and 2.17 µm respectively. Table 5.2 shows the different parameter values for each of these frequencies.

In Chapter 6 we will investigate the forces and the resulting flows for sources with frequencies corresponding to these three points of interest.

λ_0 [µm]	λ [µm]	n [-]	κ [-]	k [m^{-1}]	α [m^{-1}]	$\delta\varepsilon'_{\mathrm{rel}}$ [-]	$\varepsilon''_{\mathrm{rel}}$ [-]
1.20	0.91	1.32	9.89×10^{-6}	6.93×10^{6}	5.18×10^{1}	0.753	2.62×10^{-5}
2.40	1.88	1.28	9.56×10^{-4}	3.35×10^{6}	2.50×10^{3}	0.635	0.0024
2.80	2.45	1.14	1.15×10^{-1}	2.56×10^{6}	2.58×10^{5}	0.291	0.2627
3.20	2.17	1.48	9.24×10^{-2}	2.90×10^{6}	1.81×10^{5}	1.176	0.2731

Table 5.2: Parameter values for the wavelengths of interest. The wavelength inside the medium is shown together with the refractive index, the wave number and the (relative) permittivity.

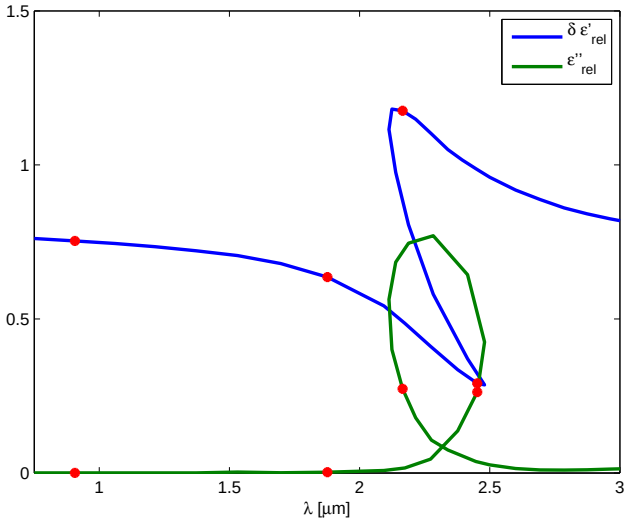

Figure 5.5: The permittivity of the wavelengths of interest as function of the fluid wavelengths, 0.91 µm, 1.88 µm, 2.45 µm and 2.17 µm respectively. We see that different vacuum wavelengths can have similar fluid wavelengths because of the index of refraction.

Chapter 6

Numerical results and simulations

In this chapter we will first investigate the numerical properties of the electromagnetic fields generated by the two different external sources we have discussed in Chapter 3. We will see what the residuals are for different parameters, and how we have to choose them to get accurate results.

Once this is settled we will investigate the flows generated by the electromagnetic fields, and again investigate the convergence behaviour of the solutions of the Navier-Stokes equations for different grid sizes.

Once we have obtained accurate enough velocity fields we will investigate what the result of the induced flow will be on small particles suspended in the fluid.

6.1 Gaussian beam accuracy

As explained in Section 3.1, the Gaussian beam approximation only satisfies the Maxwell equations approximately, and the error is of order $|\hat{s}|^2$, with

$$\hat{s} = \frac{\lambda_0}{2\pi w_0 \hat{n}}.$$

We will now investigate this approximation, by looking at both the analytical and numerical residual of the Maxwell equations. We determine both the numerical and analytical residual for the wavelengths 2.4 µm, 2.8 µm and 3.2 µm. The waist size w_0 varies from 1 µm to 5 µm. The residuals are determined on grids consisting of 32, 64, 96 and 128 grid points. Figure (6.1) shows the results.

We see that in both cases the residual decreases for smaller $|\hat{s}|$ values. This is expected since the analytical error will become less and less. In Figure 6.1(b) we see the analytical residual. For values $|\hat{s}| < 0.2$ the residuals coincide for all different grid sizes. Furthermore the order of this residual is converging to $\mathcal{O}(|\hat{s}^2|)$, which can be seen fro the reference line, which is parallel to the $|\hat{s}^2|$ lines. This is exactly the order we expect from the theoretical derivation. For all lines, the residual passes 0.01 at approximately $|\hat{s}| = 0.09$. This corresponds to a waist size

$$w_0 \approx 1.77 \frac{\lambda_0}{|\hat{n}|}.$$

So for highly focussed beams we cannot expect the Gaussian beam model to give very accurate results, while these beams are exactly the ones we are interested in. In Figure 6.1(b) the numerical

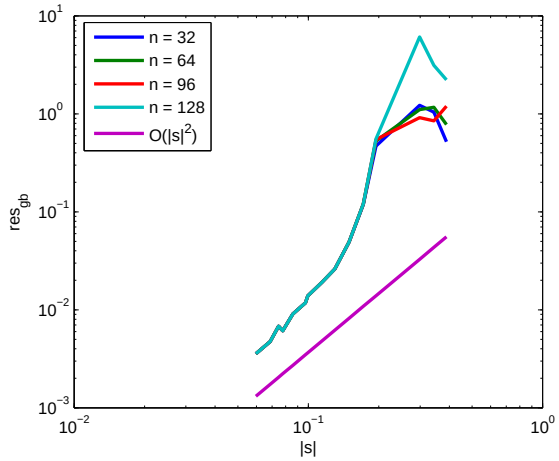

(a) Analytical residual.

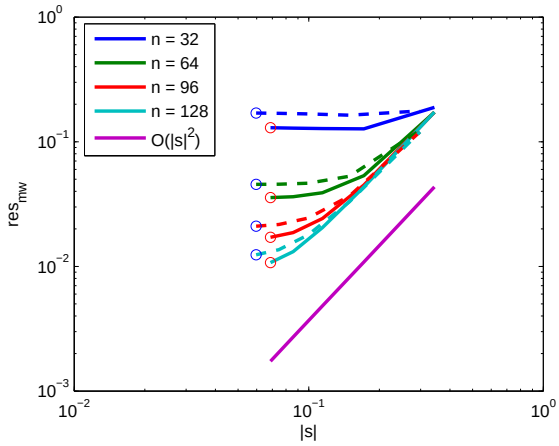

(b) Numerical residual.

Figure 6.1: Residuals for the Gaussian beam approximation.

residuals can be found for two vacuum wavelengths, the full lines correspond to $\lambda_0 = 3.2\,\mu\text{m}$ and the dashed lines to $\lambda_0 = 2.4\,\mu\text{m}$. We see that the larger wavelength is in general better than the smaller wavelength, on a constant grid, which is a results of the fields of the smaller wavelength oscillating with a smaller period. We see that for large $|\hat{s}|$ for all grid sizes the residuals seem to follow the reference line, suggesting that in this region of $|\hat{s}|$ the analytical error is dominant over the numerical error. Then, for decreasing $|\hat{s}|$ this decrease in residual starts to stagnate, resulting in no further decrease. The point at which this stagnation starts depends on the grid size, reflecting that it is the numerical error that 'kicks in'. When $|\hat{s}|$ decreases more, the residuals will converge to a value depending on both λ_0 and the grid size. If we focus on the encircled point in Figure 6.1(b) and plot them as function of the grid size we get as result Figure 6.2.

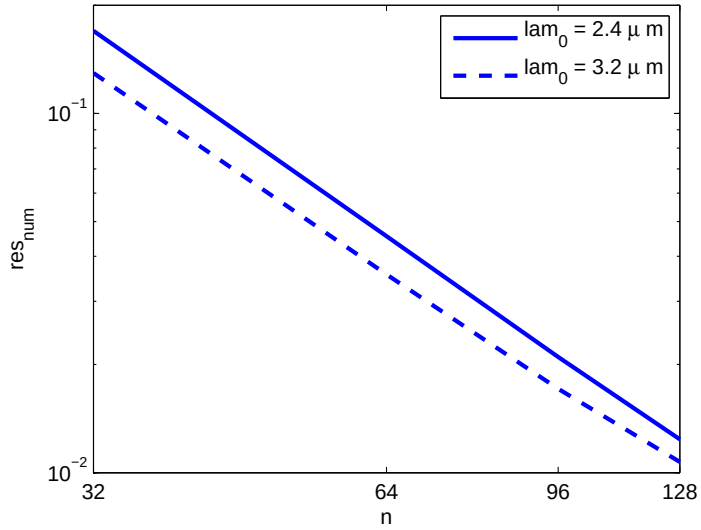

Figure 6.2: Numerical error for small $|\hat{s}|$ values.

We see that in the $|\hat{s}| \to 0$ limit, the error gets of constant order in the grid size. Using least squares to fit a linear line to both lines results in orders -1.89 and -1.81 for $\lambda_0 = 2.4\,\mu\text{m}$ and $\lambda_0 = 3.2\,\mu\text{m}$ respectively, close to the theoretical value -2, reflecting that all the numerical procedures are of order $\mathcal{O}(h^2)$ in the cell size h.

Until now we have looked at the field values them selves. For our purposes we are more interested in the derived force density. We can quantitatively estimate how accurate this force density is by considering how well momentum conservation from (2.111) is satisfied. We will do this by integrating the force density directly using the midpoint integration scheme, and applying the divergence theorem to the term containing the time-averaged stress tensor. This transforms the volume integral of the divergence of the stress tensor to a surface integral of the normal component of the stress tensor. More precisely we have

$$\int_V \nabla \cdot \overleftrightarrow{T}\, \mathrm{d}V = \int_S \hat{\mathbf{n}} \cdot \overleftrightarrow{T}\, \mathrm{d}A,$$

where V is the specific control volume, and S is its surface, consisting of six faces. The integration is performed by using a midpoint scheme for each face and adding the result. Finally the sum of all absolute values is taken over the control volumes, and this quantity is normalized, using the sum of the absolute values of the force density. The momentum residuals are plotted as function of $|\hat{s}|$, resulting in Figure 6.3.

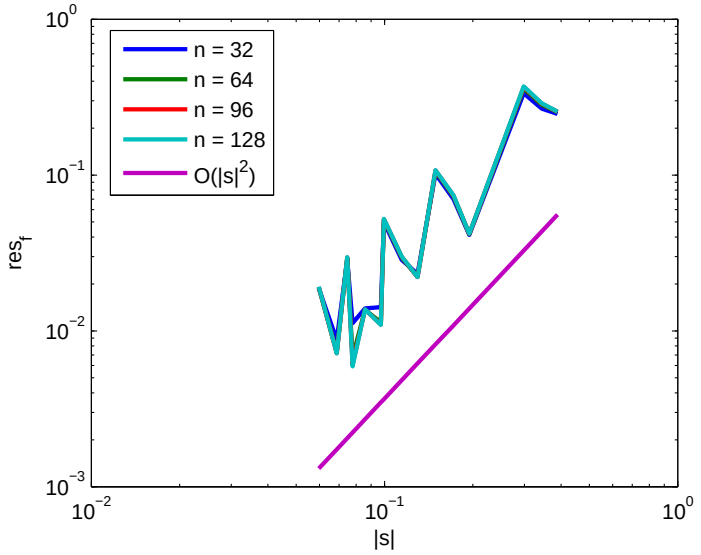

Figure 6.3: Numerical residual of the momentum equation.

We see that for all grid sizes that lines almost coincides, suggesting that the analytical error is dominant for these choice of parameters. Furthermore the error decreases following the reference line of order $\mathcal{O}(|\hat{s}|^2)$, also pointing towards the analytical error. The reason why for the same range of $|\hat{s}|$ values we do not see any numerical error, is that the force density is smoother than the field quantities them selves. From (2.24) we see that the force density is the product of a field component multiplied with the conjugate of another field component. This means that the $\exp(\imath kz)$ factor, which is highly oscillatory in the propagation direction is cancelled by a factor $\exp(-\imath kz)$ from the conjugate field component. The result is much smoother function. This will be illustrated in a later section for specific choices of parameters. The jumpy behaviour of the momentum residual implies a dependency on a parameter other than $|\hat{s}|$, most likely λ or w_0.

We have seen that not only in the fields themselves but also the derived quantities such as the force density the analytical error is dominant for our choices of parameters. This strengthens our motivation for using a different external source.

6.2 Discretization of Gaussian dipole array

As mentioned in Section 3.2.3 we have to make sure the discretization grid for the Gaussian plane is fine enough. We will compute the fields for four different grid sizes to show the effect of the

discretization of the source domain. We will use as wavelength $\lambda_0 = 2.4\,\mu\text{m}$, and the aperture will be a square patch of $15\lambda \times 15\lambda$, with λ the wavelength in the medium. The distance between the source plane and the domain of interest is $2\,\mu\text{m}$. We will use as number of dipoles the values $n_\text{d} = 8, 16, 32, 64$. For the domain on which we determine the fields we have chosen $n = 128$ grid points. Figure 6.4 shows the electric field intensity, $|E|^2$, in the xz-plane for $y = y_\text{s}$.

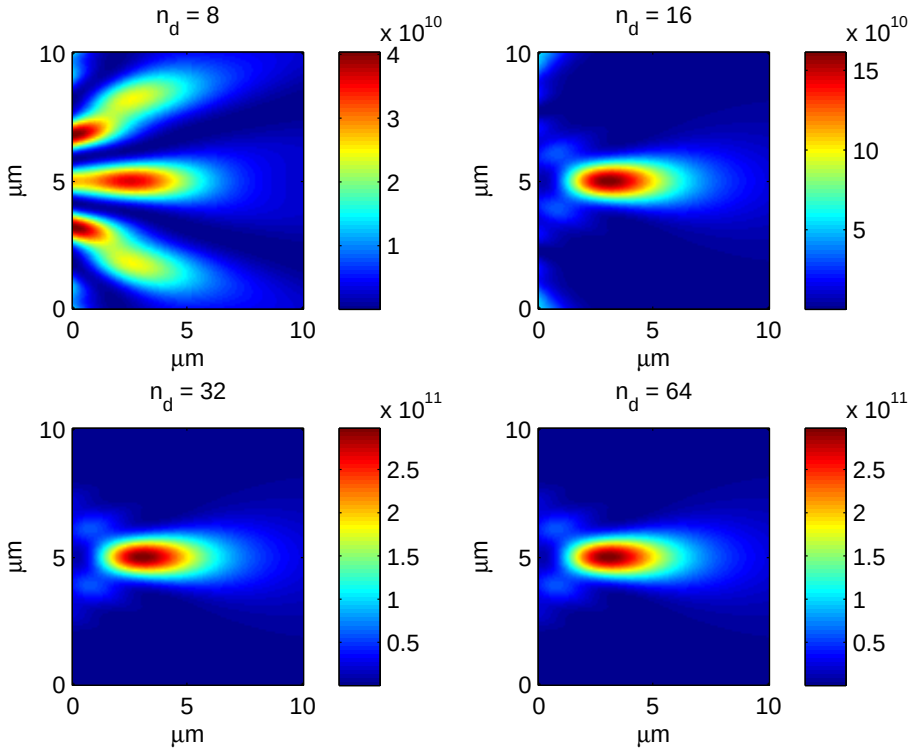

Figure 6.4: Intensities for different source resolutions.

We see that for $n_\text{d} = 8$ the result is completely different from the other cases, suggesting that the discretization is too crude. For $n_\text{d} = 16$ the qualitative result looks much like the $n_\text{d} = 32$ and $n_\text{d} = 64$ result, although the intensity is smaller, and side loops are still visible. The results for $n_\text{d} = 32$ and $n_\text{d} = 64$ are almost equal. If we calculate the difference of the intensity fields compared to the results of $n_\text{d} = 64$, using

$$e_{n_\text{d}} = \sqrt{\frac{\sum_i \left(|E_i^{n_\text{d}}|^2 - |E_i^{64}|^2\right)}{\sum_i |E_i^{64}|^2}},$$

we get $e_8 = 0.903$, $e_{16} = 0.469$ and $e_{32} = 4.57 \times 10^{-6}$, so we see the difference for the finest two grids are also quantitatively very small, showing that $n_\text{d} = 32$ already is fine enough to determine the fields. This confirms that even though the resolution is only about 2 dipoles per wavelength this

is not a problem since the source current in the source plane does not oscillate with this wavelength, but has a higher period as we noticed earlier. For our simulations we will use $n_{\mathrm{d}} = 32$ unless stated otherwise.

6.3 Convergence on different grids

In this section we will investigate the convergence of the resulting velocity and temperature fields given by the Navier-Stokes equations, for different grid sizes and wavelengths. In order to make quantitative estimates, we select four grid sizes, with 32, 64, 96 and 128 grid points in each direction.

Of course we expect the values to be more accurate for finer and finer grids, but due to time and memory limitation we cannot keep improving the grid size. We want to see how the (average) quantities behave as function of the grid size. First some notation will be introduced, after which we will define quantitatively how we will compare different quantities on the different grids, and finally the results for different cases are presented.

6.3.1 Grid notation and error definition

We are working with a rectangular grid, with equal dimensions in all three directions. We denote the number of cells in each direction as n. We will investigate the convergence properties for $n = 32, 64, 96, 128$.

The complete domain is denoted D and for each n it is divided into n^3 control volumes so that

$$D = \bigcup_{i=1}^{n^3} D_i^{(n)}.$$

Each control volume has volume $V_i^{(n)}$.

To investigate the convergence properties, we will consider as reference volumes C_i the control volumes on the coarsest grid, so $C_i = D_i^{(32)}$. We denote the volume of C_i as V_i. For the different grid sizes these reference volumes consist of a number of control volumes. To make this more explicit, we (implicitly) relabel the $D_i^{(n)}$ control volumes, so that

$$C_i = \bigcup_{j=1}^{m_n} D_{i,j}^{(n)},$$

with $m_{32} = 1$, $m_{64} = 2^3 = 8$, $m_{96} = 3^3 = 27$, and $m_{128} = 4^3 = 64$. In particular we have $D_i^{(32)} = D_{i,1}^{(32)}$ and $V_i = V_i^{(32)}$. We now have a way of identifying the (constant) references volumes for each grid size. See Figure (6.5) for a two dimensional illustration of the division of the grid.

To be able to quantify how well our solutions coincide for the different grid sizes, we need to identify analytical quantities related to the reference volumes, that are invariant with respect to the grid size, and for which we have estimates for each of the different grids. Since we are using a finite volume method, these quantities naturally arise as the average values of the different physical quantities. If we consider an arbitrary quantity $u(\mathbf{x})$, $\mathbf{x} \in D$, we define the average for each reference volume C_i as

$$\bar{u}_i = \frac{1}{V_i} \int_{C_i} u(\mathbf{x}) \, \mathrm{d}\mathbf{x}.$$

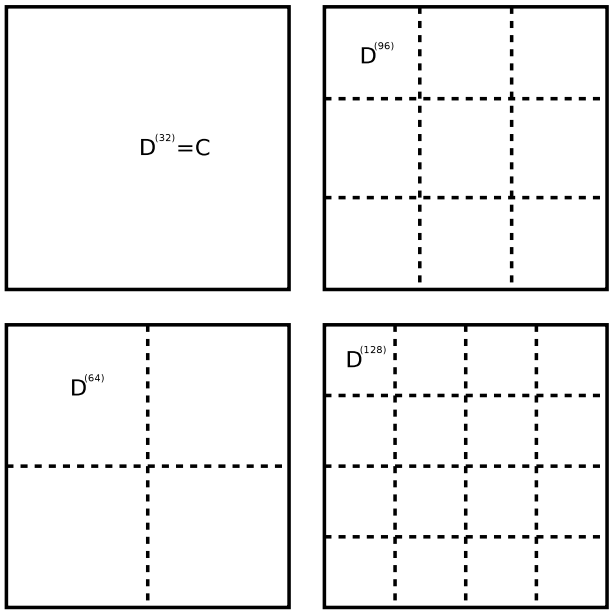

Figure 6.5: Division of grid for the different grid sizes.

Now for each grid size we have an estimate for these values, given by

$$\tilde{u}_i = \frac{1}{V_i}\int_{C_i} u(\mathbf{x})\,\mathrm{d}\mathbf{x} = \frac{1}{V_i}\sum_{j=1}^{m_n}\int_{D_{i,j}^{(n)}} u(\mathbf{x})\,\mathrm{d}\mathbf{x} = \frac{1}{V_i}\sum_{j=1}^{m_n} u_{ij}^{(n)} V_{ij}^{(n)}.$$

Note that this method is valid for arbitrary grids, as long as we can write each reference volume as a finite union of disjoint control volumes.

We now define the error for each reference volume as

$$e_i = |\bar{u}_i - \tilde{u}_i|.$$

The total error is defined as the sum of these errors over all the reference volumes,

$$E = \sum_{i=1}^{m_n} |\bar{u}_i - \tilde{u}_i|.$$

A motivation for this choice is that is resembles the standard 1-norm on the function space, although we have the inequality

$$\sum_i \left|\int_{D_i} (v - \tilde{v})\,\mathrm{d}\mathbf{x}\right| \leq \sum_i \int_{D_i} |v - \tilde{v}|\,\mathrm{d}\mathbf{x} = \int_D |v - \tilde{v}|\,\mathrm{d}\mathbf{x} = \|v - \tilde{v}\|_1.$$

The idea is that for grids fine enough both sides of the inequality are close to each other, that is, the quantities do not vary too much on the scale of the control volumes.

One difficulty is that value $\bar{u}_i$ is unknown. This would be the exact value, as given by the exact solution $u(\mathbf{x})$. To tackle this problem, we assume that the estimates $\tilde{u}_i$ for the finest grid are close to the analytical value, and we use this estimate as reference value. Since we run our simulations for four different grid sizes, this means we get error estimates for the coarsest three.

After we have determined the error, we normalize is by dividing by the mean values of the finest grid, so our final expression for the error will be

$$E_h = \frac{\sum_{i=1}^{m_n} |\bar{u}_i - \tilde{u}_i|}{\sum_{i=1}^{m_n} |\bar{u}_i|}, \tag{6.1}$$

where the h denotes the implicit dependency on the grid size.

6.3.2 Error results

We will determine the error for the velocity field and temperature field. We investigate four different wavelengths, $\lambda_0 = 1.2\,\mu\text{m}$, $\lambda_0 = 2.4\,\mu\text{m}$, $\lambda_0 = 2.8\,\mu\text{m}$ and $\lambda_0 = 3.2\,\mu\text{m}$. The corresponding wavelengths in the medium are respectively $\lambda = 0.91\,\mu\text{m}$, $\lambda = 1.88\,\mu\text{m}$, $\lambda = 2.45\,\mu\text{m}$ and $\lambda = 2.17\,\mu\text{m}$. The Gaussian dipole model is used, with a beam width parameter $w_0 = 1\,\mu\text{m}$ and the aperture extended to catch the full source current profile in the source plane, located at $z_\text{s} = -1.0\,\mu\text{m}$. The power is normalized to $P_0 = 1\,\text{mW}$.

Figure (6.6) shows the result for the velocity and temperature fields. We see that all errors are dropping for finer grids. The very small errors in the temperature for the wavelengths $\lambda_0 = 1.2\,\mu\text{m}$ and $\lambda_0 = 2.4\,\mu\text{m}$ are a result of the small values of κ and thus ε'' for these wavelengths, resulting in almost zero heat dissipation. It is interesting to see that the error in the x and y component of the velocity is small for $\lambda_0 = 1.2\,\mu\text{m}$ compared to the other wavelengths, while in the z it is relatively large. There is no direct explanation for this, but it is likely to be a result of the difference in the scale of the velocity in the direction of propagation and the radial plane.

The errors in all the quantities are dropping for finer grids, with the maximum discrepancy between the $n = 96$ and $n = 128$ grid already being less than 0.0014, the value for the z component of the velocity, for $\lambda_0 = 1.2\,\mu\text{m}$. This is the smallest wavelength we will use, giving us confidence that our resulting fields are close enough to the real solutions. We will always use grid sizes between $n = 96$ and $n = 128$ for the simulations.

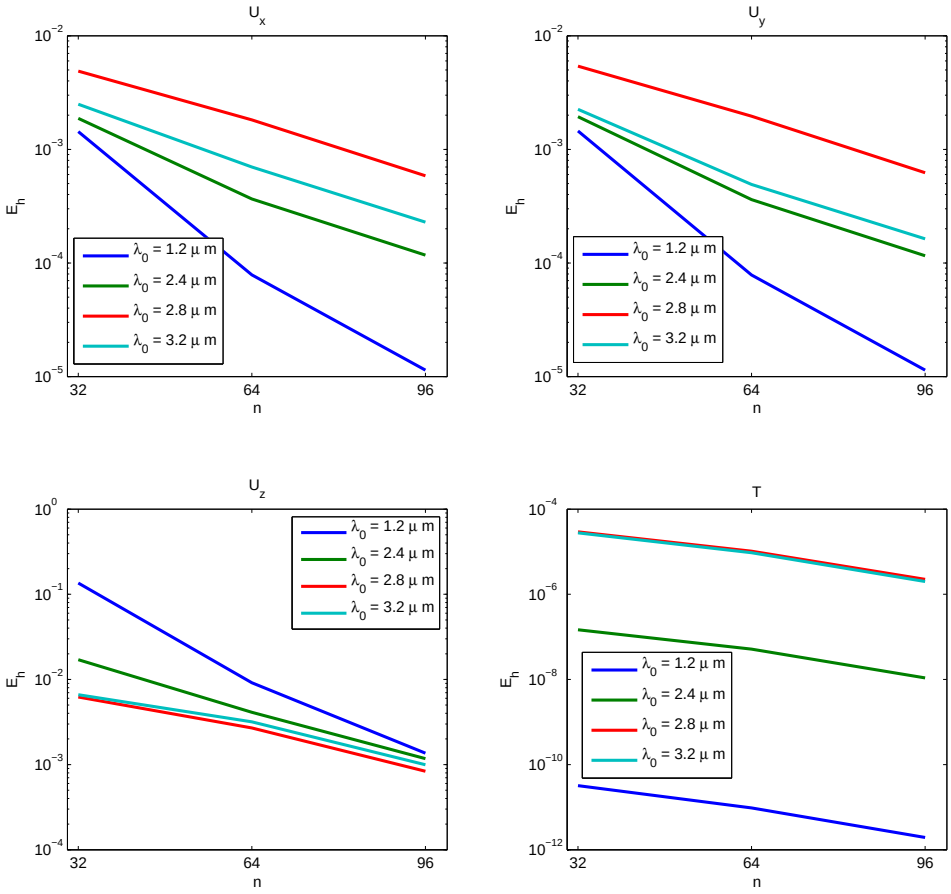

Figure 6.6: Convergence of the velocity and temperature for different wavelengths.

6.4 Simulations

We have now covered all the numerical aspects of the discretizations, and are confident that they are accurate enough, and that the fields and flows we calculate are indeed the solutions to the equations we have derived in the previous chapters.

6.4.1 General setting

In Chapter 5 we have already discussed the domain they we are looking at, and the parameters of the fluid, purified water, we will consider.

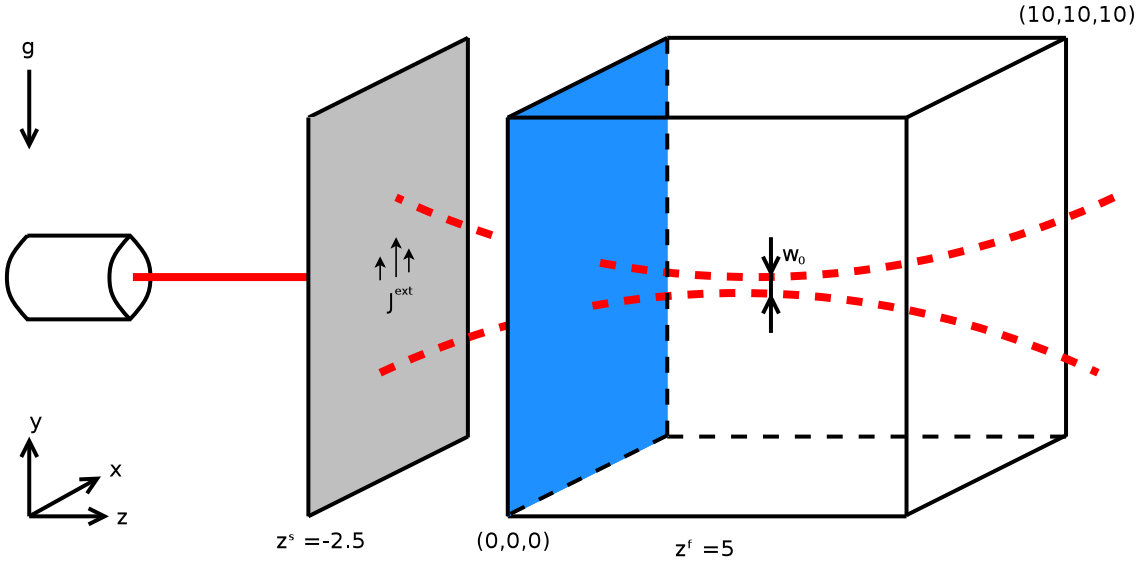

Figure 6.7: Schematic overview including the source domain and parameter values. All coordinates are in µm.

Figure 6.7 is similar to Figure 5.1, but some details are added to further clarify the choices of parameters. The grey plane is the source plane, located at $z_s = -2.5\,\mu m$. As focussing point we chose $\mathbf{x}_s = (5\,\mu m, 5\,\mu m, 5\,\mu m)$. Notice that since we are not using the Gaussian beam approximation, this choice does not automatically means the point of highest intensity will be located at this parameter value. We will see that it usually is located at slightly smaller z value. The value w_0 is the parameter we choose as waist size. In the Gaussian beam approximation this would be the radius at which the intensity drops by a factor $\exp(-2)$, but again we cannot expect this to be true for our dipole model, particularly for small values of w_0, at which the Gaussian beam approximation does not hold. We will choose $w_0 = 1\,\mu m$ as default value. The blue plane, one of the boundaries of our domain, is used to normalize the incoming time-averaged power to $P_0 = 1\,mW$. The domain is divided in $n = 101$ grid points in each direction. The values stated here are the default values used, unless mentioned otherwise.

λ_0 (µm)	λ (µm)	$w_{\mathrm{f},x}$ (µm)	$w_{\mathrm{f},y}$ (µm)
1.2	0.91	0.98	1.01
2.4	1.88	1.03	1.22
2.8	2.45	1.49	1.88
3.2	2.16	1.15	1.48

Table 6.1: Waist size at focal point.

6.4.2 Intensities for different wavelengths

We will now determine the electromagnetic fields for the different wavelengths mentioned in Chapter 5. Figure 6.8 shows the electric field intensity, $|\mathbf{E}|^2$ in the different planes through the focal point. The normalization is equal for all images. We can see from the figures of the xz-plane and yz-plane that the focal points in general do not coincide with the parameter value $z_{\mathrm{f}} = 5\,\mu\mathrm{m}$. For larger wavelengths the focal point moves to smaller z values. The point of highest intensity are found at $z = 4.2\,\mu\mathrm{m}$, $z = 2.9\,\mu\mathrm{m}$, $z = 1.4\,\mu\mathrm{m}$ and $z = 1.9\,\mu\mathrm{m}$ respectively. This shows that how smaller the wavelength in the fluid, the closer the focal point is at the values prescribed by the parameter. Table 6.1 shows the wavelength inside the medium. This seems reasonable, for as smaller the wavelength in the medium, the closer we get to the Gaussian beam approximation.

The red lines are equipotential lines which show the waist size as function of $\rho = \sqrt{x^2 + y^2}$. This is the distance from the axial line at which the intensity has dropped by a factor $\exp(-2)$. For $\lambda_0 = 1.2\,\mu\mathrm{m}$ we see the shape resembles the Gaussian beam approximation, while for the other wavelengths we see some distortion for small z. This distortion is the contribution of the near- and intermediate field. Even though the distance to the source plane is equal for each wavelength, the distance expressed in number of wavelengths gets smaller for larger wavelengths, resulting in a larger contribution of the terms proportional to kr^{-1} and k^2r^{-2}.

In the xy-plane plots we see that for the smallest wavelength the equipotential lines of the intensity are circles centred around the axial line. For larger wavelengths they get more spread out in the y direction, resulting in an inhomogeneity of the intensity with respect to the radial angle. The electric field is polarized in the y direction, so we see that the intensity is spread out in the direction of polarization. As we will see later this results in smaller gradient forces on the y direction compared to the x direction.

We estimate the waist size for each wavelength at the point of focus in both the x and y direction. The results can be found in Table 6.1. To determine this values we interpolated the intensity values along the $(x, y_{\mathrm{f}}, z_{\mathrm{f}}$ and $(x_{\mathrm{f}}, y, z_{\mathrm{f}}$ lines and determined how far from the axial line the intensity dropped by a factor $\exp(-2)$. The interpolation is done using splines.

6.4.3 Force density on fluid

Given the electric and magnetic fields, we can determine the complex Poynting vector, and use (2.109) to determine the force density on the fluid. From Figure 6.8 we see that the intensities are concentrated around the focal point, and drop off quickly when moving away from this point. This suggest that the force density is also largest around the focal point and quickly drops off.

Figure 6.9 shows the total force density in the xy-plane at the focal point. We see indeed that most of the contribution is centred around the focal point, and it quickly dies off. The figures show

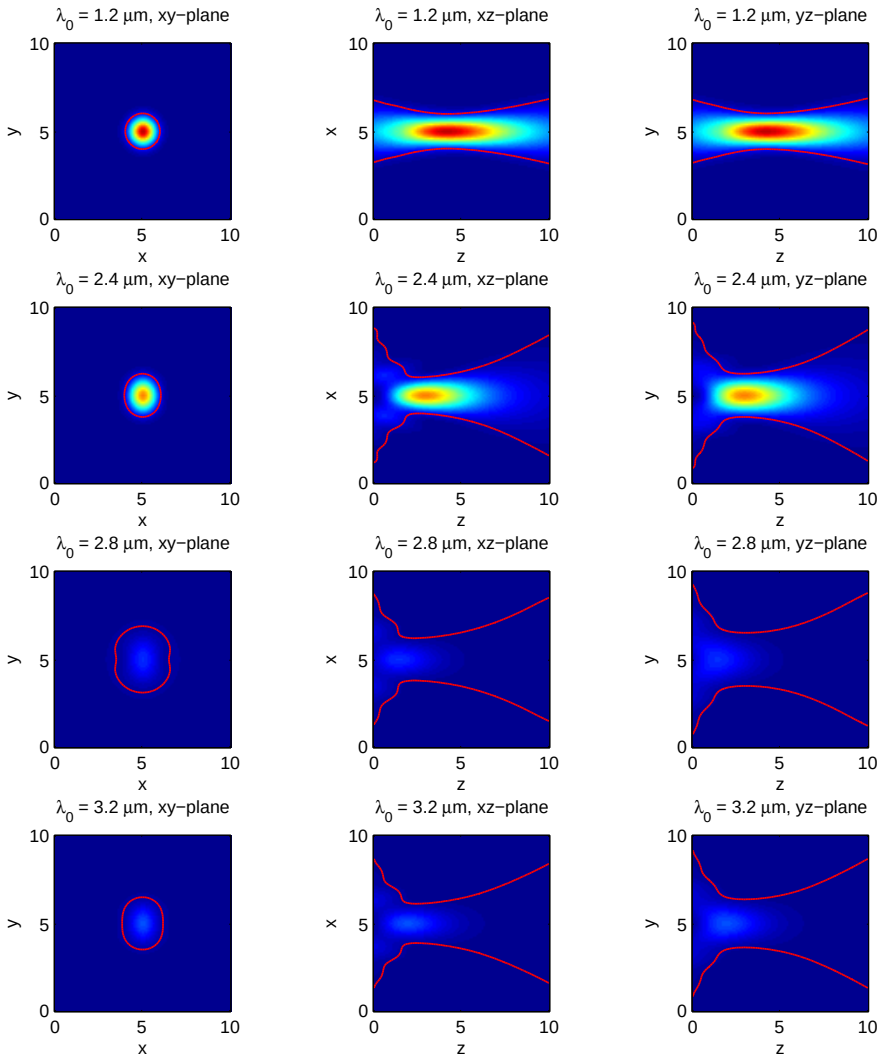

Figure 6.8: Electric field intensities for different wavelengths, all coordinates are in µm.

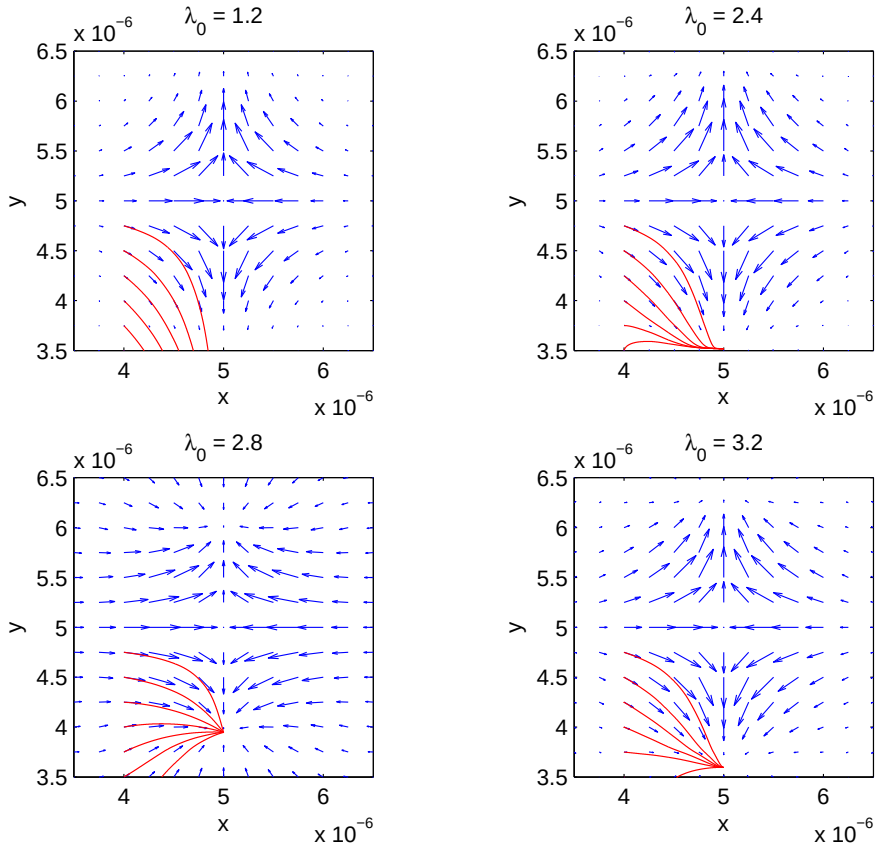

Figure 6.9: Force density on the fluid in the xy-plane, through the focal point. In the x direction the force is pointing towards the centre, while in the y direction, the direction of polarization of the electric field, is it pointing away from the centre. The red lines are streamlines, showing the additional stationary point for the larger wavelengths.

patches of $3\,\mu\text{m} \times 3\,\mu\text{m}$. The focal point itself is a stationary point. The most important feature is that the force density is in opposite direction for the x and y direction. In the x direction it is pointed towards the middle, while in the y direction, the direction of polarization of the electric field, the force density is pointing away from the centre. This suggests that there will be a flow that is pointing away from the focal point, the point which is used as trapping point for particles. We will see that indeed this flow will occur, and later on we will estimate the force this will exert on particles. Another important feature is that for the larger wavelengths we see that there are additional stationary points, located on the line with $x = x_\text{f}$ going through the focal point. The location depends on the wavelength, the larger is it the closer the point is to the focal point. The red lines are stream lines showing one of these additional points. It is important to realise this is only a projection of the force field on the xy-plane, so the z component is likely to be non-zero at these points.

In Figure 6.10 the force density in the xz- and yz-plane for $\lambda_0 = 1.2\,\mu\text{m}$ and $\lambda_0 = 2.4\,\mu\text{m}$ are shown. The z axis is centred around the focal point. We see that the z component is relatively small, especially for $\lambda_0 = 1.2\,\mu\text{m}$ and around the focal point, where it nearly vanishes. In the xz-plane the force density is directed towards the centre while in the yz-plane it is directed away from the centre, showing that the force density in the vicinity of the focal point has the same structure as we saw in Figure 6.9. On the axial line the force density is nearly zero, which is a result of the small value of ε'' for these wavelengths, so that $\mathbf{f}_\text{dis}$ is negligible. These force densities in combination with the no-slip boundary conditions suggest that the fluid will start moving away from the axial line in the y-direction and start moving towards the axial line in the x direction, creating loops in each of the four quadrants defined by the lines $x = y = 5\,\mu\text{m}$ in Figure 6.9. We will see that this is indeed what will happen.

For the two larger wavelengths the force density in the xz- and yz-plane is shown in Figure 6.11. Here we see a different structure. For these wavelengths there is a significant z component of the force density, suggesting that the $\mathbf{f}_\text{dis}$ term from (2.110) starts to contribute due to the relatively large values of ε'' for these wavelengths. Again we see the x component in the xz-plane pointing towards the centre while the y component is pointing away from the center. This suggest that again there will be a rotating behaviour of the fluid, but due to the relatively large z component is it likely that the flow will follow a spiral movement instead of loops.

6.4.4 Velocity profiles

Until now we have looked only at the electromagnetic fields and quantities that are derived from them. We will now consider the resulting velocity fields, which are determined using the SIMPLE algorithm described in Section 4.7. We will show the same planes as for the force density in the previous section.

Figure 6.12 shows the velocity in the xy-plane through the focal point for each wavelength. The red lines are streamlines. We see for $\lambda_0 = 1.2\,\mu\text{m}$ and $\lambda_0 = 2.4\,\mu\text{m}$ that velocity fields look alike, and form closed loops in this plane, implying a zero z component in this plane. For $\lambda_0 = 3.2\,\mu\text{m}$ we also see a loop structure but here the streamlines are not closed, but converge to a singular point, implying a non-zero z component of the velocity. For $\lambda_0 = 2.8\,\mu\text{m}$ we do not see any loop-like streamlines at all. This confirms what we conjectured earlier from the force density. For the wavelengths with relatively large values of ε'' the z component of the velocity gets dominant. The two streamlines for $\lambda_0 = 1.2\,\mu\text{m}$ and $\lambda_0 = 2.4\,\mu\text{m}$ seem to coincide very closely, but it is important to note that all four quiver plots are independently normalized, so they can differ in magnitude.

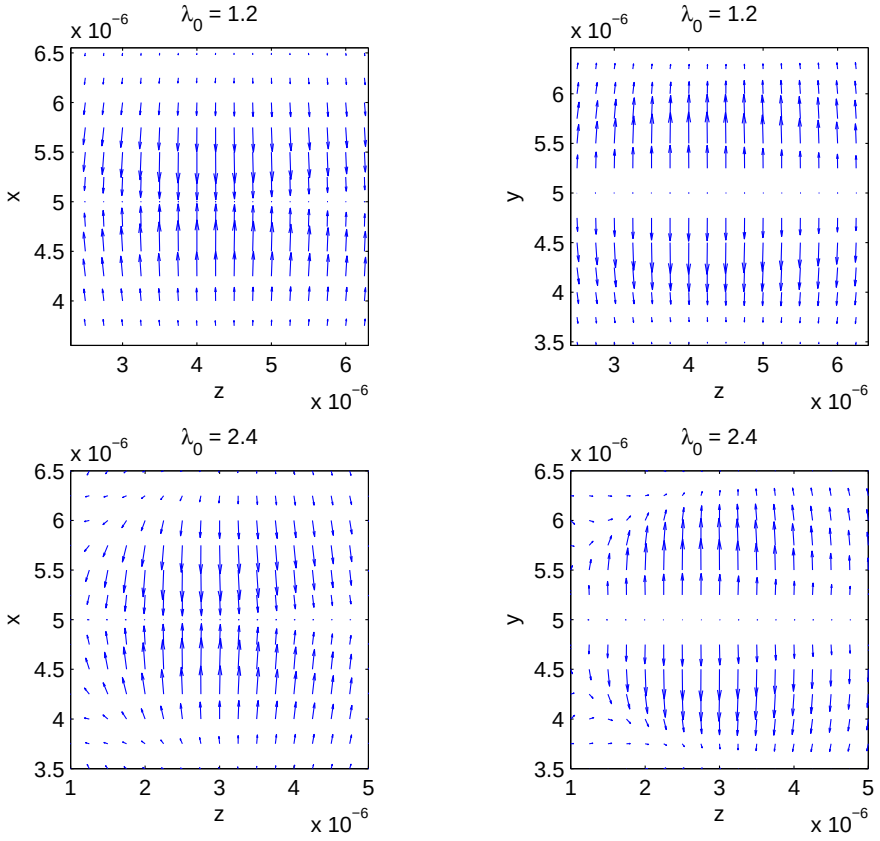

Figure 6.10: Force density in the xz- and yz-plane for $\lambda_0 = 1.2\,\mu\text{m}$ and $\lambda_0 = 2.4\,\mu\text{m}$, centred around the focal points. We see that the z component is relatively small, especially for $\lambda_0 = 1.2\,\mu\text{m}$. In the xz-plane the force density is direction towards the centre while in the yz-plane it is direction away from the centre.

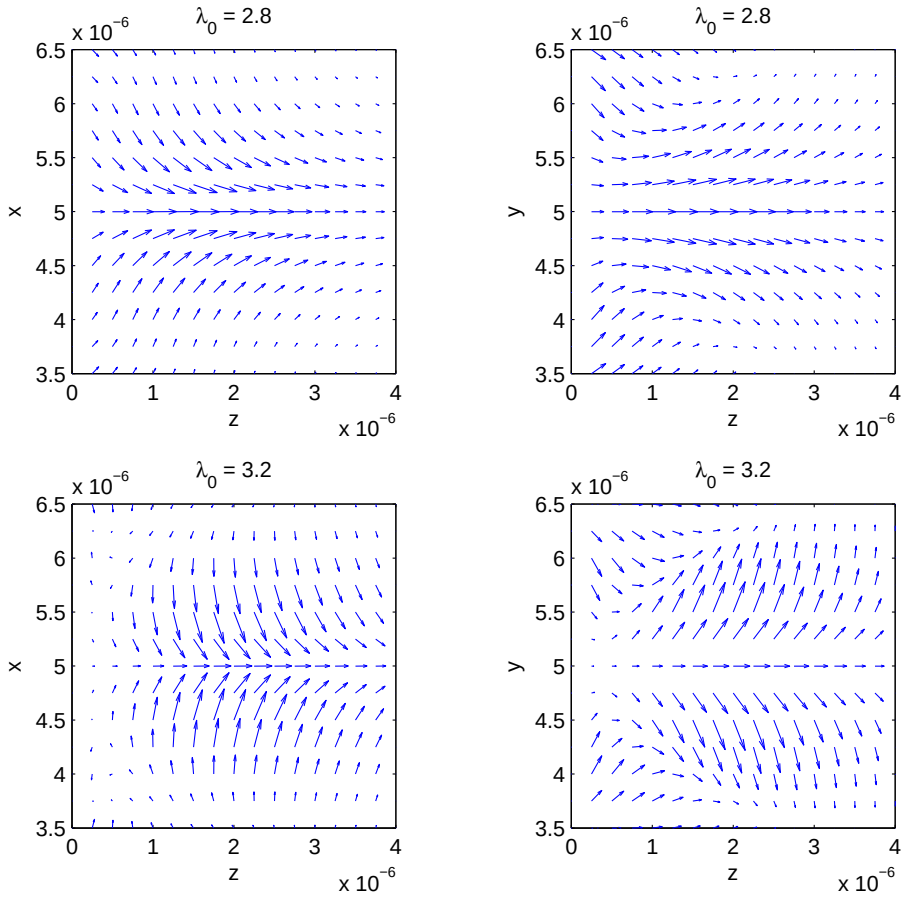

Figure 6.11: Force density in the xz- and yz-plane for $\lambda_0 = 2.8\,\mu\text{m}$ and $\lambda_0 = 3.2\,\mu\text{m}$. For these wavelengths there is a significant z component of the force density, suggesting that the $\mathbf{f}_{\text{dis}}$ term from (2.110) starts to contribute due to the relatively large values of ε'' for these wavelengths.

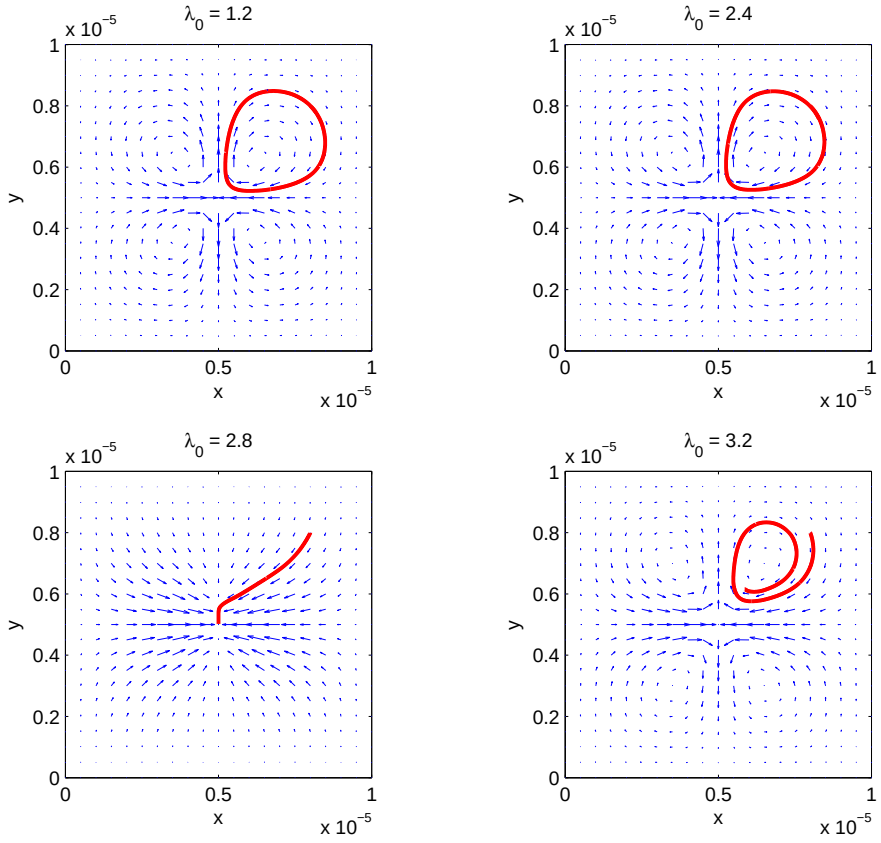

Figure 6.12: Resulting velocity field in the xy-plane, through the focal point. The red lines are streamlines. We see for $\lambda_0 = 1.2\,\mu\text{m}$ and $\lambda_0 = 2.4\,\mu\text{m}$ that velocity fields look alike, and form closed loops. For $\lambda_0 = 3.2\,\mu\text{m}$ we also see a loop structure but here the streamlines are not closed, implying a non-zero z component of the velocity. For $\lambda_0 = 2.8\,\mu\text{m}$ we do not see any loop-like streamlines at all.

Indeed we find as maximum velocity components in this plane the values $87\,\mu\mathrm{m\,s^{-1}}$, $64\,\mu\mathrm{m\,s^{-1}}$, $11\,\mu\mathrm{m\,s^{-1}}$ and $39\,\mu\mathrm{m\,s^{-1}}$ respectively.

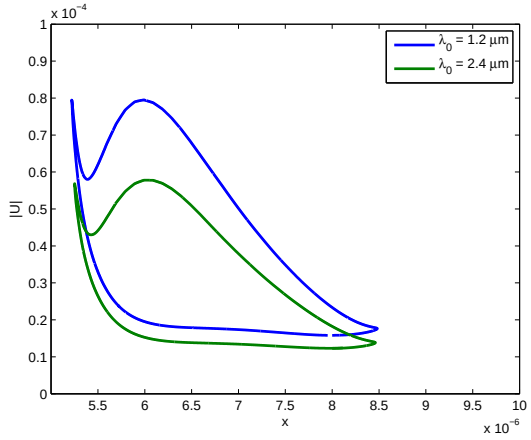

Figure 6.13: Magnitude of the velocity corresponding to the two closed loops in Figure 6.12, for $\lambda_0 = 1.2\,\mu\mathrm{m}$ and $\lambda_0 = 2.4\,\mu\mathrm{m}$. The curves are traversed counter-clockwise in time by the fluid particles. We see that the shape for both wavelengths is alike.

Figure 6.13 shows the magnitude of the velocity for the closed loops in Figure 6.12. The larger velocity corresponds to $\lambda_0 = 1.2\,\mu\mathrm{m}$ while the smaller velocity corresponds to $\lambda_0 = 2.4\,\mu\mathrm{m}$. We see that except for the magnitude, the shape of the two curved is identical. The curved in 6.12 are traversed clockwise by the velocity field, so increasing speeds correspond to decreasing x values. This means the curves in 6.13 are traversed counter-clockwise in time.

In Figure 6.14 we see the velocity field in the xz- and yz-plane for the wavelengths $\lambda_0 = 1.2\,\mu\mathrm{m}$ and $\lambda_0 = 2.4\,\mu\mathrm{m}$. Near the focal point we have zero z component in all plots. As for the force density, in the xz-plane the velocity is pointing toward the central axis, while in the yz-plane it is pointing away from the axis, following our conjecture based on the force density. At the central axis the velocity is zero in both planes, and it is growing to a maximum when moving radially outward, after which it quickly gets smaller again. The maximum magnitude in these planes are again $87\,\mu\mathrm{m\,s^{-1}}$ and $64\,\mu\mathrm{m\,s^{-1}}$ respectively, just as in the xy-plane, which implies that this maximum magnitude is attained at the radial axes going through the focal point.

In Figure 6.15 shows the velocity fields in the same planes but now for the wavelengths $\lambda_0 = 2.8\,\mu\mathrm{m}$ and $\lambda_0 = 3.2\,\mu\mathrm{m}$. We see a qualitatively different picture. The most important feature is that the z component is dominant near the focal axis. This confirms our conclusions from Figure 6.12, that the $\mathbf{f}_{\mathrm{dis}}$ term starts contributing for these wavelengths. Because this non-zero z component we now see circulation in both the xz- and yz-plane. This suggest that in contrast to the smaller wavelengths, where the circulation is in the xy-plane, we now have circulation in all three directions. Furthermore we see that the flow in the y direction is no longer away from the central axis for all z values. For small z values it is actually flowing towards the centre.

Figure 6.16 shows some streamlines for the different wavelengths. For $\lambda_0 = 1.2\,\mu\mathrm{m}$ and $\lambda_0 = 2.4\,\mu\mathrm{m}$ the streamlines show circulation in the xy-plane just was predicted earlier from Figure

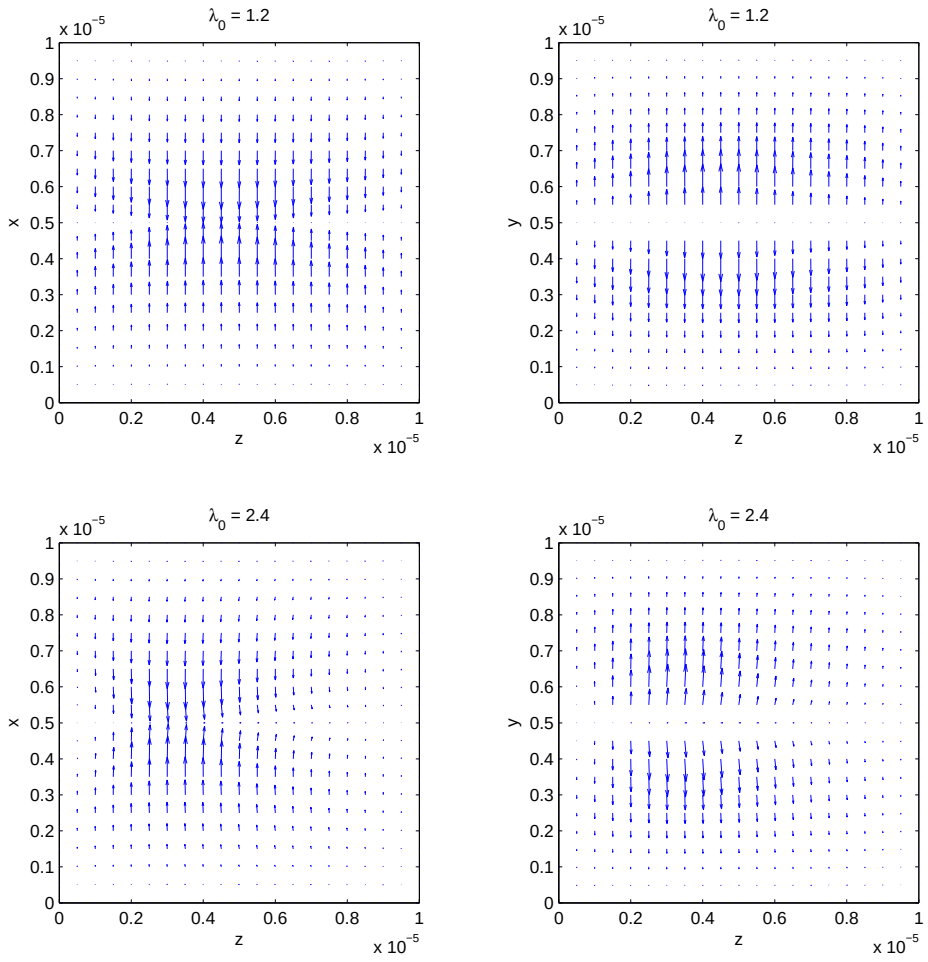

Figure 6.14: Velocity field in the xz- and yz-plane, through the focal point for $\lambda_0 = 1.2\,\mu\text{m}$ and $\lambda_0 = 2.4\,\mu\text{m}$. Near the focal point we have a zero z component in all the plots. Also in the xz-plane we have the velocity pointing towards the central axis while in the yz-plane is it pointing away from the central axis.

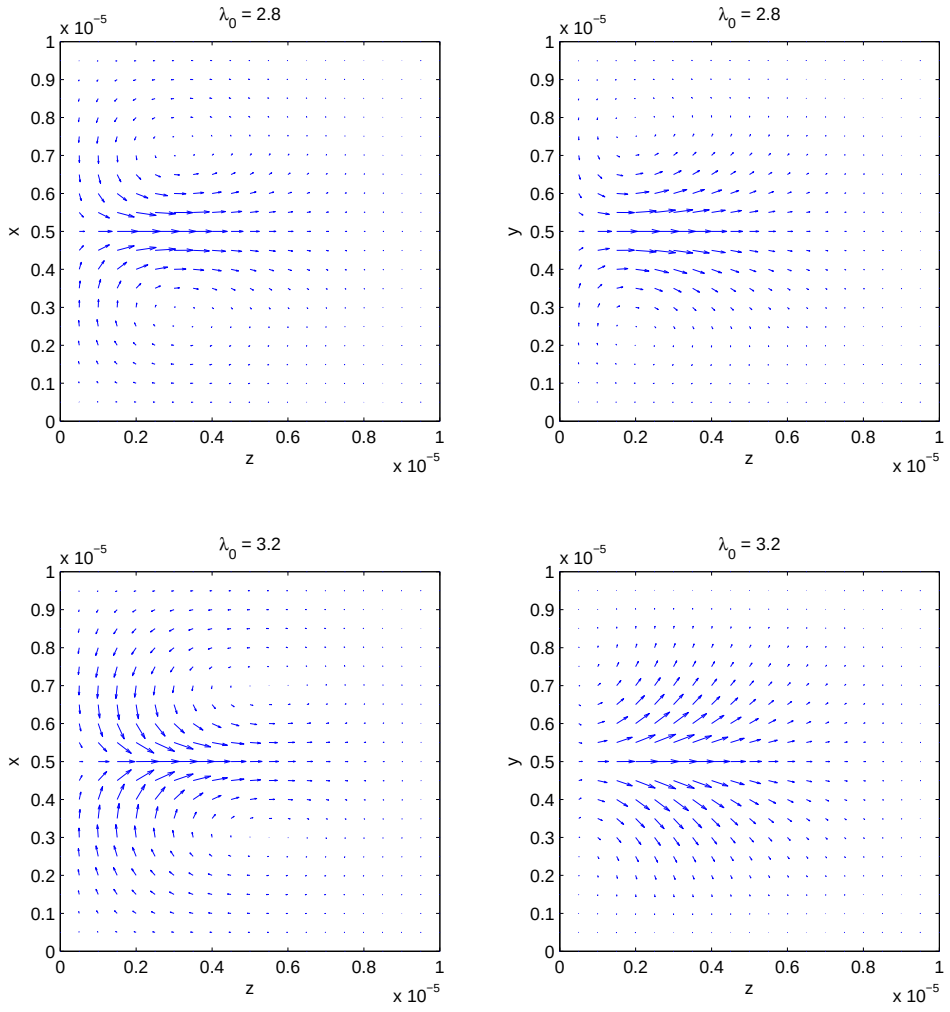

Figure 6.15: Velocity field in the xz- and yz-plane, through the focal point for $\lambda_0 = 2.8\,\mu\text{m}$ and $\lambda_0 = 3.2\,\mu\text{m}$. For these wavelength we have a large z component at the focal axis, pointing away from the source. This is the contribution of the $\mathbf{f}_{\text{dis}}$ force density term.

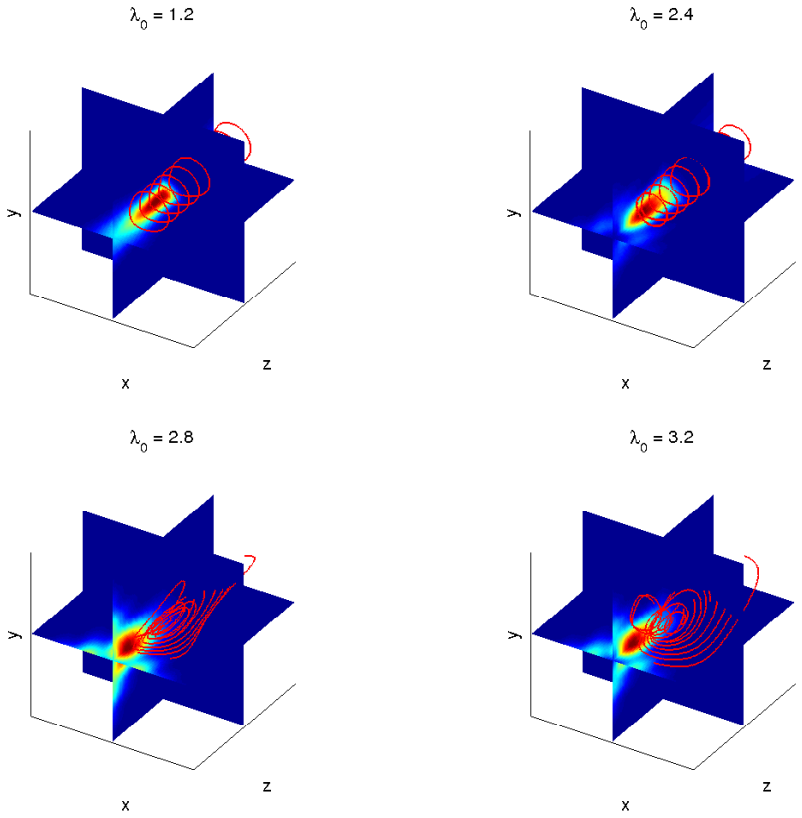

Figure 6.16: Velocity field in the xz- and yz-plane, through the focal point for $\lambda_0 = 1.2\,\mu\text{m}$ and $\lambda_0 = 2.4\,\mu\text{m}$. Near the focal point we have a zero z component in all the plots. Also in the xz-plane we have the velocity pointing towards the central axis while in the yz-plane is it pointing away from the central axis, following our conjecture based on the force density.

6.12. Furthermore they do not pass through the planes $x = x_\mathrm{f}$ and y_f, confining the flow to a specific quadrant in the xy-plane. Although the streamlines for the larger wavelengths move in the z direction, they are still confined to a specific quadrant in the xy-plane, like with the smaller wavelengths. This suggest that in the plane defined by $x = x_\mathrm{f}$, the x component of the velocity is (nearly) zero for all the wavelengths. Also the y component in the plane defined by $y = y_\mathrm{f}$ will be nearly zero. Because of this none of the streamlines passes through these planes. This means that the fluid is circulating through a specific region of the domain, not passing, or barely passing, certain 'boundary' planes. This is exactly what we see in 6.16 for $\lambda_0 = 2.8\,\mu\mathrm{m}$ and $\lambda_0 = 3.2\,\mu\mathrm{m}$, where all the streamlines fall in the quadrant with $x > x_\mathrm{f}$ and $y > y_\mathrm{f}$. The reason why for these wavelengths the streamlines are not confined in the z direction is because of the significant $\mathbf{f}_\mathrm{dis}$ term, which has a large z value, pointing in positive z direction.

As a particular example we will investigate the y component of the velocity through the plane $y = y_\mathrm{f} = 5\,\mu\mathrm{m}$. Figure 6.17 shows this component for all four wavelengths. Each wavelength is scaled independently to show the structure of the velocity component. For $\lambda_0 = 1.2\,\mu\mathrm{m}$ and $\lambda_0 = 2.4\,\mu\mathrm{m}$ the order of the velocity is $10^{-10}\mathrm{m\,s^{-1}}$ and $10^{-9}\mathrm{m\,s^{-1}}$ respectively, which is negligible compared to the velocities we saw earlier, in the order of $10^{-5}\mathrm{m\,s^{-1}}$. The apparent asymmetry in the x direction is a numerical artefact because of these small values. For the larger wavelengths, $\lambda_0 = 2.8\,\mu\mathrm{m}$ and $\lambda_0 = 3.2\,\mu\mathrm{m}$ we see that the velocity component is two orders larger, and more local. This is a consequence of the heat dissipation and the buoyancy flow induced because of the resulting temperature differences. But still velocities of the order of $10^{-8}\mathrm{m\,s^{-1}}$ are very small compared to the maximum velocities $11\,\mu\mathrm{m\,s^{-1}}$ and $39\,\mu\mathrm{m\,s^{-1}}$ we saw earlier for these wavelengths.

6.4.5 Temperature increase due to dissipation.

Up until now we have focussed on the resulting velocity fields for the different wavelengths. In Section 4.4 we described the Boussinesq approximation for modelling buoyancy flows induced by density differences, resulting from temperature differences. In Figure 6.17 we saw the first signs of this phenomenon. For the larger wavelengths, with larger values of the ε'', which is proportional to the heat dissipation, we saw a relatively large flow in the y direction, compared to the smaller, transparent, frequencies. From (2.108) we see that the heat dissipation is proportional to $|\mathbf{E}|^2$. Figure 6.8 shows that the heat dissipation is highly localized at the point of focus. Using a midpoint scheme to numerically integrate q_em we can determine the total (time-averaged) absorbed power for each wavelength. This results in

$$Q = \int_V q_\mathrm{em}\,\mathrm{d}V,$$

with V the total domain.

In Table 6.2 the results are stated, together with the maximum temperature deviation from the reference temperature. The reference temperature is set to 300 K in all cases. We see that for the small wavelengths the absorption is low and also the temperature difference is very small. For $\lambda_0 = 2.4\,\mu\mathrm{m}$, we are under the 2 K difference mentioned at the end of Section 4.4. For the larger wavelengths the temperature differences are much larger, and is it here where our approximation loses its validity. For wavelengths having such a high heat dissipation, we have to look beyond the Boussinesq approximation in order to get the right, physical, flows. One of the possibilities would be to consider the flow compressible, so to allow density variations along the streamlines.

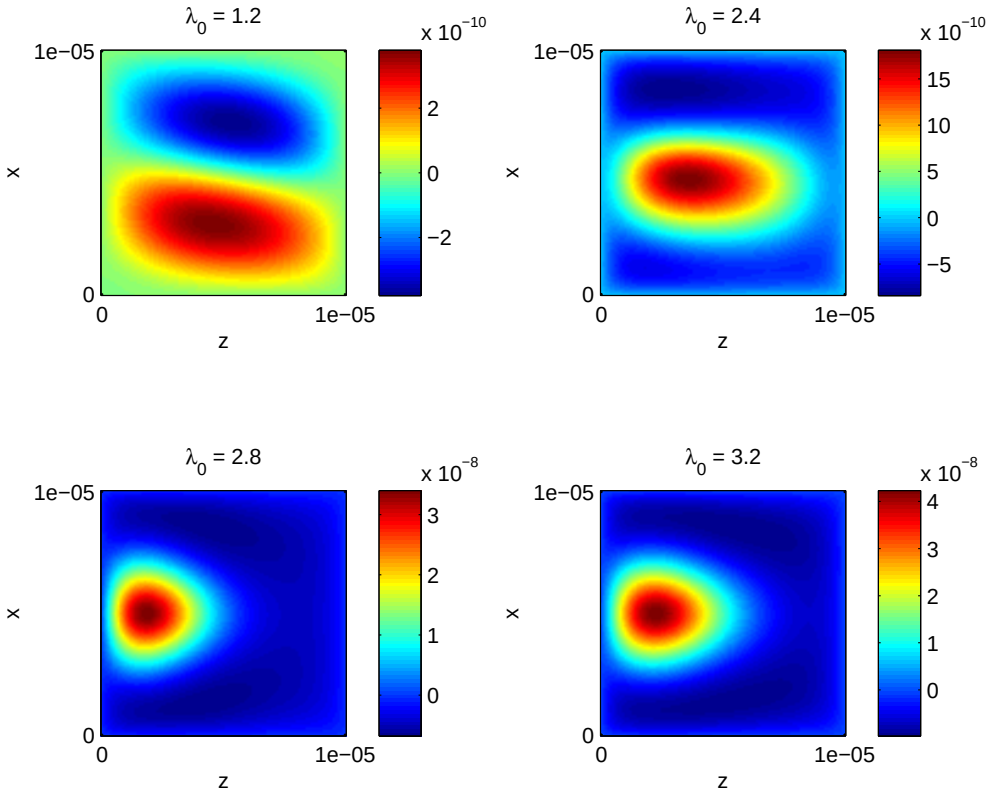

Figure 6.17: Velocity field in the xz- and yz-plane, through the focal point for $\lambda_0 = 1.2\,\mu\text{m}$ and $\lambda_0 = 2.4\,\mu\text{m}$. Near the focal point we have a zero z component in all the plots. Also in the xz-plane we have the velocity pointing towards the central axis while in the yz-plane is it pointing away from the central axis, following our conjecture based on the force density.

λ_0 [µm]	Q [mW]	max. ΔT [K]
1.2	0.001	0.047
2.4	0.053	1.906
2.8	0.998	37.653
3.2	0.110	42.654

Table 6.2: Heat dissipation and temperature difference for all four wavelengths. We see that for the larger wavelengths the temperature differences are significantly higher, making the Boussinesq approximation invalid in these cases.

6.4.6 Higher power beams

All simulation are run using a normalization power of $P_0 = 1\,\mathrm{mW}$. In most experimental set-ups more powerful laser beams are used, varying from less than $5\,\mathrm{mW}$ up to $50\,\mathrm{mW}$ [19]. In the previous section we saw that for the larger wavelengths, $\lambda_0 = 2.8\,\mu\mathrm{m}$ and $\lambda_0 = 3.2\,\mu\mathrm{m}$ the temperatures already rise above the limits of our approximation. We will now focus on $\lambda_0 = 1.2\,\mu\mathrm{m}$ and $\lambda_0 = 2.4\,\mu\mathrm{m}$, and examine the resulting velocity and temperature fields when we rise the ingoing power to $P_0 = 50\,\mathrm{mW}$. Of course we expect the total heat absorbed to increase, and so also the resulting temperatures. We have to be careful to stay within the boundaries of the Boussinesq approximation. When increasing the incoming power, the fields will have the same structure, only multiplied by a constant, since $P_0 \propto I_0^2$, so for the field structure we refer to the previous sections. Since $|\mathbf{E}|^2 \propto I_0^2$ and $\mathbf{S} \propto I_0^2$, both q_{em} and f_{em} will be 50 times larger when we increase the power from $P_0 = 1\,\mathrm{mW}$ to $P_0 = 50\,\mathrm{mW}$.

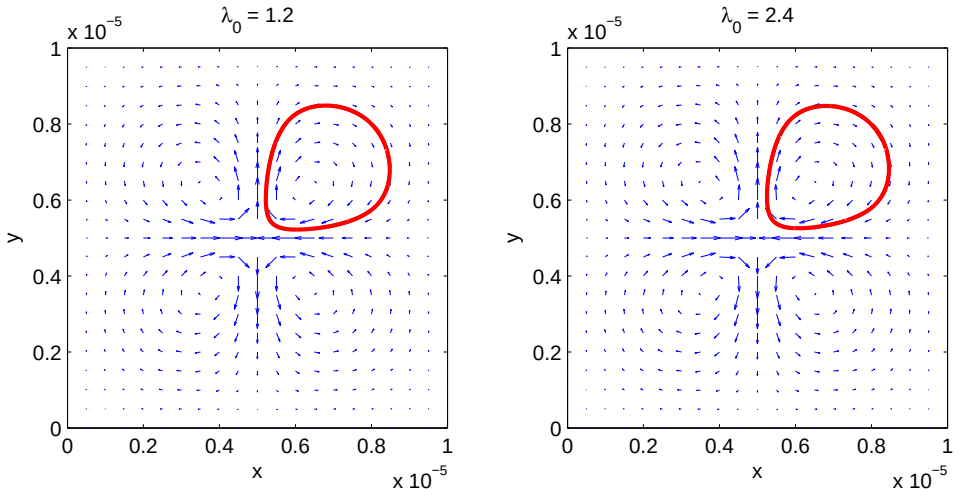

Figure 6.18: Resulting velocity field in the xy-plane, through the focal point. The red lines are streamlines. The velocity fields look very similar to the two corresponding plots in Figure 6.12.

Figure 6.18 shows the resulting velocity profile in the xy-plane. It looks very similar to the two corresponding plots in Figure 6.12. Also the curves of the magnitude of the velocity of the streamlines outlined has the exact same shape but is multiplied by approximately 50, the factor with which the power increased. Table 6.3 shows the minimum and maximum velocity magnitude for the streamlines outlined in Figure 6.18 compared to the corresponding ones in Figure 6.12. The values in parentheses are for $P_0 = 1\,\mathrm{mW}$. All values are exactly multiplied by 50, showing that in this regime the flow is linear in the external force density $\mathbf{f}_{\mathrm{em}}$, confirming that we are in the laminar Stokes regime.

As mentioned earlier, with larger power comes larger heat dissipation and higher temperatures. Figure 6.19 shows the temperature distribution in the xy-plane through the focal point, with $z = z_{\mathrm{f}}$. For $\lambda_0 = 1.2\,\mu\mathrm{m}$ the maximum temperature rise is $2.34\,\mathrm{K}$, still small enough for the Boussinesq

λ_0 [µm]	$u_{\min}$ [µm s^{-1}]	$u_{\max}$ [µm s^{-1}]
1.2	790 (15.8)	3975 (79.5)
2.4	614 (12.3)	2889 (57.8)

Table 6.3: Minimum and maximum velocity magnitudes for the streamlines from Figure 6.18 and Figure 6.12. The values in parentheses are for the $P_0 = 1\,\mathrm{mW}$ case. The values are proportional with a factor 50.

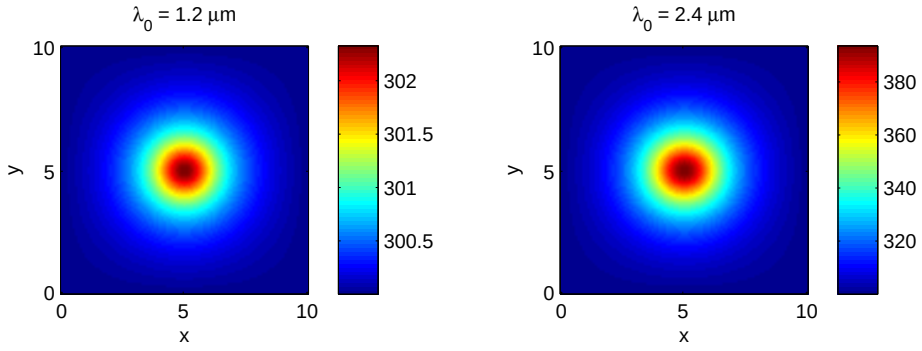

Figure 6.19: Temperature in the xy-plane through the focal point. For $\lambda_0 = 1.2\,\mu\mathrm{m}$ the increase is about 2 K, still small enough for the Boussinesq approximation to be valid, but for $\lambda_0 = 2.4\,\mu\mathrm{m}$ the increase is almost 100 K, so our assumption is not valid in this case.

approximation to be valid, but for $\lambda_0 = 2.4\,\mu\text{m}$ the increase is 95.2 K, so our assumption is not valid in this case, and the resulting flow is not the one we expect physically. This implies that our suggestion that the flow is linear in the external force density is only valid for the most transparent wavelengths. For wavelengths at which heat dissipation is significant, non-linear phenomena can occur, resulting in (possibly quantitatively) different flows.

6.4.7 Influence of boundaries

The domain size we are using is relatively small, having length $L = 10\,\mu\text{m}$ in each direction. The result is that the no-slip boundary condition can be of big influence to the resulting flow. On obvious solution to rule this out would be to enlarge the domain, but using a similar grid size this means we would need to solve a larger system. This becomes quickly infeasible, since we are working with a three dimensional domain. One option we will explore is to double the domain size, without changing the number of cells, thus effectively we will have cells that are twice as large in each direction. We then have $L = 20\,\mu\text{m}$. It is not likely that the flow patterns will change qualitatively, we already saw that away from the focal axis the velocity gets smaller quickly. This is why we will focus on the amplitude of the velocity, especially near the focal point. We will also consider the results of the Stokes equations. The Stokes equations follow from the Navier-Stokes equations if we assume the non-linear advective term $v_j \partial_j v_i$ from (4.22) is negligible. Furthermore the buoyancy is neglected. This results in the linear equations

$$\partial_i p = \mu \partial_j^2 v_i + f_i^{\text{em}}.$$

These equations are valid for small Reynolds numbers. The Reynolds number is given by

$$Re = \frac{vL}{\nu},$$

where v and L are the characteristic velocity and length respectively. We will consider the smallest wavelength $\lambda_0 = 1.2\,\mu\text{m}$, with power $P_0 = 1\,\text{mW}$, so that the velocity is relatively small, and the effect of the buoyancy is negligible since the total absorbed heat is very small. For our case we have $Re \ll 1$, so the Stokes equations can be used to approximate our solution. In order to solve them we use the corresponding Green's function, the so-called Stokeslet. Here we assume there are no physical boundaries, so we have an infinite domain. The Green's function is derived in [11].

In Figure 6.20 we see the velocity in plane $z = z_\text{f}$ for the three cases with $L = 10\,\mu\text{m}$, $L = 20\,\mu\text{m}$ and the Stokes flow. We translated the coordinates so that the focal planes coincide at $x_\text{f} = y_\text{f} = 10\,\mu\text{m}$. The x component it taken for $y = y_\text{f}$ and vice-versa the y component it taken for $x = x_\text{f}$, so both are evaluated on a line through the focal point. All three cases coincide near the focal point itself, but the maximum values differ slightly. For the full Navier-Stokes equations the maximum amplitudes are smaller than for the Stokes flow, so ignoring the advective term leads to larger velocities. This can be understood because the advective term states that the velocity is 'carried away by itself', resulting in smaller velocity values. For points further away from the focus we see that the velocity is larger when the boundaries are further away. The difference between $L = 10\,\mu\text{m}$, $L = 20\,\mu\text{m}$ are relatively large, so indeed the close boundaries do temper the flow. The larger domain is already getting close to the Stokes flow. Although the amplitudes to change with a changing domain, overall qualitative picture seems to coincide in all cases. For the Stokes flow this is as expected since we are in the Stokes domain with small Reynolds numbers.

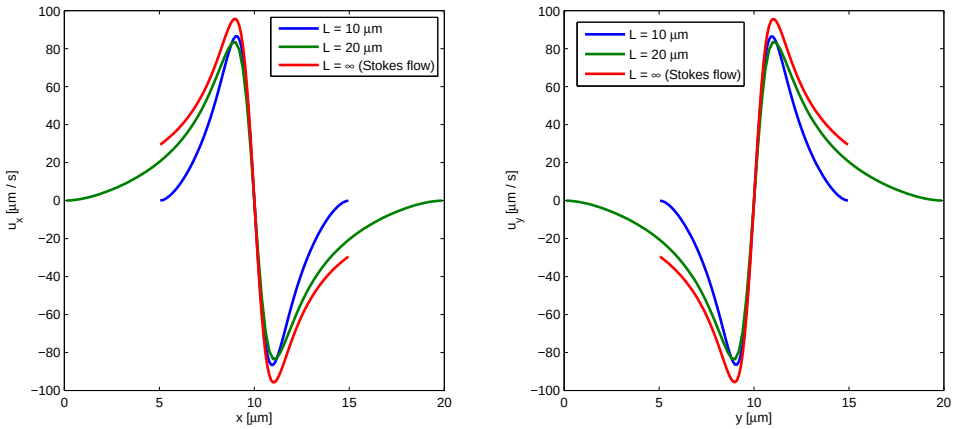

Figure 6.20: Velocity components along two lines through the focal point. The x component is shown as function of x for $y = y_\mathrm{f}$ and $z = z_\mathrm{f}$, and likewise the y component is shown as function of y for $x = x_\mathrm{f}$ and $z = z_\mathrm{f}$. We see that for the full Navier-Stokes equations the amplitude drops slightly for the bigger domain, while for the approximation of the Stokes flow it increases slightly.

Chapter 7

Conclusions

Using the Maxwell equations and the Navier-Stokes equations we have formulated a number of equations to simulate fluid flows induced by electromagnetic fields, in particular those produced by laser beams.

Our first concern was which electromagnetic source to use. An often used approximation for laser beams is the Gaussian beam approximation. We have showed that this approximation leads to large analytical errors for the most interesting parameters choices, and this might lead to non-physical force densities. To circumvent this problem we have designed the dipole approximation, which is an exact solution of the Maxwell equations. We also showed that the numerical accuracy is high enough for our choice of parameters. Also for small wavelengths we get resulting fields much alike the Gaussian beam, suggesting that our model is an adequate one, and the derived quantities are indeed similar to the physical ones.

Using these dipole sources we have run several simulations, for four different wavelengths, the relatively transparent short wavelengths, $\lambda_0 = 1.2\,\mu\text{m}$ and $\lambda_0 = 2.4\,\mu\text{m}$ and the more absorbing wavelengths $\lambda_0 = 2.8\,\mu\text{m}$ and $\lambda_0 = 3.2\,\mu\text{m}$. For the different wavelengths we noticed different flows and resulting temperatures.

For the smaller wavelengths the force density has no component in the direction of propagation. In the plane orthogonal to this propagation direction, the component in the direction of polarization of the electric field is pointing away from the focal axis, while the component orthogonal to the polarization direction is pointing towards the focal axis.

For the low power beams the heat dissipation is very small and the resulting temperatures are within the Boussinesq approximation, but the resulting buoyancy flow does not lead to any significant effect. The flow generated by the force density is highly dominant and leads to circulation in the planes orthogonal to the direction of propagation of the beam. The direction of the circulation depends on the polarization of the electric field as described earlier. As a consequence of this circulating motion the streamlines are confined to a specific quadrant in the planes orthogonal to the propagation direction.

For the high power beams we see two different things. For the smallest wavelength, $\lambda_0 = 1.2\,\mu\text{m}$, the resulting flow is nearly proportional, suggesting that the flow is linear in the force density. This shows that we have a Stokes flow with small Reynolds number. Again the resulting temperatures are within the Boussinesq approximation, but there is not significant flow because of the buoyancy.

For $\lambda_0 = 2.4\,\mu\text{m}$ we see the same proportionality with the high power beam, but now the resulting

temperature rise is large, and we are far outside the Boussinesq regime, so this proportional flow is not necessarily the physical flow we would expect, and a more thorough model is needed to coop with the large temperature differences. The fluid density will become inhomogeneous, and also the variation in viscosity might become significant. We conclude that for this wavelength at higher powers our model is not and we need a more complete approach.

The fact that we use a limited domain has some influence on the flow, but leads to the same qualitative results. Away from the focus, the magnitude of the velocity will drop off more slowly in larger domains, but near the focus the results are similar. Since this is the region of most interest to us, using a smaller domain is not a real drawback for investigating these flows.

For the larger wavelengths we see qualitatively different results. These wavelengths are much less transparent, leading to big losses of electromagnetic energy to heat. The most obvious consequence is that the beams do not penetrate the domain very far, and the focal point is closer to the source plane. Furthermore the contribution of the dissipative term of the force density, which was negligible for the shorter wavelengths, is now significant, leading to a large force component in the direction of propagation. The non-dissipative force term is still there, and the total force density, which is the sum of these two contributions, leads to a complicated flow pattern. The streamlines are still confined to a specific quadrant in the xy-plane, but will move in the direction of propagation.

As a consequence of the large heat dissipation, the resulting temperatures are much higher than for the smaller wavelengths. Even for the low power beam the temperatures are well above the Boussinesq regime, so our approximation is not valid for these wavelengths. As a consequence we cannot claim that the flows we observe are physical. The large temperature differences can lead to different flows that are not captured in our model. Again a variable density and viscosity is needed to model these situations adequately.

Finally there is the question of the force density itself. Although derived in a very thorough manner, there are still assumptions about the interaction of the electromagnetic field with the matter inside the medium that we cannot answer by any simulations. In particular, the correct form of the stress tensor that governs all these forces. Thorough experimental investigation is needed to see whether the flows we predict are indeed there, to confirm that these assumptions are correct.

Chapter 8

Future work

As mentioned in the previous chapter, there is still a lot of interesting work to be done in this research area. Considering the flows we have investigated, the most important next step would be to drop the Boussinesq approximation and work with the full compressible Navier-Stokes equations. The large temperature differences due to heat absorption lead to significant differences in density. Also the viscosity changes with temperature and should be taken as a variable quantity.

Another interesting point would be the boundary conditions for the temperature. We assumed the boundaries were at a constant ambient temperature, while in a physical set-up there would be some heat transfer coefficient governing the temperatures at the boundary of the domain. This might be of particular interest when the focal point if very close to one of the sides of the domain.

An important next step will be an experimental set-up where the induced flows we predict can be measured directly. This will settle the question of the electromagnetic stress tensor and would justify further investigation of this phenomenon. One thing that is needed to model such a set-up is a more complex domain. A difficulty might be the electromagnetic boundary conditions. When a domain with small scale structure is introduced the permittivity could start varying over the domain, leading to inhomogeneous heating, scattering and all sorts of electromagnetic phenomena. A different way to model the fields is then needed. A possible way to overcome these electromagnetic difficulties is to use a solid material with equal index of refraction as the liquid, a so-called index-matching material. The electromagnetic field will then be unaltered by the solid material, but the flows will be channelled by the geometry of the solid.

As we saw in Chapter 6, for the high frequency beams, with low losses, we have a very distinctive structure of the force density near the focal point. In the polarization direction the force is pointing away from the focal point, while in the orthogonal direction it is pointing towards the focal point. This is also the region where the force density is at its maximum magnitude, so it is a logical choice to focus on this region. A problem is that the loops created by this force density depend on the size of the domain. To overcome this, we could use the index matching material to create a channel to guide the fluid around. This channel could for example coincide with one of the closed loops from Figure 6.16. There is still the matter of measuring the velocity through this small channel.

Finally we have neglected the possible back-action of the fluid to the fields. Since the fluid velocities are small the terms involved in this interaction are small too, but at some point they might no longer be neglected. Especially when certain parameters such as the density are considered variable, since the permittivity depends on this quantity.

Appendix A

Four-vector notation

In order to determine the right constitutive relations, and energy and momentum equations, we will use the four-vector notation from special relativity. Since the Maxwell equations are Lorentz invariant, we can get compact notation in this way. Once we have the correct expressions for the constitutive relations and energy and momentum equations, we will make assumptions about the fluid velocity being non-relativistic, in order to simplify things

We change to the coordinates $x^0 = ct$ and $x^i = x_i$ for $i = 1, 2, 3$. We use the notations of [7] and [21]. The partial derivatives are now given by

$$\partial_\mu = \begin{pmatrix} \frac{1}{c}\partial_t & \partial_1 & \partial_2 & \partial_3 \end{pmatrix}.$$

We will use the so-called $(-+++)$ convention, meaning that the metric tensor is given by

$$\eta^{\mu\nu} = \eta_{\mu\nu} = \begin{pmatrix} -1 & 0 & 0 & 0 \\ 0 & 1 & 0 & 0 \\ 0 & 0 & 1 & 0 \\ 0 & 0 & 0 & 1 \end{pmatrix}. \tag{A.1}$$

We will need the four-vectors for the velocity and the electric and magnetic current densities. For the velocity we have

$$V^\mu = \begin{pmatrix} \gamma c & \gamma v_1 & \gamma v_2 & \gamma v_3 \end{pmatrix}, \tag{A.2}$$

where γ is the famous gamma factor, given by

$$\gamma = \frac{1}{\sqrt{1 - \frac{\|v\|^2}{c^2}}}.$$

For ordinary velocities we have $\gamma \approx 1$, and we will use this simplification when applicable. We define the electric current density four-vector

$$J^\mu = \begin{pmatrix} c\rho_{\mathrm{e}} & J_1 & J_2 & J_3 \end{pmatrix}, \tag{A.3}$$

and the magnetic current density four-vector

$$K^\mu = \begin{pmatrix} c\rho_\mathrm{m} & K_1 & K_2 & K_3 \end{pmatrix}, \tag{A.4}$$

where J_i and K_i are the components of the normal current densities. If we separate the vector in a time and space part, we can write the space part in vector notation. We then get

$$V^\mu = \begin{pmatrix} \gamma c & \gamma \mathbf{v} \end{pmatrix}, \; J^\mu = \begin{pmatrix} c\rho_\mathrm{e} & \mathbf{J} \end{pmatrix} \text{ and } K^\mu = \begin{pmatrix} c\rho_\mathrm{m} & \mathbf{K} \end{pmatrix}.$$

We can now define the field tensor $F^{\nu\mu}$ as

$$F^{\mu\nu} = \begin{pmatrix} 0 & \frac{E_1}{c} & \frac{E_2}{c} & \frac{E_3}{c} \\ -\frac{E_1}{c} & 0 & \mu_0 H_3 & -\mu_0 H_2 \\ -\frac{E_2}{c} & -\mu_0 H_3 & 0 & \mu_0 H_1 \\ -\frac{E_3}{c} & \mu_0 H_2 & -\mu_0 H_1 & 0 \end{pmatrix}, \tag{A.5}$$

and the dual field tensor $G^{\nu\mu}$ as

$$G^{\mu\nu} = \frac{1}{2}\epsilon^{\mu\nu\rho\sigma} F^{\rho\sigma} = \begin{pmatrix} 0 & \mu_0 H_1 & \mu_0 H_2 & \mu_0 H_3 \\ -\mu_0 H_1 & 0 & -\frac{E_3}{c} & \frac{E_2}{c} \\ -\mu_0 H_2 & \frac{E_3}{c} & 0 & -\frac{E_1}{c} \\ -\mu_0 H_3 & -\frac{E_2}{c} & \frac{E_1}{c} & 0 \end{pmatrix}. \tag{A.6}$$

In vector notation these tensors are equal to

$$F^{\nu\mu} = \begin{pmatrix} 0 & \frac{1}{c}\mathbf{E} \\ -\frac{1}{c}\mathbf{E} & \cdot \times (\mu_0 \mathbf{H}) \end{pmatrix}$$

and

$$G^{\nu\mu} = \begin{pmatrix} 0 & \mu_0 \mathbf{H} \\ -\mu_0 \mathbf{H} & \cdot \times (\frac{1}{c}\mathbf{E}) \end{pmatrix},$$

where $\cdot \times \mathbf{E}$ means that vector with which is multiplied is inserted in the curl operator.
The Maxwell equations can now be stated as

$$\partial_\nu F^{\mu\nu} = J^\mu, \tag{A.7}$$
$$\partial_\nu G^{\mu\nu} = K^\mu. \tag{A.8}$$

Conversation of electric and magnetic charge are expressed as

$$\partial_\mu J^\mu = 0, \tag{A.9}$$
$$\partial_\mu K^\mu = 0. \tag{A.10}$$

Further expression can be derived for the Lorentz force and Poynting theorem as the gradient of the energy-stress tensor. At this point we will not need these results since we already derived them directly from the Maxwell equations.

Appendix B

Implementation

In this appendix we will discuss how we have implemented the simulations. We have mainly used OpenFOAM, a free open-source software package written in C++. OpenFOAM is originally developed for numerically solving fluid mechanics problems, but applications include for example electro-hydrodynamics or partial differential equations in general. The main advantages of using OpenFOAM is that it contains the algorithms needed to solve the fluid dynamics equations, and it gives the possibility to use high-level syntax for manipulating scalar and vector fields on the mesh, using concepts such as operator-overloading. One major disadvantage is the lack of support for complex numbers, which is the reason why we have split all expressions in a real and imaginary part in Chapter 2 and Chapter 3.

The OpenFOAM package consists of a number of libraries, responsible for certain physical models, algorithms or general tasks such as mesh control or the implementation of boundary conditions. These libraries are used by the executable programs themselves, usually referred to as the solvers. The package comes with a number of basic solvers that can be used out-of-the-box. For example there are solvers for solving problems with incompressible flow, with or without turbulence. Also there are solvers for compressible flow, and solvers for certain specific problems containing for example natural convection.

Each problem, or case, consist of a file-tree containing configuration files, or dictionary files, to control the process of solving. Furthermore they contain the value of the parameters used by the specific solver. Through these dictionary files the user has a lot of flexibility in solving the problem. Almost everything can be tweaked to meet the needs of the specific case problem. For example the convergence criteria for the solving algorithm, in our case the SIMPLE algorithm, the discretization schemes used to discretized the differential operators in the equations, the algorithms used to solve the linear systems that need to be solved during the whole process, and what pre-conditioners are used.

Furthermore OpenFOAM comes with basic meshing and post-processing tools. For simple domains, such as the one we have used, the `blockMesh` tool can be used. This tool can create meshes consisting of one or more rectangular boxes. For more complicated domains, there are tools specifically designed for this task, and OpenFOAM can handle most common formats (or has tools to convert them to a format it can handle). For data gathering there is the `sample` tool, that extracts user-defined data points from the solution fields, using the interpolation method of the user's choice.

A lot of information on the general settings and the solvers and tools that come with OpenFOAM can be found in the user guide [14].

For our simulations we have developed several solvers for the different tasks. First the electromagnetic fields are calculated on the mesh points. For both the Gaussian beam model and the dipole array we have analytic expressions of the electric and magnetic fields for all positions in the domain. This means that we can determine all the field components explicitly given the position vectors of the grid. This is where the advantage of the high-level syntax comes in. For example, to calculate the real part of the Green's function from (3.46),

$$\mathrm{Re}\,\{g(\mathbf{r})\} = \frac{1}{4\pi\|\mathbf{r}\|}e^{-\alpha\|\mathbf{r}\|}\cos k\|\mathbf{r}\|,$$

we use three lines of code,

```
volVectorField x = mesh.C();
volScalarField dr = Foam::mag(x - y);
volScalarField g = 0.25 / Foam::constant::mathematical::pi / dr *
                    Foam::exp(-alpha * dr) * Foam::cos(k * dr);
```

The `volVectorField` and `volScalarField` objects are defined in an OpenFOAM library and contain a vector and scalar field, defined in all the centres of the grid points of the mesh. The mesh itself is contained in the `mesh` object. The expression `mesh.C()` simply returns the coordinates of the centres of all the grid points in the mesh as a `volVectorField`. After the total electric and magnetic fields are determined, the derived quantities such as the Poynting vector and the intensity of the electric field are calculated. This is easily done using the lines

```
volVectorField S_real = 0.5 * ((E_real ^ H_real) + (E_imag ^ H_imag));
volVectorField S_imag = 0.5 * ((E_imag ^ H_real) - (E_real ^ H_imag));
volScalarField E_sq = (E_real & E_real) + (E_imag & E_imag);
```

Here we see how the operator over-loading works. Where normally in C++ the `^` and `&` operators are bitwise operators on the integer types, OpenFOAM defines them on the `volVectorField` and `surfaceVectorField` objects, their meaning being the cross-product and the inner-product respectively. Again we see the explicit splitting in real and imaginary part.

Two other useful objects are the `surfaceVectorField` and `surfaceScalarField`. These also contain vector and scalar fields over the mesh, but now defined in the centres of all the faces of each grid point. There is also support for tensor fields over the mesh, where a distinction is made between symmetric and non-symmetric tensors.

OpenFOAM also takes care of the creation of the linear systems used during the different stages of the solving algorithm. In order to achieve this there are expressions that convert a differential operator on a field quantity and other explicit terms to a discrete system of the famous form $A\mathbf{x} = \mathbf{b}$. Here a distinction is made between implicit and explicit discretization. Implicit discretization means the field considered is actually the field that is solved for and is treated as unknown. The discretization scheme defined through the dictionary files is applied and the term is added to the system matrix A. Explicit discretization works similar in that again the discretization scheme from the dictionary files is applied, but now the field itself is considered to be known. In simple words, the values of the previous iteration are substituted and the contribution goes to the $\mathbf{b}$ term. Of course when explicit discretization is used, it is essential that the field is initialized to some

initial value for the first step. The implicit discretization terms are found in the name-space `fvm` and the explicit discretization terms in the name-space `fvc`. The programmer does not manipulate the system matrices directly. However there are procedures available to manipulate them, for example to apply the relaxation described in Section 4.7.

Another advantage of the fact that OpenFOAM is open-source, and you compile and link your own solvers is that it is easy to combine it with functionalities from other libraries. For example when implementing the dipole array explained in Section 3.2, the fields of a lot of individual dipoles are needed to be calculated and in the end all their contributions need to be summed. Since for each dipole the calculations are alike, except a different source vector $\mathbf{y}$ is used, these calculations are very suitable to perform in parallel. During the project a small CUDA implementation was developed and linked with the solver. This results in significantly higher performance. Other useful applications might be for example the use of LAPACK routines for certain tasks.

As mentioned earlier OpenFOAM can handle complicated meshes that are created using other tools. It can solve the fluid dynamical equations governing the flows in these complex domains. One thing that is not supported at this point is to solve the (full) Maxwell equations on such complex meshes. In order to achieve this, either an external method has to be used, or such a Maxwell solver has to be implemented in OpenFOAM.

Our implementation of the fluid dynamics solver is based on existing solvers in OpenFOAM. We used the standard incompressible flow solver without a turbulence model, and added the buoyancy concepts from the natural convection solver. The essential part of the SIMPLE algorithm is given by the lines

```
while (simple.loop())
{

    // --- Pressure-velocity SIMPLE corrector
    {
        #include "UEqn.H"
        #include "TEqn.H"
        #include "pEqn.H"
    }

    runTime.write();

}
```

The included files contain the solution procedures of the different equations. The code for the momentum equation is given by

```
// Momentum predictor
tmp<fvVectorMatrix> UEqn
(
    fvm::div(phi, U)
  - fvm::laplacian(nu, U)

 == f_em / rho_0
);
```

```
    UEqn().relax();

    if (simple.momentumPredictor())
    {
        solve
        (
            UEqn()
            ==
            fvc::reconstruct
            (
                (
                    - ghf*fvc::snGrad(rhok)
                    - fvc::snGrad(p_rgh)
                ) * mesh.magSf()
            )
        );
    }
```

Here we see how in the first lines the implicit part containing the velocity field is created and relaxed. In the second part the explicit terms containing the (modified) pressure are added. The energy equation given by (4.23), can be rewritten as

$$\partial_i(v_i T) - T\partial_i v_i - \frac{k}{\rho_0 c_\mathrm{p}}\partial_i^2 T = \frac{q_\mathrm{em}}{\rho_0 c_\mathrm{p}}.$$

The discretization of this equation in our implementation is given by the lines

```
    fvScalarMatrix TEqn
    (
        fvm::div(phi, T)
      - fvm::Sp(fvc::div(phi), T)
      - fvm::laplacian(k / rho_0 / c_p, T)
      // Added source term, divided by correct quantities
      == H
    );

    TEqn.relax();
    TEqn.solve();

    rhok = 1.0 - beta*(T - T_0);
```

We see that the temperature field is discretized implicitely in all three terms. The expression `phi` is the fluid flux, determined in the pressure equation. Also the new density is determined. The pressure equation takes more effort. The code is given by

```
{
    volScalarField rAU("rAU", 1.0/UEqn().A());
```

```
surfaceScalarField rAUf("(1|A(U))", fvc::interpolate(rAU));

U = rAU*UEqn().H();
UEqn.clear();

phi = fvc::interpolate(U) & mesh.Sf();
adjustPhi(phi, U, p_rgh);

surfaceScalarField buoyancyPhi(rAUf*ghf*fvc::snGrad(rhok)*mesh.magSf());
phi -= buoyancyPhi;

while (simple.correctNonOrthogonal())
{
    fvScalarMatrix p_rghEqn
    (
        fvm::laplacian(rAUf, p_rgh) == fvc::div(phi)
    );

    p_rghEqn.setReference(pRefCell, getRefCellValue(p_rgh, pRefCell));

    p_rghEqn.solve();

    if (simple.finalNonOrthogonalIter())
    {
        // Calculate the conservative fluxes
        phi -= p_rghEqn.flux();

        // Explicitly relax pressure for momentum corrector
        p_rgh.relax();

        // Correct the momentum source with the pressure gradient flux
        // calculated from the relaxed pressure
        U -= rAU*fvc::reconstruct((buoyancyPhi + p_rghEqn.flux())/rAUf);
        U.correctBoundaryConditions();
    }
}

#include "continuityErrs.H"

p = p_rgh + rhok*gh;

if (p_rgh.needReference())
{
    p += dimensionedScalar
    (
        "p",
```

```
            p.dimensions(),
            pRefValue - getRefCellValue(p, pRefCell)
        );
        p_rgh = p - rhok*gh;
    }
}
```

We see the modified pressure being determined and the pressure equation being solved. After this the velocity field is corrected. The final part makes sure the reference value for the pressure is taken into account.

Bibliography

[1] A. Ashkin, J. M. Dziedzic, J. E. Bjorkholm, and Steven Chu. Observation of a single-beam gradient force optical trap for dielectric particles. *Opt. Lett.*, 11(5):288–290, May 1986.

[2] G. K. Batchelor. *An Introduction to Fluid Dynamics*. Cambridge University Press, cambridge mathematical library edition, 2000.

[3] L. W. Davis. Theory of electromagnetic beams. *Phys. Review A*, 19:1177–1179, 1979.

[4] Maria Dienerowitz, Michael Mazilu, and Kishan Dholakia. Optical manipulation of nanoparticles: a review. *Journal of Nanophotonics*, 2(1):021875–021875–32, 2008.

[5] J. H. Ferziger and M. Perić. *Computational Methods for Fluid Dynamics*. Springer, 3rd edition, 2002.

[6] Winston Frias and Andrei I. Smolyakov. Electromagnetic forces and internal stresses in dielectric media. *Phys. Rev. E*, 85:046606, Apr 2012.

[7] David J. Griffiths. *Introduction to Electrodynamics*. Prentice Hall, 3rd edition, 1999.

[8] George M. Hale and Marvin R. Querry. Optical constants of water in the 200-nm to 200-µm wavelength region. *Appl. Opt.*, 12(3):555–563, Mar 1973.

[9] Kolumban Hutter, Yongqi Wang, and IrinaP. Chubarenko. Phenomenological coefficients of water. In *Physics of Lakes*, Advances in Geophysical and Environmental Mechanics and Mathematics, pages 389–418. Springer Berlin Heidelberg, 2011.

[10] H. Jasak. *Error analysis and estimation for the Finite Volume method with applications to fluid flows*. PhD thesis, Imperial College, University of London, 1996.

[11] Sangtae Kim and Seppo J. Karrila. *Microhydrodynamics: Principles and Selected Applications*. Butterworth-Henemann, Boston, June 1991.

[12] L. D. Landau and E. M. Lifshitz. *Electrodynamics of Continuous Media*. Pergamon Press, 2nd edition, 1984.

[13] L. D. Landau and E. M. Lifshitz. *Fluid Mechanics*. Pergamon Press, 2nd edition, 1984.

[14] OpenCFD Limited. *OpenFOAM 2.1.1 User Guide*, 2012.

[15] S. V. Patankar. *Numerical heat transfer and fluid flow*. Hemisphere Publishing Corporation, 1981.

[16] Demetri Psaltis, Stephen R. Quake, and Changhuei Yang. Developing optofluidic technology through the fusion of microfluidics and optics. *Nature*, 442(7101):381–386, July 2006.

[17] Maria L. V. Ramires, Carlos A. Nieto de Castro, Yuchi Nagasaka, Akira Nagashima, Marc J. Assael, and William A. Wakeham. Standard reference data for the thermal conductivity of water. *Journal of Physical and Chemical Reference Data*, 24(3):1377–1381, 1995.

[18] C. M. Rhie and W. L. Chow. Numerical study of the turbulent flow past an airfoil with trailing edge separation. *AIAA Journal*, 21:1525–1532, November 1983.

[19] Alexander Rohrbach. Stiffness of optical traps: Quantitative agreement between experiment and electromagnetic theory. *Phys. Rev. Lett.*, 95:168102, Oct 2005.

[20] Ross T. Schermer, Colin C. Olson, J. Patrick Coleman, and Frank Bucholtz. Laser-induced thermophoresis of individual particles in a viscous liquid. *Opt. Express*, 19(11):10571–10586, May 2011.

[21] Jack Vanderlinde. *Classical Electromagnetic Theory*. Kluwer Academic Publishers, 2nd edition, 2004.

[22] Pinyu Wu, Rongxin Huang, Christian Tischer, Alexandr Jonas, and Ernst-Ludwig Florin. Direct measurement of the nonconservative force field generated by optical tweezers. *Phys. Rev. Lett.*, 103:108101, Sep 2009.